IMPROVED ABSORBING BOUNDARY CONDITIONS FOR TIME-DOMAIN METHODS IN ELECTROMAGNETICS

by

YOTKA RICKARD, M.Sc. (Eng.), M.Sc. (Math.)

A Thesis
Submitted to the School of Graduate Studies
In Partial Fulfilment of the Requirements
For the Degree
Doctor of Philosophy

McMaster University

DOCTOR OF PHILOSOPHY (2002) McMASTER UNIVERSITY
(Electrical and Computer Engineering) Hamilton, Ontario

TITLE: Improved Absorbing Boundary Conditions for Time-Domain Methods in Electromagnetics

AUTHOR: Yotka Spasova Rickard
M.Sc. (Eng) (Technical University Sofia, Bulgaria)
B.Sc. (Math) (Sofia University "St. Kl. Ochridski", Bulgaria)
M.Sc. (Math) (McMaster University, Hamilton, Ontario)

SUPERVISOR: Prof. W. -P. Huang, Department of Electrical and Computer Engineering

NUMBER OF PAGES: xvi, 175

Abstract

This thesis contributes to the development of novel absorbing boundary conditions (ABCs) for two finite-difference time-domain (FDTD) methods in computational electromagnetics: the well-known FDTD method to the solution of Maxwell's equations and the wave equation in the time-domain (WETD) method.

The conventional approach to create a perfectly matched layer (PML) ABC for the FDTD solution to Maxwell's equations is reviewed, as well as several other state-of-the-art techniques to define a PML medium.

The novel WETD technique is described for applications in numerical algorithms both for optical waveguides and structures, and in the microwave and millimetre-wave structure analysis. The new algorithm requires a reliable and efficient ABC, which can handle both open problems (i.e., radiation and scattering) and problems involving port terminations (such as high-frequency circuit problems and optical guiding structures).

A new degree of freedom is introduced in the definition of the PML variable profiles and thus improved algorithms for PML ABCs are formulated and developed both for the WETD method and for the FDTD solution to Maxwell's equations. The proposed modified PML profiles handle equally well both port

terminations in guided-wave problems and truncations of the computational domain of open problems.

The performance of the proposed PML absorber is further improved by new types of PML termination walls using single-layer ABCs. For that, a lossy version of Mur's second order ABC and a lossy version of the second order dispersive boundary condition (DBC) have been developed and implemented. The current implementation is formulated and developed on orthogonal non-uniform grids. It handles inhomogeneous dielectrics intersecting the PML boundaries. Various numerical simulations have been carried out to validate the theoretical models at microwave and optical frequencies, as well as in depth detailed comparison with commonly used PML ABCs is presented.

Suggestions for further research are provided.

Acknowledgements

The author wishes to express her sincere appreciation to Dr. N. Georgieva and Dr. W. -P. Huang, both from the Department of Electrical and Computer Engineering at McMaster University, for their expert suggestions, continuing support and interest throughout the course of this work.

The author gratefully acknowledges the financial assistance provided by the Department of Electrical and Computer Engineering at McMaster University through a Teaching Assistantship; by the Ministry of Training for Colleges and Universities in Ontario through an Ontario Graduate Scholarship and Ontario Graduate Scholarship in Science and Technology.

Last but not least, the author wishes to express her greatest gratitude to her husband, Brian, for his understanding, patience and loving support. This work would not be possible without his continuous encouragement and help.

Contents

List of Abbreviations

ABC	Absorbing Boundary Condition
AR	Anti-Reflection
BC	Boundary Condition
BHW	Blackman-Harris Window
BPM	Beam Propagation Method
DBC	Dispersive Boundary Condition
EM	Electromagnetic
FDFD	Finite-Difference Frequency-Domain
FDTD	Finite-Difference Time Domain
FEM	Finite-Element Method
FETD	Finite-Element Time-Domain
GPML	Generalized Perfectly Matched Layer
IPML	Improved Perfectly Matched Layer
IPML-FDTD	Improved Perfectly Matched Layer for the FDTD solution to Maxwell's equations
IPML-WETD	Improved Perfectly Matched Layer for the Wave Equation in the Time Domain Method
MoM	Method of Moment

MPML	Modified Perfectly Matched Layer
ODE	Ordinary Differential Equation
PDE	Partial Differential Equation
PEC	Perfect Electric Conductor
PMC	Perfect Magnetic Conductor
PML	Perfectly Matched Layer
TDIE	Time-Domain Integral Equation
TDWP	Time-Domain Wave Potentials
TE	Transverse Electric
TM	Transverse Magnetic
VP	Vector Potential
WE	Wave Equation
WETD	Wave Equation in the Time Domain
2-D	Two-Dimensional
3-D	Three-Dimensional

List of Figures

Chapter 1

Introduction

Up to the late 1980s, the modeling of engineering systems involving electromagnetic wave interactions was dominated by frequency-domain techniques, mainly based on solving frequency-domain integral equations by the Method of Moment (MoM); see e.g. Harrington (1968). MoM includes setting up and solving dense, complex-valued systems of thousands, even tens of thousands of linear equations by direct or iterative techniques. Its drawbacks include not only a huge computational burden, but also the necessity of the integral equations reformulation including difficult derivations of geometry-specific Green's functions; as well as incapability to deal with electrically large objects of complex geometry.

To resolve the above mentioned difficulties, since the late 1980s the focus of the computational electromagnetic research changed towards the direct solution of the fundamental Maxwell's curl equations or the derived from them wave equation, on spatial grids in either time or frequency domain. The solutions of those partial differential equations (PDE) have proven to be robust and provide highly accurate modeling for variety of free-space and guided-wave

electromagnetic interaction problems. They deal easily with geometrical and material complexity and inhomogeneities.

Time-domain methods can be classified according to the analytical form in which the fields are represented. Any field problem can be described either by its PDE, or by its corresponding time-domain integral equations (TDIE). The first type of models (the PDE models) can be further classified as finite-difference or finite-element methods depending on the discretization scheme used. The second type of models (the TDIE models) leads to the boundary-value integral formulation that can be also treated by a variety of discretization schemes.

Time domain finite-difference PDE solvers have two versions: based on the discretization of Maxwell's equations or based on the discretization of the wave equation. They both provide the means to model ultrahigh-speed microwave and photonic circuits and devices, since those have electromagnetic wave transport and interaction phenomena as a critical operating factor. Simulation techniques of this type also permit the visualization of the electromagnetic wave propagation dynamics in those devices which otherwise is difficult, costly and sometimes impossible to implement.

When open problems are treated by a 3-D space-domain discretization of PDE solvers, the real infinite space has to be truncated to a reasonably sized numerical domain. The boundaries of that numerical domain have to simulate the reflectionless propagation of the field or potential quantities, which is done by the application of Absorbing Boundary Conditions (ABCs).

Kane Yee (1966) placed the basis for the time domain PDE solvers by introducing the finite-difference time-domain (FDTD) approximation of derivatives on interleaved (dual) spatial Cartesian meshes for the electric and magnetic field in Maxwell's equations.

The second alternative for the time domain finite-difference PDE solvers is the wave equation, either derived for the electric (or the magnetic) field, see e.g. Krupezevic (1993), or derived for the magnetic (and/or electric) vector potential, see e.g. Georgieva (1997). FDTD potential formulation has the advantages of significant memory and CPU-time savings in comparison to the FDTD field formulation, since all six components of the electric and magnetic field can be described by three or even two scalar quantities: either by the three components of one (magnetic or electric) vector potential, or by two collinear scalar wave functions, which are components of the magnetic and electric vector potential in one preferred direction. The advantages of using vector potentials (VP) include the facts that they are less singular in the vicinity of sources and sharp discontinuities, such as edges and wedges of infinite conductivity; they are also smoother functions of space than the field components at interfaces between regions of different permittivities and/or permeabilities. Each component of the vector potential is decoupled from the other ones. This implies fewer numerical errors and no late time-step instability.

Despite its attractiveness, the time-domain wave potential (TDWP) approach (see Georgieva (2001)) has not been implemented until recently,

because of many unsolved problems, mainly related to the proper application of boundary conditions at material interfaces, conducting edges and corners, etc. The right choice of wave-potential preferred direction posed another serious problem. The first finite-difference application of the time-domain wave potential (TDWP) method was presented by Georgieva and Rickard (1999), (2000). In Georgieva (2001), the construction of solutions based on the TDWP approach is rigorously analyzed for general inhomogeneous media.

The practical application of the above-mentioned new time-domain methods, based on the use of the wave equation, requires the formulation and development of reliable and problem-independent ABCs. It has to be an efficient ABC, which can handle both open problems (i.e. radiation and scattering) and problems involving port terminations (high-frequency circuit problems).

During the last decade or two, various ABCs have been developed. However, intensive research is still going on in this area because numerical reflections, even if small, affect badly the stability of the algorithms, as well as the frequency-domain results, which appear to be very sensitive to numerical errors in the transient response.

Jean-Pierre Berenger (1994) introduced the Perfectly Matched Layer (PML) ABC, which has been proven to be the best ABC capable of suppressing all sources of computational noise to amplitudes below 10^{-4} of the incident wave amplitude. The PML ABC introduced by Berenger (1994), (1996) has attracted immense attention in the last years. It has been used both in the frequency domain

and in the time domain. In the time domain it has been applied mainly in conjunction with the FDTD solution to Maxwell's equations. In the frequency domain, PMLs have been developed for the Finite-Element Method (FEM) and for the Finite-Difference Frequency-Domain (FDFD) formulations. PML has been modified and improved for various applications.

There are only few attempts to apply PML to the wave equation, mainly in the frequency domain [for example see W.P. Huang *et al.* (1996), AlSunaidi *et al.* (1999), Tang *et al.* (1998), Cuccinotta *et al.* (1999), Yassui *et al.* (1999)]. To the author's knowledge there is only one publication on one-direction of PML absorption for the time-domain 2-D wave equation by D. Zhou *et al.* (2001).

In this thesis, improved algorithms for PML ABCs for the 3-D time-domain wave equation (WETD) in lossless and lossy inhomogeneous dielectric media have been developed and their possible applications to the analysis of microwave and optical wave passive elements have been investigated. A new degree of freedom is introduced in the definition of the PML variable profiles and improved PML ABCs are developed both for the WETD method and for the FDTD method to the solution of Maxwell's equations. New types of PML termination walls are developed. The objective of this research is to develop the theoretical and numerical aspects of the problem. It opens a wide range of possibilities for further improvement of numerical implementation and practical applications. Various numerical simulations have been carried out to validate the

theoretical models as well as comparisons to other well-known ABCs are presented.

Chapter 2 outlines the most powerful time domain method in the computational electrodynamics – Yee's finite-difference time-domain (FDTD) method. The fundamental concepts are reviewed and the non-uniform orthogonal algorithm is presented.

Chapter 3 focuses on the perfectly matched layer (PML) absorbing boundary condition (ABC) for Yee's FDTD method to the solution of Maxwell's equations. Some of the existing PML ABCs are reviewed which are related to the development of an improved PML (IPML) ABC, where the IPML variables profiles are modified by incorporating a new degree of freedom in the existing algorithms.

Chapter 4 describes the wave equation in the time domain (WETD) techniques using vector potentials. These new techniques developed by Georgieva (2001), and by Georgieva and Rickard (1999), (2000) are the first successful attempts to apply the vector potential theory into finite-difference time-domain algorithms. First, the time-domain algorithm based on the magnetic vector potential and the second-order wave equation is presented. Then, the application of a pair of two collinear wave potentials of a fixed direction is outlined and its advantages are considered.

Chapter 5 describes the improved PML ABC developed for the 3-dimensional WETD method. Modified PML variable profiles are proposed whose

superior performance is validated in the numerical examples in Chapter 6. New types of PML termination walls that improve the performance of the absorber are developed.

Chapter 6 deals with the validation of the proposed PML models – for both the WETD method and the FDTD method to the solution of Maxwell's equations. The numerical aspects of their implementation are considered. Examples of both open (radiation) problems and port terminations in high-frequency circuit problems are presented. The algorithms are tested for homogeneous and inhomogeneous media. The modified PML variable profiles developed for both the WETD and Yee's FDTD method are shown to offer lower reflections in a wider frequency band in comparison with the commonly used profiles. The effect of the termination walls on the overall performance of the PML absorber is studied and the best options are singled out.

The thesis concludes in Chapter 7 where the results are discussed and some suggestions for further research are provided.

The author's original contributions in this thesis are:

1. New degree of freedom is added in the formulation of the PML variable profiles. Based on it, an Improved Perfectly Matched Layer (IPML) ABC for the FDTD solution of Maxwell's equations on orthogonal non-uniform grids is developed and implemented in a FORTRAN program.

2. An Improved Perfectly Matched Layer ABC for the 3-dimensional wave equation in the time-domain (WETD) method is formulated and developed on orthogonal non-uniform grids and is implemented in a FORTRAN program. New degree of freedom is incorporated in the formulation of the PML variable profiles.
3. New types of termination walls for the IPML ABC are formulated and implemented.
4. In depth detailed comparison with commonly used PML ABCs is presented.
5. Prescription for suitable values of all IPML parameters is given based on extensive numerical experiments.

However, in the author's opinion the most important contribution is the introduction of the new degree of freedom in the definition of the PML variables profiles. This represents a problem-independent approach to the improvement and optimization of the PML performance, in contrast to the attempts to optimize one PML variable in a problem-specific environment. Finding PML variable profiles suitable for the wave equation in the time domain was crucial to the development of an efficient and reliable ABC for the WETD, which was the primary goal of this research. The PML ABC proposed here is not limited to electromagnetic problems only. It can be applied to any physical phenomenon modeled by the general lossy 3-D scalar wave equation, which requires reflection-free boundaries.

Chapter 2

The Finite-Differences Time-Domain Method

2.1 Introduction

The solution of every electromagnetic field problem is based on (the exact) Maxwell's equations:

$$\nabla \times \vec{E} = -\mu \frac{\partial \vec{H}}{\partial t} - \sigma^m \vec{H} + \vec{J}_m^i \tag{2.1}$$

$$\nabla \times \vec{H} = \varepsilon \frac{\partial \vec{E}}{\partial t} + \sigma \vec{E} + \vec{J}^i \tag{2.2}$$

$$\nabla \cdot \vec{H} = 0 \tag{2.3}$$

$$\nabla \cdot \left(\varepsilon \vec{E}\right) = \rho \tag{2.4}$$

where:

$\vec{E}$ is the electric field intensity [V/m];

$\vec{H}$ is the magnetic field intensity [A/m];

μ is the magnetic permeability at the given point in space [H/m];

ε is the dielectric permittivity [F/m];

σ is the electric conductivity [S/m];

σ^m is the magnetic conductivity [ohm/m];

$\vec{J}^i$ is the induced electric current density [A/m^2];

$\vec{J}_m^i$ is the induced magnetic current density [V/m^2].

The equations (2.1) to (2.4) are always endowed with certain boundary conditions (BCs) depending on the problem.

The solutions to practical problems depend on numerical methods to solve the above equations since their analytical solution is available for very limited simple structures only. Starting with the first application to 2-D problems (TE and TM wave propagation in a waveguide structure) in the fundamental publication of K. Yee (1966), the FDTD method evolved to the most powerful time-domain approach in electromagnetics nowadays.

2.2. Outline of Yee's algorithm on orthogonal non-uniform meshes

The idea of Kane Yee (1966) is to discretize directly Maxwell's curl equations in their differential form, replacing them by a set of *finite difference equations*. This initially was done on an orthogonal uniform grid, i.e. the increments Δx, Δy, Δz in *x*-, *y*-, and *z*-directions, respectively, were constant in all directions.

As shown on Fig. 2.1, the $\vec{E}$ and $\vec{H}$ components are located so that each $\vec{E}$ component is surrounded by four circulating $\vec{H}$ components and vice versa, thus providing an interlinked array of Faraday's Law and Ampere's Law

contours. Hence, Yee's algorithm simultaneously simulates the point-wise differential form and the macroscopic integral form of Maxwell's equations, which together with the central difference operations (using the so called leapfrog scheme) implicitly enforces the two Gauss' Law relations, too.

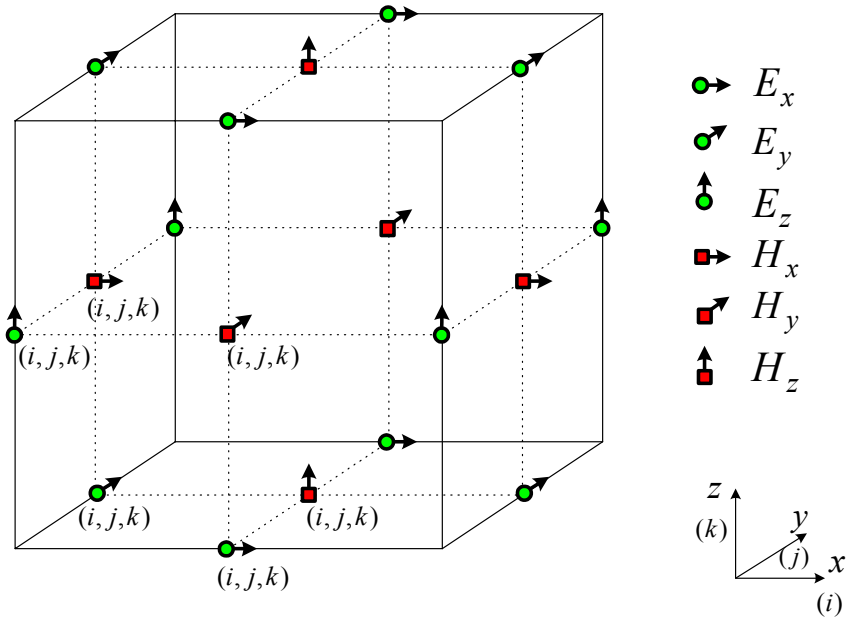

Fig. 2.1. Yee's discretization cell showing the orientations and positions of the $\vec{E}$ - and $\vec{H}$ - field components.

The method is known as FDTD, the "*Finite-Differences Time-Domain*" method. It can be readily put in terms of an *orthogonal non-uniform grid*, i.e. the increments $\Delta x(i)$, $\Delta y(j)$, $\Delta z(k)$ could change along their corresponding direction, so that at the time step *n*, the following discretization holds:

$$H_x^{n+\frac{1}{2}}(i,j,k)=\left[\frac{1-r^m(i,j,k)}{1+r^m(i,j,k)}\right]H_x^{n-\frac{1}{2}}(i,j,k)+\frac{\Delta t}{\mu\left[1+r^m(i,j,k)\right]}\times \left[\frac{E_y^n(i,j,k+1)-E_y^n(i,j,k)}{\Delta z(k)}-\frac{E_z^n(i,j+1,k)-E_z^n(i,j,k)}{\Delta y(j)}\right] \tag{2.5}$$

$$H_y^{n+\frac{1}{2}}(i,j,k)=\left[\frac{1-r^m(i,j,k)}{1+r^m(i,j,k)}\right]H_y^{n-\frac{1}{2}}(i,j,k)+\frac{\Delta t}{\mu\left[1+r^m(i,j,k)\right]}\times \left[\frac{E_z^n(i+1,j,k)-E_z^n(i,j,k)}{\Delta x(i)}-\frac{E_x^n(i,j,k+1)-E_x^n(i,j,k)}{\Delta z(k)}\right] \tag{2.6}$$

$$H_z^{n+\frac{1}{2}}(i,j,k)=\left[\frac{1-r^m(i,j,k)}{1+r^m(i,j,k)}\right]H_z^{n-\frac{1}{2}}(i,j,k)+\frac{\Delta t}{\mu\left[1+r^m(i,j,k)\right]}\times \left[\frac{E_x^n(i,j+1,k)-E_x^n(i,j,k)}{\Delta y(j)}-\frac{E_y^n(i+1,j,k)-E_y^n(i,j,k)}{\Delta x(i)}\right] \tag{2.7}$$

$$E_x^{n+1}(i,j,k)=\left[\frac{1-r(i,j,k)}{1+r(i,j,k)}\right]E_x^n(i,j,k)+\frac{\Delta t}{\varepsilon\left[1+r(i,j,k)\right]}\times \left[\frac{H_z^{n+\frac{1}{2}}(i,j,k)-H_z^{n+\frac{1}{2}}(i,j-1,k)}{\Delta y_H(j)}-\frac{H_y^{n+\frac{1}{2}}(i,j,k)-H_y^{n+\frac{1}{2}}(i,j,k-1)}{\Delta z_H(k)}\right] \tag{2.8}$$

$$E_y^{n+1}(i,j,k)=\left[\frac{1-r(i,j,k)}{1+r(i,j,k)}\right]E_y^n(i,j,k)+\frac{\Delta t}{\varepsilon\left[1+r(i,j,k)\right]}\times \left[\frac{H_x^{n+\frac{1}{2}}(i,j,k)-H_x^{n+\frac{1}{2}}(i,j,k-1)}{\Delta z_H(k)}-\frac{H_z^{n+\frac{1}{2}}(i,j,k)-H_z^{n+\frac{1}{2}}(i-1,j,k)}{\Delta x_H(i)}\right] \tag{2.9}$$

$$E_z^{n+1}(i,j,k)=\left[\frac{1-r(i,j,k)}{1+r(i,j,k)}\right]E_z^n(i,j,k)+\frac{\Delta t}{\varepsilon\left[1+r(i,j,k)\right]}\times \left[\frac{H_y^{n+\frac{1}{2}}(i,j,k)-H_y^{n+\frac{1}{2}}(i-1,j,k)}{\Delta x_H(i)}-\frac{H_x^{n+\frac{1}{2}}(i,j,k)-H_x^{n+\frac{1}{2}}(i,j-1,k)}{\Delta y_H(j)}\right] \tag{2.10}$$

where $r(i,j,k)=\dfrac{\sigma(i,j,k)\cdot\Delta t}{2\varepsilon(i,j,k)}$; $r^m(i,j,k)=\dfrac{\sigma^m(i,j,k)\cdot\Delta t}{2\mu(i,j,k)}$.

Here, the 3-dimensional (3-D) computational domain is divided into non-uniform orthogonal mesh with mesh sizes in each direction $\Delta x(i)$, $\Delta y(j)$, $\Delta z(k)$, depending on the position of the mesh point ($1\le i\le n_{x_{\max}}$, $1\le j\le n_{y_{max}}$, $1\le k\le n_{z_{\max}}$), see Fig. 2.2. The use of non-uniform gird increases the efficiency of the FDTD method since a fine mesh can be used only where details are present thus allowing for large savings in memory and computational time.

In order to represent the time and space derivatives properly, the figure shows how the $\vec{E}$- and $\vec{H}$- field components are displaced in time and space by half a step, e.g., in the *z*-direction E_z, H_x and H_y are half step above E_x, E_y and H_z. Also, $\vec{H}$-field components are spatially offset by half a grid with respect to $\vec{E}$-field components (”after” $\vec{E}$ components) and are calculated half a time step in advance. As a result of the spatial offset of $\vec{H}$-field components, their spatial increments are actually:

$$\Delta x_H(i)=\frac{\Delta x(i)+\Delta x(i+1)}{2} \tag{2.11}$$

$$\Delta y_H(j)=\frac{\Delta y(j)+\Delta y(j+1)}{2} \tag{2.12}$$

$$\Delta z_H(k)=\frac{\Delta z(k)+\Delta z(k+1)}{2} \tag{2.13}$$

where $\Delta x(i)$, $\Delta y(j)$, and $\Delta z(k)$ are the increments for the $\vec{E}$-field components.

The advantage of such a discretization is obvious: it removes the necessity of the less accurate forward-in-time finite differentiation and uses only central difference (leapfrog) schemes.

In order for the above numerical scheme to be stable, it has been rigorously derived that the step size with respect to time, Δt, has to meet Courant's stability condition, see e.g. Taflove (1995):

$$\Delta t \le \frac{1}{c} \min_{i,j,k} \frac{1}{\sqrt{\left(\frac{1}{\Delta x(i)}\right)^2 + \left(\frac{1}{\Delta y(j)}\right)^2 + \left(\frac{1}{\Delta z(k)}\right)^2}} \tag{2.14}$$

or

$$\Delta t \le \frac{1}{c} \cdot \frac{1}{\sqrt{\left(\frac{1}{\Delta x_{\min}}\right)^2 + \left(\frac{1}{\Delta y_{\min}}\right)^2 + \left(\frac{1}{\Delta z_{\min}}\right)^2}} \tag{2.15}$$

where $c = \left(\sqrt{\mu\varepsilon}\right)^{-1}$ is the highest velocity of light in the analyzed structure.

The minimal spatial step can be defined as

$$\Delta l_{\min} = \min_{\substack{1 \le i \le n_{x_{\max}} \\ 1 \le j \le n_{y_{\max}} \\ 1 \le k \le n_{z_{\max}}}} \left\{\Delta x(i), \Delta y(j), \Delta z(k)\right\} \tag{2.16}$$

and Courant's stability condition on Δt usually used in practice is:

$$\Delta t \le \frac{1}{c} \cdot \frac{\Delta l_{\min}}{\sqrt{3}}$$

In the programs developed in this research, Δt is defined as:

$$\Delta t = \frac{\Delta l_{\min}}{2c} \tag{2.17}$$

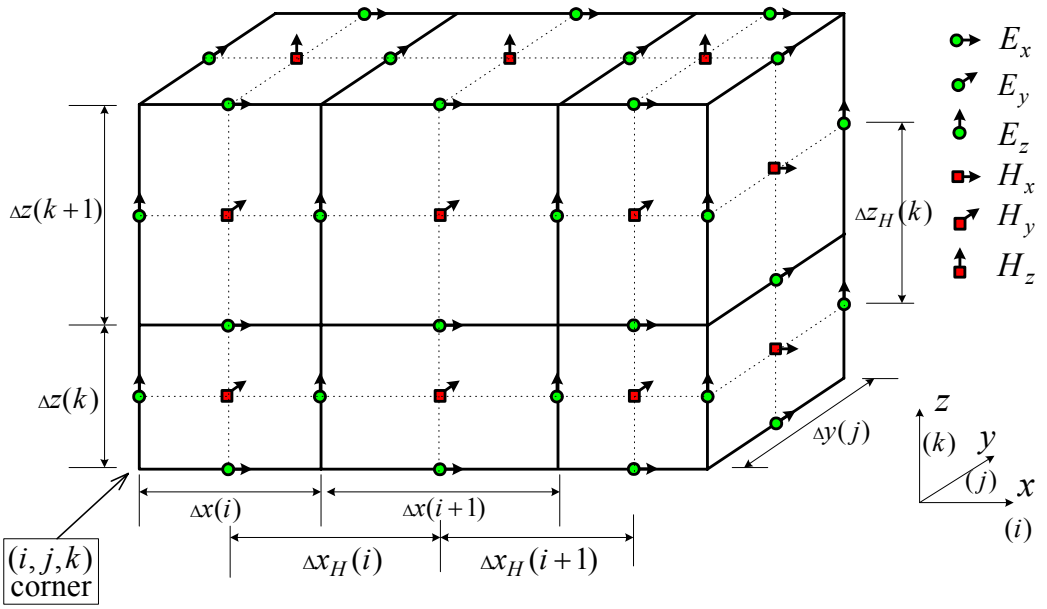

Fig. 2.2. Orthogonal non-uniform mesh layout showing the space increments in x-, y-, and z-directions for the $\vec{E}$- and $\vec{H}$- field components, respectively.

The central finite differences used in Yee's algorithm have second-order accuracy and the resulting time-stepping algorithm is nondissipative, i.e. the numerical wave propagation does not experience any decay resulting from non-physical numerical- algorithm artefacts. Regardless of its mesh non-uniformity, Monk and Suli (1994) proved the second order convergence of the non-uniform orthogonal FDTD. In their proof only Dirichlet homogeneous boundary

conditions are considered. Navaro *et al.* (1996) presented a numerical investigation of the accuracy and showed that the non-uniform orthogonal FDTD yields numerical values of the fields that have second-order accuracy. In the latter paper the results obtained from FDTD simulations are compared to the analytical values for different boundary conditions.

Chapter 3

Improved Absorbing Boundary Conditions for the FDTD

In this chapter, an improvement of the existing modified perfectly matched layer (MPML) ABC will be described, which is based on the introduction of a new degree of freedom in the definition of the PML variable profiles. The resulting PML will be referred to as the improved PML (IPML). As an introduction to the subject, the original Berenger's PML and B. Chen's MPML are outlined. Then a detailed derivation procedure for the IPML parameters is presented, which is based on the method outlined by D.G. Fang (1998). The new degree of freedom is defined, namely the PML variables are allowed to grow at different exponent rates. The resulting IPML parameter profiles are enlisted for the 3-D FDTD method to the solution of Maxwell's equations. Finally, alternative methods to define a PML medium are outlined.

3.1 Outline of Berenger's perfectly matched layer (PML)

One of the disadvantages while using Yee's FDTD method is the necessity to make the computational domain very large. The boundaries of the computational domain have to be far away from the modeled structure in order to separate the desired solution from the boundary effects which give rise to spurious solutions - because the FDTD method does not model the evanescent modes properly: in reality, the structures are open, that is, they exist in an open region and no energy comes back; while in the FDTD model we are confined in a finite computational domain.

This challenge has been addressed in many papers. During the last two decades few types of Absorbing Boundary Conditions (ABCs) have been proposed, such as Engquist-Majda's one-way Wave Equation ABC [Engquist and Majda (1977)], Mur's ABC of first, second, and third order [Mur (1981)], Litva's second order Dispersive Boundary Condition (DBC) [Z. Bi *et al.* (1992)], etc. These provide effective reflection coefficients of order -35 to -45 dB for most FDTD simulations.

To attain a dynamic range of 70 dB, comparable to current RCS measurement technology, a new type of ABC was proposed by Berenger (1994) with "a perfectly matched layer (PML) for the absorption of electromagnetic waves".

Berenger's PML ABC is a *non-physical lossy absorbing medium*, adjacent to the outer grid boundary and has its wave impedance independent of the angle

of incidence and frequency of the outgoing scattered waves. Berenger reported reflection coefficients as low as 1/3000th of those from the standard second and third order analytical ABC's such as Mur's.

The underlying idea of PML ABC is to separate each field component in Yee's algorithm for Maxwell's curl equations into two quantities, each depending on one spatial derivative only, thus giving an additional degree of freedom of the algorithm. This way instead of the six field variables, twelve are defined, in the following way:

$$E_x = E_{xy} + E_{xz} \tag{3.1}$$

$$E_y = E_{yx} + E_{yz} \tag{3.2}$$

$$E_z = E_{zx} + E_{zy} \tag{3.3}$$

$$H_x = H_{xy} + H_{xz} \tag{3.4}$$

$$H_y = H_{yx} + H_{yz} \tag{3.5}$$

$$H_z = H_{zx} + H_{zy} \tag{3.6}$$

By definition, a perfectly matched interface is an interface between two media, one of which is lossy, such that the interface does not reflect a plane wave for all frequencies and all angles of incidence. That is achieved by *matching the phase velocities and the wave impedances* on both sides of the interface.

In his first example for a 2-D TE case - E_x, E_y, H_z, Berenger (1994) starts with Maxwell's equations in the most general case, which is a medium with an electric conductivity σ and a magnetic conductivity σ^m:

$$\varepsilon_0 \frac{\partial E_x}{\partial t} + \sigma E_x = \frac{\partial H_z}{\partial y} \tag{3.7}$$

$$\varepsilon_0 \frac{\partial E_y}{\partial t} + \sigma E_y = \frac{\partial H_z}{\partial x} \tag{3.8}$$

$$\mu_0 \frac{\partial H_z}{\partial t} + \sigma^m H_z = \frac{\partial E_x}{\partial y} - \frac{\partial E_y}{\partial x} \tag{3.9}$$

As it is well known, if the condition

$$\frac{\sigma}{\varepsilon_0} = \frac{\sigma^m}{\mu_0} \tag{3.10}$$

is satisfied, this matches the wave impedance of a lossy free-space medium to that of vacuum so that no reflection occurs when a plane wave propagates normally across an interface between true vacuum and the lossy free-space medium.

To define the PML medium in the TE case, the magnetic component H_z is broken into two subcomponents, denoted as H_{zx} and H_{zy}, depending on the *x*- and *y*-derivatives, respectively. Thus the electromagnetic field has four components, E_x, E_y, H_{zx} and H_{zy}, connected through the four equations:

$$\varepsilon_0 \frac{\partial E_x}{\partial t} + \sigma_y E_x = \frac{\partial \left(H_{zx} + H_{zy} \right)}{\partial y} \tag{3.11}$$

$$\varepsilon_0 \frac{\partial E_y}{\partial t} + \sigma_x E_y = \frac{\partial \left(H_{zx} + H_{zy} \right)}{\partial x} \tag{3.12}$$

$$\mu_0 \frac{\partial H_{zx}}{\partial t} + \sigma_x^m H_{zx} = -\frac{\partial E_y}{\partial x} \tag{3.13}$$

$$\mu_0 \frac{\partial H_{zy}}{\partial t} + \sigma_y^m H_{zy} = -\frac{\partial E_x}{\partial y} \tag{3.14}$$

where the parameters (σ_x, σ_x^m, σ_y, σ_y^m) are homogeneous to electric and magnetic conductivities. From this simple example, it is immediately clear that if, for example, $\sigma_y = \sigma_y^m = 0$, the PML medium can absorb a plane wave (E_y, H_{zx}) propagating along x, but it would not absorb a wave (E_x, H_{zy}) propagating along y.

Similarly, in the 3-D case, in order to make the absorber a lossy medium, for each direction a PML electric conductivity σ_i and a PML magnetic conductivity (loss) σ_i^m, $i = x,\ y,\ z$, are assigned to the outer boundary layer to absorb the outgoing waves, that meet the requirements:

$$\frac{\sigma_i}{\varepsilon_0} = \frac{\sigma_i^m}{\mu_0};\ i = x,\ y,\ z \tag{3.15}$$

Then the equations of Yee's algorithm are separated to obtain the PML scheme as follows:

$$\mu_0 \frac{\partial H_{xy}}{\partial t} + \sigma_y^m H_{xy} = -\frac{\partial \left(E_{zx} + E_{zy} \right)}{\partial y} \tag{3.16}$$

$$\mu_0 \frac{\partial H_{xz}}{\partial t} + \sigma_z^m H_{xz} = \frac{\partial \left(E_{yx} + E_{yz} \right)}{\partial z} \tag{3.17}$$

$$\mu_0 \frac{\partial H_{yz}}{\partial t} + \sigma_z^m H_{yz} = -\frac{\partial \left(E_{xy} + E_{xz} \right)}{\partial z} \tag{3.18}$$

$$\mu_0 \frac{\partial H_{yx}}{\partial t} + \sigma_x^m H_{yx} = \frac{\partial \left(E_{zx} + E_{zy} \right)}{\partial x} \tag{3.19}$$

$$\mu_0 \frac{\partial H_{zx}}{\partial t} + \sigma_x^m H_{zx} = -\frac{\partial \left(E_{yx} + E_{yz} \right)}{\partial x} \tag{3.20}$$

$$\mu_0 \frac{\partial H_{zy}}{\partial t} + \sigma_y^m H_{zy} = \frac{\partial \left(E_{xy} + E_{xz} \right)}{\partial y} \tag{3.21}$$

$$\varepsilon_0 \frac{\partial E_{xy}}{\partial t} + \sigma_y E_{xy} = \frac{\partial \left(H_{zx} + H_{zy} \right)}{\partial y} \tag{3.22}$$

$$\varepsilon_0 \frac{\partial E_{xz}}{\partial t} + \sigma_z E_{xz} = -\frac{\partial \left(H_{yx} + H_{yz} \right)}{\partial z} \tag{3.23}$$

$$\varepsilon_0 \frac{\partial E_{yz}}{\partial t} + \sigma_z E_{yz} = \frac{\partial \left(H_{xy} + H_{xz} \right)}{\partial z} \tag{3.24}$$

$$\varepsilon_0 \frac{\partial E_{yx}}{\partial t} + \sigma_x E_{yx} = -\frac{\partial \left(H_{zx} + H_{zy} \right)}{\partial x} \tag{3.25}$$

$$\varepsilon_0 \frac{\partial E_{zx}}{\partial t} + \sigma_x E_{zx} = \frac{\partial \left(H_{yx} + H_{yz} \right)}{\partial x} \tag{3.26}$$

$$\varepsilon_0 \frac{\partial E_{zy}}{\partial t} + \sigma_y E_{zy} = -\frac{\partial \left(H_{xy} + H_{xz} \right)}{\partial y} \tag{3.27}$$

Following the 2-D example in Berenger (1994), for the 3-D case it can be shown that in PML, each field component, call it Ψ, decays as

$$\Psi = \Psi_0 e^{j\omega\left(t - \frac{x\cos\phi\cos\psi + y\sin\phi\cos\psi + z\sin\psi}{cG} \right)} e^{-\frac{\sigma_x \cos\phi\cos\psi}{\varepsilon_0 cG} x} e^{-\frac{\sigma_y \sin\phi\cos\psi}{\varepsilon_0 cG} y} e^{-\frac{\sigma_z \sin\psi}{\varepsilon_0 cG} z}$$

where

$G = \sqrt{w_x \cos^2\phi\cos^2\psi + w_y \sin^2\phi\cos^2\psi + w_z \sin^2\psi}$;

(ϕ, ψ) define the angle of incidence of the wave electric field vector;

$$\omega_x = \frac{1-\frac{j\sigma_x}{\omega\varepsilon_0}}{1-\frac{j\sigma_x^m}{\omega\mu_0}}; \qquad \omega_y = \frac{1-\frac{j\sigma_y}{\omega\varepsilon_0}}{1-\frac{j\sigma_y^m}{\omega\mu_0}}; \qquad \omega_z = \frac{1-\frac{j\sigma_z}{\omega\varepsilon_0}}{1-\frac{j\sigma_z^m}{\omega\mu_0}} \tag{3.28}$$

and the ratio Z of the electric field magnitude to the magnetic field magnitude is

$$Z = \sqrt{\frac{\mu_0}{\varepsilon_0}} \cdot \frac{1}{G} \tag{3.29}$$

When the above mentioned requirements for σ_i and σ_i^m are met, namely

$$\frac{\sigma_x}{\varepsilon_0} = \frac{\sigma_x^m}{\mu_0}, \qquad \frac{\sigma_y}{\varepsilon_0} = \frac{\sigma_y^m}{\mu_0}, \qquad \frac{\sigma_z}{\varepsilon_0} = \frac{\sigma_z^m}{\mu_0} \tag{3.30}$$

it follows that $\omega_x = \omega_y = \omega_z = G = 1$ for *all* frequencies; the decay of any field component Ψ becomes:

$$\Psi = \Psi_o e^{j\omega\left(t - \frac{x\cos\phi\cos\psi + y\sin\phi\cos\psi + z\sin\psi}{c}\right)} e^{-\frac{\sigma_x\cos\phi\cos\psi}{\varepsilon_0 c}x} e^{-\frac{\sigma_y\sin\phi\cos\psi}{\varepsilon_0 c}y} e^{-\frac{\sigma_z\sin\psi}{\varepsilon_0 c}z} \tag{3.31}$$

and

$$Z = \sqrt{\frac{\mu_0}{\varepsilon_0}} \tag{3.32}$$

Thus the first term in (3.31) shows that the wave in PML travels normally to the electric field with the speed of light in vacuum; next terms show its magnitude exponential decay along the three Cartesian axes. Equation (3.32) shows that the wave impedance of PML medium equals that of vacuum *regardless of angle of propagation*.

Berenger proposed the PML conductivity σ_i to increase gradually with the depth ρ_i in the absorber, $i = x,\ y,\ z$, as the wave travels in the PML medium:

$$\sigma_i(\rho) = \sigma_{\max}\left(\frac{\rho}{\delta_i}\right)^n,\ 0 \le \rho \le \delta_i \tag{3.33}$$

where ρ is the depth in PML; δ_i is the entire thickness of the PML medium in the respective direction (see Fig. 3.1), and *n* is the user defined rate of increase.

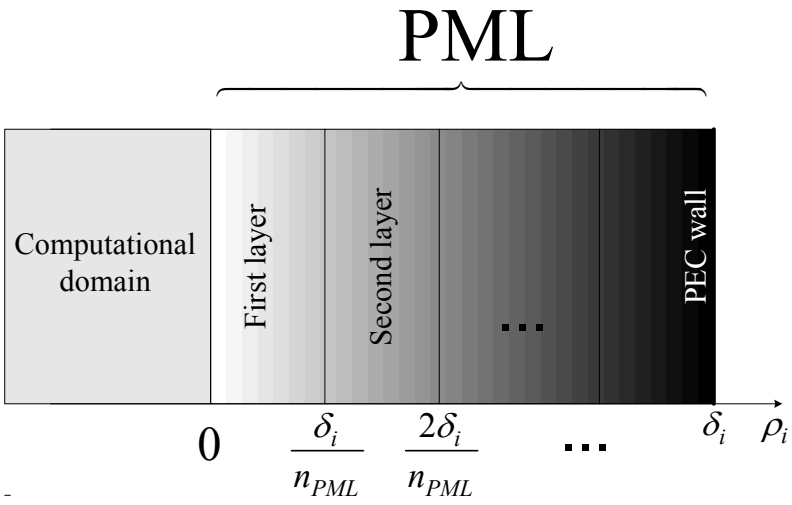

Fig. 3.1. FDTD computational domain endowed with a PML medium showing the depth in PML ρ_i, $i = x,\ y,\ z$ and a PEC wall termination layer.

The reflection factor for an angle of incidence θ is:

$$R(\theta) = e^{-\frac{2\cos\theta}{\varepsilon_0 c}\int_0^{\delta}\sigma(\rho)d\rho} \tag{3.34}$$

and hence for normal incidence:

$$R(0) = e^{-2\sigma_{\max}\delta/(n+1)\varepsilon_0 c} \tag{3.35}$$

This is a user-defined parameter prescribing the level of reflection; for all practical purposes it is enough to choose $R(0) \le 10^{-6}$.

In PML so called "exponential time-advance scheme" can also be used (see derivation in Section 3.3.4), since the field decays much faster than in the rest of the computational domain; thus, for example for the split-field components E_{yx} and E_{yz} the update equations will be:

$$E_{yx}^{n+1}(i,j,k) = e^{-\frac{\sigma_x(i)\Delta t}{\varepsilon_0}} \cdot E_{yx}^{n}(i,j,k) - \frac{\left(e^{-\frac{\sigma_x(i)\Delta t}{\varepsilon_0}} - 1\right)}{\sigma_x(i)} \times \left[\frac{H_{zx}^{n+\frac{1}{2}}(i,j,k) - H_{zx}^{n+\frac{1}{2}}(i-1,j,k)}{\Delta x_H(i)} + \frac{H_{zy}^{n+\frac{1}{2}}(i,j,k) - H_{zy}^{n+\frac{1}{2}}(i-1,j,k)}{\Delta x_H(i)} \right] \tag{3.36}$$

$$E_{yz}^{n+1}(i,j,k) = e^{-\frac{\sigma_z(k)\Delta t}{\varepsilon_0}} \cdot E_{yz}^{n}(i,j,k) - \frac{\left(e^{-\frac{\sigma_z(k)\Delta t}{\varepsilon_0}} - 1\right)}{\sigma_z(k)} \times \left[\frac{H_{xy}^{n+\frac{1}{2}}(i,j,k) - H_{xy}^{n+\frac{1}{2}}(i,j,k-1)}{\Delta z_H(k)} + \frac{H_{xz}^{n+\frac{1}{2}}(i,j,k) - H_{xz}^{n+\frac{1}{2}}(i,j,k-1)}{\Delta z_H(k)} \right] \tag{3.37}$$

Similar expressions hold for all other field components.

3.2 Outline of the modified perfectly matched layer (MPML)

Although PML is matched to evanescent modes, too, it is not possible to increase the attenuation rate of the evanescent modes by adjusting parameters of the matched layers (since that rate is the same as in free space). For evanescent modes with low attenuation rate it is necessary to use thick PMLs, and usually not less than 16 layers are necessary. Alternatively, the PMLs have to be located far from discontinuities and sources. In either case the computer time and memory usage increase significantly.

To overcome this drawback, B. Chen *et al.* (1995) proposed a Modified Perfectly Matched Layer (MPML). The idea is to add *additional degree of freedom* in the algorithm, in order to *adjust the parameters of PML*. In result the authors claim that the thickness of PML is reduced at least by half, and that it can be allocated very close to sources and discontinuities, down to two spatial steps.

To this goal, new coefficients α_x, α_y, α_z, κ_x, κ_y, κ_z are introduced. Together with the previously introduced PML conductivities, they meet the following requirements:

$$\frac{\sigma_x}{\varepsilon_0} = \frac{\sigma_x^m}{\mu_0}, \qquad \frac{\sigma_y}{\varepsilon_0} = \frac{\sigma_y^m}{\mu_0}, \qquad \frac{\sigma_z}{\varepsilon_0} = \frac{\sigma_z^m}{\mu_0}, \tag{3.38}$$

$$\kappa_x = \alpha_x; \qquad \kappa_y = \alpha_y; \qquad \kappa_z = \alpha_z \tag{3.39}$$

The new scheme is called a Modified Perfectly Matched Layer (MPML) for the FDTD solution to Maxwell's equations.

Using the new parameters, the MPML for the FDTD equations become:

$$\mu_0\kappa_y\frac{\partial H_{xy}}{\partial t}+\sigma_y^m H_{xy}=-\frac{\partial\left(E_{zx}+E_{zy}\right)}{\partial y} \tag{3.40}$$

$$\mu_0\kappa_z\frac{\partial H_{xz}}{\partial t}+\sigma_z^m H_{xz}=\frac{\partial\left(E_{yx}+E_{yz}\right)}{\partial z} \tag{3.41}$$

$$\mu_0\kappa_z\frac{\partial H_{yz}}{\partial t}+\sigma_z^m H_{yz}=-\frac{\partial\left(E_{xy}+E_{xz}\right)}{\partial z} \tag{3.42}$$

$$\mu_0\kappa_x\frac{\partial H_{yx}}{\partial t}+\sigma_x^m H_{yx}=\frac{\partial\left(E_{zx}+E_{zy}\right)}{\partial x} \tag{3.43}$$

$$\mu_0\kappa_x\frac{\partial H_{zx}}{\partial t}+\sigma_x^m H_{zx}=-\frac{\partial\left(E_{yx}+E_{yz}\right)}{\partial x} \tag{3.44}$$

$$\mu_0\kappa_y\frac{\partial H_{zy}}{\partial t}+\sigma_y^m H_{zy}=\frac{\partial\left(E_{xy}+E_{xz}\right)}{\partial y} \tag{3.45}$$

$$\varepsilon_0\alpha_y\frac{\partial E_{xy}}{\partial t}+\sigma_y E_{xy}=\frac{\partial\left(H_{zx}+H_{zy}\right)}{\partial y} \tag{3.46}$$

$$\varepsilon_0\alpha_z\frac{\partial E_{xz}}{\partial t}+\sigma_z E_{xz}=-\frac{\partial\left(H_{yx}+H_{yz}\right)}{\partial z} \tag{3.47}$$

$$\varepsilon_0\alpha_z\frac{\partial E_{yz}}{\partial t}+\sigma_z E_{yz}=\frac{\partial\left(H_{xy}+H_{xz}\right)}{\partial z} \tag{3.48}$$

$$\varepsilon_0\alpha_x\frac{\partial E_{yx}}{\partial t}+\sigma_x E_{yx}=-\frac{\partial\left(H_{zx}+H_{zy}\right)}{\partial x} \tag{3.49}$$

$$\varepsilon_0\alpha_x\frac{\partial E_{zx}}{\partial t}+\sigma_x E_{zx}=\frac{\partial\left(H_{yx}+H_{yz}\right)}{\partial x} \tag{3.50}$$

$$\varepsilon_0\alpha_y\frac{\partial E_{zy}}{\partial t}+\sigma_y E_{zy}=-\frac{\partial\left(H_{xy}+H_{xz}\right)}{\partial y} \tag{3.51}$$

In each direction towards the edges of the computational domain, the MPML variables have the following profiles:

1. The proposed by Berenger (1994) PML conductivity:

$$\sigma_i(\rho) = \sigma_{\max}\left(\frac{\rho}{\delta_i}\right)^n = \frac{(n+1)\varepsilon_0 c \cdot \ln\left(\frac{1}{R(0)}\right)}{2\delta_y}\left(\frac{\rho}{\delta_i}\right)^n \tag{3.52}$$

where $0 \le \rho \le \delta_i,\ i = x, y, z$ and

2. The proposed by B. Chen *et al.* (1995) PML loss factor:

$$\alpha_i(\rho) = 1 + \varepsilon_{\max}\left(\frac{\rho}{\delta_i}\right)^n \tag{3.53}$$

Here,

$R(0)$ is the user selected reflection coefficient at normal incidence, usually in the range $R(0) \in \left[10^{-2},\ 10^{-6}\right]$;

δ_i is the thickness of the MPML;

ρ is the depth in MPML, $0 \le \rho \le \delta_i$;

$\varepsilon_{\max}$ is user defined parameter, controlling the rate of the evanescent mode attenuation; originally proposed to be in the range $\varepsilon_{\max} \in [0,10]$;

n is user defined rate of increase; Berenger proposes n = 1,2,3; Chen uses n=2.

3.3 Improved perfectly matched layer (IPML)

In this section, an improvement of the existing MPML proposed by B. Chen *et al.* (1995) will be described. This improvement consists of including a new degree of freedom in the definition of the MPML variable profiles; namely, the PML variables are allowed to grow at different exponent rates. The resulting PML will be referred to as the improved PML (IPML). The conventional method of derivation of the PML parameters, as outlined by D.G. Fang (1998), will be followed.

3.3.1 Derivation of IPML parameters

Following the general approach of Berenger (1994), each of the (six) field components is represented as a sum of two (artificially created) sub-components, as defined in equations (3.1) to (3.6). Those sub-components have no specific physical meaning. They are defined so that each of them depends on only one spatial derivative. Then, following the approach of B. Chen *et al.* (1995), the Maxwell equations in IPML are split (defined) as in equations (3.40) to (3.51).

The latter equations are obtained through direct separation of each of the Maxwell equations into two equations, in such a way, that there remains ***only one*** spatial derivative on the right-hand side. Also, by definition, the second subscript of each field component corresponds to the variable with respect to which the spatial derivative on the right-hand side remains. The (purely artificial) PML loss

variables σ_i and α_i, σ_i^m and κ_i, $i = x,\ y,\ z$, are chosen in such a way that the PML can absorb, to any prescribed extent, any outgoing wave. Their presence gives the opportunity to create "a reflectionless interface between any medium and vacuum, for a plane wave striking the interface at any frequency and at any incidence angle", see details for the 2-D case in the original paper by Berenger (1994).

The procedure to obtain the IPML parameters in the 3-D case is the same as that for MPML parameters. It will be presented here, following the method outlined briefly by D.G. Fang (1998). Combining back the twelve sub-components into the original six field components, the split equations (3.40) to (3.51), for time-harmonic fields, can be rearranged in the following way:

$$j\omega\mu_0 H_x = \frac{1}{\kappa_z - \dfrac{j\sigma_z^m}{\omega\mu_0}}\frac{\partial E_y}{\partial z} - \frac{1}{\kappa_y - \dfrac{j\sigma_y^m}{\omega\mu_0}}\frac{\partial E_z}{\partial y} \tag{3.54}$$

$$j\omega\mu_0 H_y = \frac{1}{\kappa_x - \dfrac{j\sigma_x^m}{\omega\mu_0}}\frac{\partial E_z}{\partial x} - \frac{1}{\kappa_z - \dfrac{j\sigma_z^m}{\omega\mu_0}}\frac{\partial E_x}{\partial z} \tag{3.55}$$

$$j\omega\mu_0 H_z = \frac{1}{\kappa_y - \dfrac{j\sigma_y^m}{\omega\mu_0}}\frac{\partial E_x}{\partial y} - \frac{1}{\kappa_x - \dfrac{j\sigma_x^m}{\omega\mu_0}}\frac{\partial E_y}{\partial x} \tag{3.56}$$

$$-j\omega\varepsilon_0 E_x = \frac{1}{\alpha_z - \dfrac{j\sigma_z}{\omega\varepsilon_0}}\frac{\partial H_y}{\partial z} - \frac{1}{\alpha_y - \dfrac{j\sigma_y}{\omega\varepsilon_0}}\frac{\partial H_z}{\partial y} \tag{3.57}$$

$$-j\omega\varepsilon_0 E_y = \frac{1}{\alpha_x - \frac{j\sigma_x}{\omega\varepsilon_0}}\frac{\partial H_z}{\partial x} - \frac{1}{\alpha_z - \frac{j\sigma_z}{\omega\varepsilon_0}}\frac{\partial H_x}{\partial z} \tag{3.58}$$

$$-j\omega\varepsilon_0 E_z = \frac{1}{\alpha_y - \frac{j\sigma_y}{\omega\varepsilon_0}}\frac{\partial H_x}{\partial y} - \frac{1}{\alpha_x - \frac{j\sigma_x}{\omega\varepsilon_0}}\frac{\partial H_y}{\partial x} \tag{3.59}$$

Using (3.38) and (3.39), the following PML quantities can be defined:

$$\gamma_x = \alpha_x - \frac{j\sigma_x}{\omega\varepsilon_0} = \kappa_x - \frac{j\sigma_x^m}{\omega\mu_0} \tag{3.60}$$

$$\gamma_y = \alpha_y - \frac{j\sigma_y}{\omega\varepsilon_0} = \kappa_y - \frac{j\sigma_y^m}{\omega\mu_0} \tag{3.61}$$

$$\gamma_z = \alpha_z - \frac{j\sigma_z}{\omega\varepsilon_0} = \kappa_z - \frac{j\sigma_z^m}{\omega\mu_0} \tag{3.62}$$

Thus, the equations (3.54) to (3.59) become:

$$j\omega\mu_0 H_x = \frac{-jk_z}{\gamma_z}E_y + \frac{jk_y}{\gamma_y}E_z \tag{3.63}$$

$$j\omega\mu_0 H_y = \frac{-jk_x}{\gamma_x}E_z + \frac{jk_z}{\gamma_z}E_x \tag{3.64}$$

$$j\omega\mu_0 H_z = \frac{-jk_y}{\gamma_y}E_x + \frac{jk_x}{\gamma_x}E_y \tag{3.65}$$

$$-j\omega\varepsilon_0 E_x = \frac{-jk_x}{\gamma_x}H_y + \frac{jk_y}{\gamma_y}H_z \tag{3.66}$$

$$-j\omega\varepsilon_0 E_y = \frac{-jk_x}{\gamma_x}H_z + \frac{jk_z}{\gamma_z}H_x \tag{3.67}$$

$$-j\omega\varepsilon_0 E_z = \frac{-jk_y}{\gamma_y} H_x + \frac{jk_x}{\gamma_x} H_y \tag{3.68}$$

The following two requirements have to be met for reflectionless wave propagation through an interface between two media:

1.The **normal impedance matching** and

2.The **tangential wave numbers matching.**

Consider a TE plane wave propagating in the *z*-direction. At the interface between the PML and the internal computational domain:

In the PML,

$$Z_{TE} = \frac{E_x}{H_y} = -\frac{E_y}{H_x} = \frac{\omega\mu_0}{k_z}\gamma_z \tag{3.69}$$

and by eliminating the field components in (3.63) to (3.68) the following eigen-equation is obtained:

$$\frac{k_x^2}{\gamma_x^2} + \frac{k_y^2}{\gamma_y^2} + \frac{k_z^2}{\gamma_z^2} = k_0^2 = \omega^2\mu_0\varepsilon_0 \tag{3.70}$$

In the air,

$$Z_{TE_0} = \frac{\omega\mu_0}{k_{z0}} \tag{3.71}$$

and the corresponding eigen-equation is:

$$k_{x0}^2 + k_{y0}^2 + k_{z0}^2 = k_0^2 \tag{3.72}$$

The reflection coefficient at the interface is:

$$R_{TE} = \frac{Z_{TE} - Z_{TE_0}}{Z_{TE} + Z_{TE_0}} \tag{3.73}$$

Since the wave propagates in the *z*-direction, by the second requirement,

$$k_x = k_{x0} \tag{3.74}$$

$$k_y = k_{y0} \tag{3.75}$$

Then from (3.69), (3.71) and (3.73), it follows that the reflectionless transmission $R_{TE} = 0$ requires:

$$k_z = k_{z0}\gamma_z = k_{z0}\left(\alpha_z - \frac{j\sigma_z}{\omega\varepsilon_0}\right) = k_{z0}\left(\kappa_z - \frac{j\sigma_z^m}{\omega\mu_0}\right) \tag{3.76}$$

A simple comparison of (3.70) and (3.72), shows that:

$$\gamma_x = \gamma_y = 1 \tag{3.77}$$

Similarly, for TM wave propagating in the *z*-direction towards PML, exactly the same results can be easily obtained.

Therefore, for a wave propagating in the *z*-direction, the following set of IPML parameters are obtained:

$$\alpha_x = \alpha_y = \kappa_x = \kappa_y = 1 \tag{3.78}$$

$$\sigma_x = \sigma_y = \sigma_x^m = \sigma_y^m = 0 \tag{3.79}$$

$$\frac{\sigma_z}{\varepsilon_0} = \frac{\sigma_z^m}{\mu_0}, \qquad \alpha_z = \kappa_z \tag{3.80}$$

$$\Psi = \Psi_0 e^{-j\left(k_{x_0}x + k_{y_0}y + \alpha_z k_{z_0} z\right)} e^{-\frac{k_{z_0}\sigma_z}{\omega\varepsilon_0}z} \tag{3.81}$$

where Ψ is any field component of amplitude Ψ_0.

Similarly, for the *y*-direction wave propagation:

$$\alpha_x = \alpha_z = \kappa_x = \kappa_z = 1 \tag{3.82}$$

$$\sigma_x = \sigma_z = \sigma_x^m = \sigma_z^m = 0 \tag{3.83}$$

$$\frac{\sigma_y}{\varepsilon_0} = \frac{\sigma_y^m}{\mu_0}, \qquad \alpha_y = \kappa_y \tag{3.84}$$

$$\Psi = \Psi_0 e^{-j\left(k_{x0}x + \alpha_y k_{y0} y + k_{z0} z\right)} e^{-\frac{k_{z0}\sigma_y}{\omega\varepsilon_0} y} \tag{3.85}$$

and for the *x*-direction wave propagation:

$$\alpha_y = \alpha_z = \kappa_y = \kappa_z = 1 \tag{3.86}$$

$$\sigma_y = \sigma_z = \sigma_y^m = \sigma_z^m = 0 \tag{3.87}$$

$$\frac{\sigma_x}{\varepsilon_0} = \frac{\sigma_x^m}{\mu_0}, \qquad \alpha_x = \kappa_x \tag{3.88}$$

$$\Psi = \Psi_0 e^{-j\left(\alpha_x k_{x0} x + k_{y0} y + k_{z0} z\right)} e^{-\frac{k_{x0}\sigma_x}{\omega\varepsilon_0} x} \tag{3.89}$$

3.3.2 Modified IPML variable profiles

The profiles of PML parameters are of utmost importance for the performance of the absorber. In resistive media, the rate of attenuation dictated by their physical properties is usually low and the electromagnetic energy dissipation is insufficient. As a result, when the wave reaches the outer boundary of the computational domain, it will be reflected back to into the region of interest, creating spurious reflections that greatly degrade the simulation results. Assigning greater values of the PML parameters can attain greater rates of attenuation but

too large attenuation rate also creates spurious numerical reflections due to the stepwise increments in the values of the PML parameters. Therefore, the PML variables' profiles should be optimized. There have been attempts to optimize the PML variable profiles, but they are to a great extent problem dependent.

There exists one degree of freedom in choosing the PML parameters that to the author's knowledge has never been used until now. Namely, the rate of change of the PML conductivity σ_i and the rate of change of the PML loss factor α_i ***can be different***. This represents a problem-independent approach to the improvement and optimization of the PML performance. The proposed approach is in contrast with the commonly used approaches:

A. Optimization of one PML variable profile as done e.g. by Lazzi *et al.* (1997b,c), Marengo *et al.* (1999), Winton *et al.* (2000), etc.;
B. Optimization in problem-specific environment as done e.g. by Johnson *et al.* (2000), Lazzi *et al.* (1997a), etc.

Thus, the newly proposed IPML conductivity profile $\sigma_i,\ i = x, y, z$ is suggested to be of different (higher) order that that of the IPML loss factor α_i:

$$\sigma_i(\rho) = \sigma_{\max}\left(\frac{\rho}{\delta_i}\right)^{n+\beta};\ \beta \in (0,2] \tag{3.90}$$

while the PML loss factor proposed by B. Chen *et al.* (1995) remains as:

$$\alpha_i(\rho) = 1 + \varepsilon_{\max}\left(\frac{\rho}{\delta_i}\right)^{n} \tag{3.91}$$

In (3.90) the upper limit for the new parameter β is chosen based on the results of an extensive numerical research. From the formula for the theoretical reflection coefficient (3.34), it directly follows that:

$$\sigma_{\max} = \frac{(n+\beta+1)\varepsilon_0 c \cdot \ln\left(\frac{1}{R(0)}\right)}{2\delta_i} \tag{3.92}$$

Here,

$R(0)$ is the user selected reflection coefficient at normal incidence, usually in the range $R(0) \in \left[10^{-2},\ 10^{-6}\right]$ but in high permittivity dielectrics values down to 10^{-12} might be used;

$\delta_i,\ i = x, y, z$ is the thickness of the MPML in the *i*-direction ;

ρ is the depth in MPML, $0 \le \rho \le \delta_i$;

$\varepsilon_{\max}$ is user defined parameter, controlling the rate of the evanescent mode attenuation; now proposed to be in the range $\varepsilon_{\max} \in [0,5]$;

n is user defined rate, now proposed to be in the range $n \in [2,6]$.

Explicitly, the IPML variables are:

At $x_{\min}$ and $x_{\max}$:

$$\sigma_x(\rho_x) = \sigma_{\max}\left(\frac{\rho_x}{\delta_x}\right)^{n+\beta};\ 0 \le \rho_x \le \delta_x \tag{3.93}$$

$$\sigma_x^m(\rho_x) = \sigma_x(\rho_x)\left(\frac{\mu_0}{\varepsilon_0}\right) \tag{3.94}$$

$$\alpha_x(\rho_x) = \kappa_x(\rho_x) = 1 + \varepsilon_{\max}\left(\frac{\rho_x}{\delta_x}\right)^n ;\ 0 \le \rho_x \le \delta_x \tag{3.95}$$

$$\sigma_y = \sigma_y^m = \sigma_z = \sigma_z^m = 0 \tag{3.96}$$

$$\alpha_y = \kappa_y = \alpha_z = \kappa_z = 1 \tag{3.97}$$

At $y_{\min}$ and $y_{\max}$:

$$\sigma_y(\rho_y) = \sigma_{\max}\left(\frac{\rho_y}{\delta_y}\right)^{n+\beta} ;\ 0 \le \rho_y \le \delta_y \tag{3.98}$$

$$\sigma_y^m(\rho_y) = \sigma_y(\rho_y)\left(\frac{\mu_0}{\varepsilon_0}\right) \tag{3.99}$$

$$\alpha_y(\rho_y) = \kappa_y(\rho_y) = 1 + \varepsilon_{\max}\left(\frac{\rho_y}{\delta_y}\right)^n ;\ 0 \le \rho_y \le \delta_y \tag{3.100}$$

$$\sigma_x = \sigma_x^m = \sigma_z = \sigma_z^m = 0 \tag{3.101}$$

$$\alpha_x = \kappa_x = \alpha_z = \kappa_z = 1 \tag{3.102}$$

At $z_{\min}$ and $z_{\max}$:

$$\sigma_z(\rho_z) = \sigma_{\max}\left(\frac{\rho_z}{\delta_z}\right)^{n+\beta} ;\ 0 \le \rho_z \le \delta_z \tag{3.103}$$

$$\sigma_z^m(\rho_z) = \sigma_z(\rho_z) \cdot \left(\frac{\mu_0}{\varepsilon_0}\right) \tag{3.104}$$

$$\alpha_z(\rho_z) = \kappa_z(\rho_z) = 1 + \varepsilon_{\max}\left(\frac{\rho_z}{\delta_z}\right)^n ;\ 0 \le \rho_z \le \delta_z \tag{3.105}$$

$$\sigma_y = \sigma_y^m = \sigma_x = \sigma_x^m = 0 \tag{3.106}$$

$$\alpha_y = \kappa_y = \alpha_x = \kappa_x = 1 \tag{3.107}$$

Where PML overlap, a corresponding combination of the non-zero/non-unity values of the parameters is used. For example, at the edge where, say, $x_{\max}$, $y_{\max}$ are approached, but not $z_{\min}$, $z_{\max}$, one uses:

$$\sigma_x(\rho_x) = \sigma_{\max}\left(\frac{\rho_x}{\delta_x}\right)^{n+\beta} ;\ 0 \le \rho_x \le \delta_x \tag{3.108}$$

$$\sigma_x^m(\rho_x) = \sigma_x(\rho_x)\left(\frac{\mu_0}{\varepsilon_0}\right) \tag{3.109}$$

$$\alpha_x(\rho_x) = \kappa_x(\rho_x) = 1 + \varepsilon_{\max}\left(\frac{\rho_x}{\delta_x}\right)^n ;\ 0 \le \rho_x \le \delta_x \tag{3.110}$$

$$\sigma_y(\rho_y) = \sigma_{\max}\left(\frac{\rho_y}{\delta_y}\right)^{n+\beta} ;\ 0 \le \rho_y \le \delta_y \tag{3.111}$$

$$\sigma_y^m(\rho_y) = \sigma_y(\rho_y)\left(\frac{\mu_0}{\varepsilon_o}\right) \tag{3.112}$$

$$\alpha_y(\rho_y) = \kappa_y(\rho_y) = 1 + \varepsilon_{\max}\left(\frac{\rho_y}{\delta_y}\right)^n ;\ 0 \le \rho_y \le \delta_y \tag{3.113}$$

$$\sigma_z = \sigma_z^m = 0 \tag{3.114}$$

$$\alpha_z = \kappa_z = 1 \tag{3.115}$$

At the corners, where there is an overlap in all three directions, say, $x_{\max}$, $y_{\max}$ and $z_{\min}$, all non-zero/non-unity PML variable values are used:

$$\sigma_x(\rho_x) = \sigma_{\max}\left(\frac{\rho_x}{\delta_x}\right)^{n+\beta};\ 0 \le \rho_x \le \delta_x \tag{3.116}$$

$$\sigma_x^m(\rho_x) = \sigma_x(\rho_x)\left(\frac{\mu_0}{\varepsilon_0}\right) \tag{3.117}$$

$$\alpha_x(\rho_x) = \kappa_x(\rho_x) = 1 + \varepsilon_{\max}\left(\frac{\rho_x}{\delta_x}\right)^{n};\ 0 \le \rho_x \le \delta_x \tag{3.118}$$

$$\sigma_y(\rho_y) = \sigma_{\max}\left(\frac{\rho_y}{\delta}\right)^{n+\beta};\ 0 \le \rho_y \le \delta_y \tag{3.119}$$

$$\sigma_y^m(\rho_y) = \sigma_y(\rho_y)\left(\frac{\mu_0}{\varepsilon_o}\right) \tag{3.120}$$

$$\alpha_y(\rho_y) = \kappa_y(\rho_y) = 1 + \varepsilon_{\max}\left(\frac{\rho_y}{\delta_y}\right)^{n};\ 0 \le \rho_y \le \delta_y \tag{3.121}$$

$$\sigma_z(\rho_z) = \sigma_{\max}\left(\frac{\rho_z}{\delta_z}\right)^{n+\beta};\ 0 \le \rho_z \le \delta_z \tag{3.122}$$

$$\sigma_z^m(\rho_z) = \sigma_z(\rho_z)\left(\frac{\mu_0}{\varepsilon_0}\right) \tag{3.123}$$

$$\alpha_z(\rho_z) = \kappa_z(\rho_z) = 1 + \varepsilon_{\max}\left(\frac{\rho_z}{\delta_z}\right)^{n};\ 0 \le \rho_z \le \delta_z \tag{3.124}$$

3.3.3 Discretization of the split-field components

There follows the discretization for one of the 12 split-field components, E_{xy}, in the IPML. Its corresponding equation (3.46) is first written in the form:

$$\frac{\partial E_{xy}}{\partial t}+\frac{\sigma_y}{\varepsilon_0\alpha_y}E_{xy}=\frac{1}{\varepsilon_0\alpha_y}\frac{\partial\left(H_{zx}+H_{zy}\right)}{\partial y} \tag{3.125}$$

Then (3.125) is discretized using central finite differences, and averaging E_{xy} with respect to time (since its value is not calculated at time $\left(n+1/2\right)$):

$$\begin{aligned}&\frac{E_{xy}^{n+1}(i,j,k)-E_{xy}^{n}(i,j,k)}{\Delta t}+\frac{\sigma_y(j)}{\varepsilon_0\alpha_y(j)}\frac{E_{xy}^{n+1}(i,j,k)+E_{xy}^{n}(i,j,k)}{2}\\&=\frac{1}{\varepsilon_0\alpha_y(j)}\left[\frac{H_{zx}^{n+\frac{1}{2}}(i,j,k)-H_{zx}^{n+\frac{1}{2}}(i,j-1,k)}{\Delta y_H(j)}\right.\\&\left.+\frac{H_{zy}^{n+\frac{1}{2}}(i,j,k)-H_{zy}^{n+\frac{1}{2}}(i,j-1,k)}{\Delta y_H(j)}\right]\end{aligned} \tag{3.126}$$

Therefore the update equation for E_{xy} is:

$$\begin{aligned}E_{xy}^{n+1}(i,j,k)=&\frac{1-\frac{\sigma_y(j)\Delta t}{2\varepsilon_0\alpha_y(j)}}{1+\frac{\sigma_y(j)\Delta t}{2\varepsilon_0\alpha_y(j)}}E_{xy}^{n}(i,j,k)+\frac{1}{1+\frac{\sigma_y(j)\Delta t}{2\varepsilon_0\alpha_y(j)}}\cdot\frac{\Delta t}{\varepsilon_0\alpha_y(j)}\times\\&\left[\frac{H_{zx}^{n+\frac{1}{2}}(i,j,k)-H_{zx}^{n+\frac{1}{2}}(i,j-1,k)}{\Delta y_H(j)}\right.\\&\left.+\frac{H_{zy}^{n+\frac{1}{2}}(i,j,k)-H_{zy}^{n+\frac{1}{2}}(i,j-1,k)}{\Delta y_H(j)}\right]\end{aligned} \tag{3.127}$$

3.3.4 Exponential time-stepping

The above standard finite-differencing scheme can be used directly. Its alternative, the so-called exponential time stepping, will be presented next. The reason for using the exponential time stepping is in the exponential decay of waves in the PML medium. For the case of such high-loss media as the PML medium is, the alternative method proposed by Holland (1994) will be presented (because of its elegancy; the same results can be obtained by some simple manipulations of the coefficients in (3.127)). Note that the coefficient before the field component to be updated is a second order approximation of the corresponding (exponential) coefficient in the solution of equation (3.125) if it is regarded as a first order ODE with respect to time.

The first order ODE will have a homogeneous and a particular solution.

The homogeneous solution is considered to be the result of excitations over previous time steps (excluding the right-hand side curl $\vec{H}$ contribution of the present time step):

$$E_{xy(\text{hom})} = Ce^{-\frac{\sigma_y t}{\varepsilon_0 \alpha_y}} \tag{3.128}$$

The decay for one time step of (3.128) is:

$$E^{n+1}_{xy(\text{hom})} = e^{-\frac{\sigma_y \Delta t}{\varepsilon_0 \alpha_y}} E^{n}_{xy(\text{hom})} \tag{3.129}$$

The particular solution is considered to be the result of only the right-hand side curl $\vec{H}$ contribution during the present time step and the time t' is measured from the beginning of the time step, so that for $0 \le t' \le \Delta t$:

$$\begin{aligned} E_{xy(part)}(t') &= \left[\frac{1}{\varepsilon_0 \alpha_y} \frac{\partial \left(H_{zx} + H_{zy} \right)}{\partial y} \int e^{\int \frac{\sigma_y}{\varepsilon_0 \alpha_y} dt'} dt' + C \right] e^{-\int \frac{\sigma_y}{\varepsilon_0 \alpha_y} dt'} \\ &= \frac{1}{\sigma_y} \frac{\partial \left(H_{zx} + H_{zy} \right)}{\partial y} + C e^{-\int \frac{\sigma_y}{\varepsilon_0 \alpha_y} dt'} \end{aligned} \tag{3.130}$$

The constant C can be obtained from (3.130) evaluated at the moment $t' = 0$:

$$\begin{aligned} E_{xy(part)}\big|_{t'=0} = 0 &= \frac{1}{\sigma_y} \frac{\partial \left(H_{zx} + H_{zy} \right)}{\partial y} + C \;\Rightarrow C = -\frac{1}{\sigma_y} \frac{\partial \left(H_{zx} + H_{zy} \right)}{\partial y} \\ E_{xy(part)}(t') &= \frac{1}{\sigma_y} \frac{\partial \left(H_{zx} + H_{zy} \right)}{\partial y} \left(1 - e^{-\int \frac{\sigma_y}{\varepsilon_0 \alpha_y} dt'} \right) \end{aligned} \tag{3.131}$$

By the end of the time step, $t' = \Delta t$,

$$E_{xy(part)}\big|_{(t'=\Delta t)} = -\frac{1}{\sigma_y} \frac{\partial \left(H_{zx} + H_{zy} \right)}{\partial y} \left(e^{-\frac{\sigma_y \Delta t}{\varepsilon_0 \alpha_y}} - 1 \right) \tag{3.132}$$

Finally, the general solution at the end of the $(n+1)^{st}$ time step is obtained as a sum of the homogeneous solution (3.129) and the particular solution (3.132), where the spatial derivative is taken as an average value at the centre of the time step $\left(n + \frac{1}{2} \right)$:

$$E_{xy}^{n+1}(i,j,k) = e^{-\frac{\sigma_y(j)\Delta t}{\varepsilon_0 \alpha_y}} \cdot E_{xy}^{n}(i,j,k) - \frac{e^{-\frac{\sigma_y(j)\Delta t}{\varepsilon_0 \alpha_y}} - 1}{\sigma_y(j)} \cdot \left[\frac{H_{zx}^{n+\frac{1}{2}}(i,j,k) - H_{zx}^{n+\frac{1}{2}}(i,j-1,k)}{\Delta y_H(j)} + \frac{H_{zy}^{n+\frac{1}{2}}(i,j,k) - H_{zy}^{n+\frac{1}{2}}(i,j-1,k)}{\Delta y_H(j)} \right] \tag{3.133}$$

For completeness, the discretized exponential time-advance scheme for all split-field components in the IPML is presented below in the case of 3-D IPML for the FDTD solution to Maxwell's equations:

$$H_{xy}^{n+\frac{1}{2}}(i,j,k) = e^{-\frac{\sigma_y^m(j)\Delta t}{\mu_0 \kappa_y}} \cdot H_{xy}^{n-\frac{1}{2}}(i,j,k) - \frac{1 - e^{-\frac{\sigma_y^m(j)\Delta t}{\mu_0 \kappa_y}}}{\sigma_y^m(j)} \cdot \left[\frac{E_{zx}^{n}(i,j+1,k) - E_{zx}^{n}(i,j,k)}{\Delta y(j)} + \frac{E_{zy}^{n}(i,j+1,k) - E_{zy}^{n}(i,j,k)}{\Delta y(j)} \right] \tag{3.134}$$

$$H_{xz}^{n+\frac{1}{2}}(i,j,k) = e^{-\frac{\sigma_z^m(k)\Delta t}{\mu_0 \kappa_z}} \cdot H_{xz}^{n-\frac{1}{2}}(i,j,k) + \frac{1 - e^{-\frac{\sigma_z^m(k)\Delta t}{\mu_0 \kappa_z}}}{\sigma_z^m(k)} \cdot \left[\frac{E_{yx}^{n}(i,j,k+1) - E_{yx}^{n}(i,j,k)}{\Delta z(k)} + \frac{E_{yz}^{n}(i,j,k+1) - E_{yz}^{n}(i,j,k)}{\Delta z(k)} \right] \tag{3.135}$$

$$H_{yz}^{n+\frac{1}{2}}(i,j,k) = e^{-\frac{\sigma_z^m(k)\Delta t}{\mu_0 \kappa_z}} \cdot H_{yz}^{n-\frac{1}{2}}(i,j,k) - \frac{1 - e^{-\frac{\sigma_z^m(k)\Delta t}{\mu_0 \kappa_z}}}{\sigma_z^m(k)} \cdot \left[\frac{E_{xy}^{n}(i,j,k+1) - E_{xy}^{n}(i,j,k)}{\Delta z(k)} + \frac{E_{xz}^{n}(i,j,k+1) - E_{xz}^{n}(i,j,k)}{\Delta z(k)} \right] \tag{3.136}$$

$$H_{yx}^{n+\frac{1}{2}}(i,j,k)=e^{-\frac{\sigma_x^m(i)\Delta t}{\mu_0\kappa_x}}\cdot H_{yx}^{n-\frac{1}{2}}(i,j,k)+\frac{1-e^{-\frac{\sigma_x^m(i)\Delta t}{\mu_0\kappa_x}}}{\sigma_x^m(i)}\cdot \left[\frac{E_{zx}^n(i+1,j,k)-E_{zx}^n(i,j,k)}{\Delta x(i)}+\frac{E_{zy}^n(i+1,j,k)-E_{zy}^n(i,j,k)}{\Delta x(i)}\right] \tag{3.137}$$

$$H_{zx}^{n+\frac{1}{2}}(i,j,k)=e^{-\frac{\sigma_x^m(i)\Delta t}{\mu_0\kappa_x}}\cdot H_{zx}^{n-\frac{1}{2}}(i,j,k)-\frac{1-e^{-\frac{\sigma_x^m(i)\Delta t}{\mu_0\kappa_x}}}{\sigma_x^m(i)}\cdot \left[\frac{E_{yx}^n(i+1,j,k)-E_{yx}^n(i,j,k)}{\Delta x(i)}+\frac{E_{yz}^n(i+1,j,k)-E_{yz}^n(i,j,k)}{\Delta x(i)}\right] \tag{3.138}$$

$$H_{zy}^{n+\frac{1}{2}}(i,j,k)=e^{-\frac{\sigma_y^m(j)\Delta t}{\mu_0\kappa_y}}\cdot H_{zy}^{n-\frac{1}{2}}(i,j,k)+\frac{1-e^{-\frac{\sigma_y^m(j)\Delta t}{\mu_0\kappa_y}}}{\sigma_y^m(j)}\cdot \left[\frac{E_{xy}^n(i,j+1,k)-E_{xy}^n(i,j,k)}{\Delta y(j)}+\frac{E_{xz}^n(i,j+1,k)-E_{xz}^n(i,j,k)}{\Delta y(j)}\right] \tag{3.139}$$

$$E_{xy}^{n+1}(i,j,k)=e^{-\frac{\sigma_y(j)\Delta t}{\varepsilon_0\alpha_y}}\cdot E_{xy}^n(i,j,k)+\frac{1-e^{-\frac{\sigma_y(j)\Delta t}{\varepsilon_0\alpha_y}}}{\sigma_y(j)}\cdot \left[\frac{H_{zx}^{n+\frac{1}{2}}(i,j,k)-H_{zx}^{n+\frac{1}{2}}(i,j-1,k)}{\Delta y_H(j)}+\frac{H_{zy}^{n+\frac{1}{2}}(i,j,k)-H_{zy}^{n+\frac{1}{2}}(i,j-1,k)}{\Delta y_H(j)}\right] \tag{3.140}$$

$$E_{xz}^{n+1}(i,j,k)=e^{-\frac{\sigma_z(k)\Delta t}{\varepsilon_0\alpha_z}}\cdot E_{xz}^{n}(i,j,k)-\frac{1-e^{-\frac{\sigma_z(k)\Delta t}{\varepsilon_0\alpha_z}}}{\sigma_z(k)}\cdot \left[\frac{H_{yx}^{n+\frac{1}{2}}(i,j,k)-H_{yx}^{n-\frac{1}{2}}(i,j,k-1)}{\Delta z_H(k)}+\frac{H_{yz}^{n+\frac{1}{2}}(i,j,k)-H_{yz}^{n-\frac{1}{2}}(i,j,k-1)}{\Delta z_H(k)}\right] \tag{3.141}$$

$$E_{yz}^{n+1}(i,j,k)=e^{-\frac{\sigma_z(k)\Delta t}{\varepsilon_0\alpha_z}}\cdot E_{yz}^{n}(i,j,k)+\frac{1-e^{-\frac{\sigma_z(k)\Delta t}{\varepsilon_0\alpha_z}}}{\sigma_z(k)}\cdot \left[\frac{H_{xy}^{n+\frac{1}{2}}(i,j,k)-H_{xy}^{n+\frac{1}{2}}(i,j,k-1)}{\Delta z_H(k)}+\frac{H_{xz}^{n+\frac{1}{2}}(i,j,k)-H_{xz}^{n+\frac{1}{2}}(i,j,k-1)}{\Delta z_H(k)}\right] \tag{3.142}$$

$$E_{yx}^{n+1}(i,j,k)=e^{-\frac{\sigma_x(i)\Delta t}{\varepsilon_0\alpha_x}}\cdot E_{yx}^{n-\frac{1}{2}}(i,j,k)-\frac{1-e^{-\frac{\sigma_x(i)\Delta t}{\varepsilon_0\alpha_x}}}{\sigma_x(i)}\cdot \left[\frac{H_{zx}^{n+\frac{1}{2}}(i,j,k)-H_{zx}^{n-\frac{1}{2}}(i-1,j,k)}{\Delta x_H(i)}+\frac{H_{zy}^{n+\frac{1}{2}}(i,j,k)-H_{zy}^{n-\frac{1}{2}}(i-1,j,k)}{\Delta x_H(i)}\right] \tag{3.143}$$

$$E_{zx}^{n+1}(i,j,k)=e^{-\frac{\sigma_x(i)\Delta t}{\varepsilon_0\alpha_x}}\cdot E_{zx}^{n}(i,j,k)+\frac{1-e^{-\frac{\sigma_x(i)\Delta t}{\varepsilon_0\alpha_x}}}{\sigma_x(i)}\cdot \left[\frac{H_{yx}^{n+\frac{1}{2}}(i,j,k)-H_{yx}^{n+\frac{1}{2}}(i-1,j,k)}{\Delta x_H(i)}+\frac{H_{yz}^{n+\frac{1}{2}}(i,j,k)-H_{yz}^{n+\frac{1}{2}}(i-1,j,k)}{\Delta x_H(i)}\right] \tag{3.144}$$

$$E_{zy}^{n+1}(i,j,k) = e^{-\frac{\sigma_y(j)\Delta t}{\varepsilon_0 \alpha_y}} \cdot E_{zy}^{n}(i,j,k) - \frac{1-e^{-\frac{\sigma_y(j)\Delta t}{\varepsilon_0 \alpha_y}}}{\sigma_y(j)} \cdot \left[\frac{H_{xy}^{n+\frac{1}{2}}(i,j,k) - H_{xy}^{n+\frac{1}{2}}(i,j-1,k)}{\Delta y_H(j)} + \frac{H_{xz}^{n+\frac{1}{2}}(i,j,k) - H_{xz}^{n+\frac{1}{2}}(i,j-1,k)}{\Delta y_H(j)} \right] \quad (3.145)$$

3.4 Outline of alternative approaches to define a PML medium

As mentioned previously, at the interface between a PML and the internal computational domain, the tangential wave numbers have to be continuous and the normal wave number should be complex in order to ensure decay in the normal direction. Therefore, a PML can always be regarded as an anisotropic medium. Numerical anisotropy can be implemented in two ways, see D.G. Fang (1998):

1. Maxwell's equations can be modified introducing stretched coordinates (i.e., using a complexification of the spatial coordinates) as proposed by Chew and Weedon (1994);

2. Anisotropic PML parameters can be directly introduced while keeping Maxwell's equations in their original form, as proposed by Sacks *et al.* (1995).

Recently Knockaert and De Zutter (2000) showed that these two approaches are mathematically equivalent.

3.4.1 Outline of the stretched coordinate approach

As in Section 3.3.1, the modified Maxwell's equations are written in the unsplit form (3.63) to (3.68). Consider TE_z or TM_z wave and match as before the normal wave impedance and the tangential phase velocities at both sides of the interface between the internal computational domain and the PML. The same requirements for the PML hold, as shown in Section 3.3.1, namely:

$$\gamma_x = \gamma_y = 1$$

and as a result the equations (3.63) to (3.68) are reduced to the form:

$$\omega\mu_0 H_x = -\frac{k_z}{\gamma_z} E_y + k_y E_z \tag{3.146}$$

$$\omega\mu_0 H_y = -k_x E_z + \frac{k_z}{\gamma_z} E_x \tag{3.147}$$

$$\omega\mu_0 H_z = -k_y E_x + k_x E_y \tag{3.148}$$

$$-\omega\varepsilon_0 E_x = -\frac{k_z}{\gamma_z} H_y + k_y H_z \tag{3.149}$$

$$-\omega\varepsilon_0 E_y = -k_x H_z + \frac{k_z}{\gamma_z} H_x \tag{3.150}$$

$$-\omega\varepsilon_0 E_z = -k_y H_x + k_x H_y \tag{3.151}$$

A comparison with the regular Maxwell's equations shows that equations (3.146) to (3.151) can be regarded as a result of introducing one new stretched coordinate, $z' = z\gamma_z$.

In the same way the complex coordinate stretching can be introduced for all directions; the rest of the analysis can be done in the same fashion as the one presented in Section 3.3.1.

Specifically, for the general case of a matched medium in the time domain, Chew and Weedon (1994) show that the curl operator is actually modified to the form:

$$\nabla_s = \hat{x}\frac{1}{s_x}\frac{\partial}{\partial x} + \hat{y}\frac{1}{s_y}\frac{\partial}{\partial y} + \hat{z}\frac{1}{s_z}\frac{\partial}{\partial z} \tag{3.152}$$

where $s_x,\ s_y,\ s_z$ are the coordinate- stretching variables that stretch the coordinates $x,\ y,\ z$. They also show that the medium becomes lossy when those stretching variables are complex:

$$s_x = 1 + \frac{j\sigma_x}{\omega\varepsilon};\ s_y = 1 + \frac{j\sigma_y}{\omega\varepsilon};\ s_z = 1 + \frac{j\sigma_z}{\omega\varepsilon} \tag{3.153}$$

The attenuation in each direction is controlled naturally through the PML variables $\sigma_x,\ \sigma_y,\ \sigma_z$.

3.4.2 Outline of the anisotropic PML approach

The PML can be introduced also by introducing an anisotropic medium, see Sacks *et al.* (1995), defined by:

$$[\mu] = \mu_0[\gamma] = \mu_0\begin{bmatrix} a & 0 & 0 \\ 0 & b & 0 \\ 0 & 0 & c \end{bmatrix};\ [\varepsilon] = \varepsilon_0[\gamma] = \varepsilon_0\begin{bmatrix} a & 0 & 0 \\ 0 & b & 0 \\ 0 & 0 & c \end{bmatrix} \tag{3.154}$$

In a medium defined by (3.154), Maxwell's equations are:

$$\begin{aligned} j\omega\mu_0 aH_x &= jk_y E_z - jk_z E_y \\ j\omega\mu_0 bH_y &= jk_z E_x - jk_x E_z \\ j\omega\mu_0 cH_z &= jk_x E_y - jk_y E_x \\ j\omega\varepsilon_0 aE_x &= -jk_y H_z + jk_z H_y \\ j\omega\mu_0 bE_y &= -jk_z H_x + jk_x H_z \\ j\omega\mu_0 cE_z &= -jk_x H_y + jk_y H_x \end{aligned} \tag{3.155}$$

Since Maxwell's equations remain unchanged, this type of PML is sometimes referred to as Maxwellian PML-like medium.

Consider a TE_z wave, i.e. $E_z = 0$, and follow the same derivation procedure as in Section 3.3.1: The normal wave impedance is:

$$Z_{TE} = \frac{E_x}{H_y} = \frac{\omega\mu_0}{k_z} b \tag{3.156}$$

Matching (3.156) to the free-space wave impedance (by the first requirement for a PML) leads to:

$$k_z = k_{z_0} b \tag{3.157}$$

By eliminating the field components in (3.155), the following eigen-equation is obtained:

$$\frac{k_x^2}{bc} + \frac{k_y^2}{ac} + \frac{k_z^2}{ab} = k_0^2 \tag{3.158}$$

The tangential wavenumbers are continuous across the interface (by the second requirement for a PML):

$$k_x = k_{x_0};\ k_y = k_{y_0} \tag{3.159}$$

and the eigen-equations in the free space yields:

$$k_{x_0}^2 + k_{y_0}^2 + k_{z_0}^2 = k_0^2 \tag{3.160}$$

Then, from (3.157) to (3.160) it follows that

$$\frac{k_{x_0}^2}{bc} + \frac{k_{y_0}^2}{ac} + k_{z_0}^2 \frac{b}{a} = k_0^2 \tag{3.161}$$

and

$$a = b = \frac{1}{c} \tag{3.162}$$

Thus the PML is defined by the complex number

$$a = b = \alpha - j\beta, \quad where \quad \alpha > 0, \ \beta > 0 \tag{3.163}$$

$$-jk_z = -jk_{z_0} b = -ik_{z_0}\alpha - k_{z_0}\beta \tag{3.164}$$

Here α determines the wavelength in the anisotropic absorber and β determines the rate of decay of the propagating wave.

3.4.3 Outline of the generalized perfectly matched layer (GPML)

J. Fang and Z. Wu (1995) follow closely the stretched coordinate approach proposed by Chew and Weedon (1994) in the derivation of their generalized PML (GPML). They modify of the form in which the stretched variables are defined:

$$s_i(i) = s_0(i)\left[1 - j\frac{\sigma_i(i)}{\omega\varepsilon}\right]; \ i = x, y, z \tag{3.165}$$

This form is equivalent to the one proposed previously for MPML. Naturally, PML constructed in the above way, can absorb both propagating and evanescent waves as long as $s_0(i) > 1$. J. Fang and Z. Wu (1995) point out that by choosing $s_0(i) > 1$, the attenuation of evanescent waves is accelerated, which is

consistent with the results presented earlier by B. Chen *et al.* (1994) in their MPML derivation.

J. Fang and Z. Wu (1995) also propose a different PML conductivity profile:

$$\sigma_i(\rho_i) = \sin^2\left(\frac{\pi\rho_i}{2\delta}\right) \tag{3.166}$$

Their loss factor is the same as the one proposed by B. Chen *et al.* (1995):

$$s_{0_i}(\rho_i) = 1 + s_m\left(\frac{\rho_i}{\delta}\right)^n \tag{3.167}$$

for $i = x, y, z$. J. Fang and Z. Wu (1995) generally work only with order $n = 2$.

In (3.167), s_m is a user-defined parameter, analogous to the parameter $\varepsilon_{\max}$ as defined in the MPML; δ is the thickness of PML; and ρ_i is the depth in PML.

Chapter 4

The Wave Equation in the Time Domain

4.1 Introduction

It is well known that the electromagnetic (EM) field can be described not only in terms of the field vectors but also in terms of scalar and vector potentials. Harrington (1961) stated for time-harmonic fields, "an arbitrary field in a homogeneous source-free region can be expresses as a sum of a TM and a TE field". That statement holds also for the general transient case. That is, the EM field can be represented in terms of the magnetic vector potential $\vec{A}$ or the electric vector potential $\vec{F}$, or both. Moreover, it is easy to show that any field can be expressed by only two scalar wave functions, which are the magnitudes of the vector potentials in a specified direction of an arbitrary (constant) unit vector $\hat{c}$. The TM (with respect to the distinguished direction) field is described by the magnetic vector potential (VP), $\vec{A} = \hat{c}A$; and the TE field is the one of the electric VP $\vec{F} = \hat{c}F$. Both potentials are solutions to the wave equation in the time domain (or the Helmholtz' equation in the frequency domain). Both vectors are collinear and parallel to the fixed direction $\hat{c}$. Their magnitudes will be referred to as wave

potentials (WPs), for details see Georgieva (2001). The choice of the wave potentials is not uniquely defined and therefore can be made (and changed) in such a way that it would fit best the geometry of the structure and its excitation.

4.2 Derivation of the wave equation in the time domain (WETD)

For the case of structures where there are no magnetic materials involved, but dielectric materials and conducting surfaces might be present, it is appropriate to express the fields in terms of the magnetic vector potential $\vec{A}$ only. There are two major reasons for such choice:

1. The structure can be excited by J_i currents, which would produce the A_i component ($i = x,\ y,\ z$);

2. With conducting patches and surfaces in the structure, the A_i component is expected to produce surface currents when the appropriate boundary conditions (BCs) for $\vec{A}$ are introduced. According to these BCs the surface currents in turn produce the other two components of $\vec{A}$.

Maxwell's curl equations for a general lossy medium are:

$$\varepsilon \frac{\partial \vec{E}^A}{\partial t} = \nabla \times \vec{H}^A - \sigma \vec{E}^A - \vec{J}^i \tag{4.1}$$

$$\mu \frac{\partial \vec{H}^A}{\partial t} = -\nabla \times \vec{E}^A - \sigma_m \vec{H}^A \tag{4.2}$$

The superscript "A" is included to underline the fact that the field vectors will be expressed in terms of the magnetic vector potential $\vec{A}$ only. In general, the magnetic field vector can be expressed in terms of the vector magnetic potential as follows:

$$\vec{H}^A = \frac{1}{\mu}\nabla \times \vec{A} \tag{4.3}$$

From the above definition it directly follows that:

$$\vec{B}^A = \mu \vec{H}^A = \nabla \times \vec{A} \tag{4.4}$$

and consequently, it is divergence-free,

$$\nabla \cdot \vec{B} = 0 \tag{4.5}$$

Therefore, the field has only electric sources (electric currents $\vec{J}^i$ and electric charges ρ_e).

The substitution of equation (4.3) into Maxwell's equations (4.1) and (4.2)leads to:

$$\varepsilon \frac{\partial \vec{E}^A}{\partial t} = \nabla \times \left(\frac{1}{\mu}\nabla \times \vec{A} \right) - \sigma \vec{E}^A - \vec{J}^i \tag{4.6}$$

and

$$\nabla \times \frac{\partial \vec{A}}{\partial t} = -\nabla \times \vec{E}^A - \frac{\sigma_m}{\mu}\nabla \times \vec{A} \tag{4.7}$$

If no magnetic inhomogeneities are present, $\nabla(\sigma_m / \mu) = 0$, then (4.7) can be written in the form:

$$-\nabla \times \vec{E}^A = \nabla \times \left(\frac{\partial \vec{A}}{\partial t} + \frac{\sigma_m}{\mu}\vec{A} \right) \tag{4.8}$$

and the definitive equation for the electric field vector becomes:

$$\vec{E}^{A} = -\frac{\partial \vec{A}}{\partial t} - \frac{\sigma_m}{\mu}\vec{A} - \nabla\Phi \tag{4.9}$$

Substitute (4.9) into (4.6). Then, if no magnetic and dielectric inhomogeneities are present, i.e.

$$\nabla\left(\frac{1}{\mu}\right) = 0;\ \nabla\left(\frac{1}{\varepsilon\mu}\right) = 0;\ \nabla\left(\frac{\sigma}{\varepsilon}\right) = 0 \tag{4.10}$$

the following equations is obtained:

$$\begin{aligned} &\frac{\partial^2 \vec{A}}{\partial t^2} + \left(\frac{\sigma}{\varepsilon} + \frac{\sigma_m}{\mu}\right)\frac{\partial \vec{A}}{\partial t} - \frac{1}{\mu\varepsilon}\nabla^2\vec{A} + \frac{\sigma\sigma_m}{\varepsilon\mu}\vec{A} + \\ &+\nabla\left(\frac{1}{\mu\varepsilon}\nabla\cdot\vec{A} + \frac{\partial\Phi}{\partial t} + \frac{\sigma}{\varepsilon}\Phi\right) = \frac{\vec{J}^{i}}{\varepsilon} \end{aligned} \tag{4.11}$$

By imposing Lorenz' gauge:

$$\mu\varepsilon\frac{\partial\Phi}{\partial t} + \mu\sigma\Phi = -\nabla\cdot\vec{A} \tag{4.12}$$

the equation (4.11) becomes:

$$\frac{1}{\mu\varepsilon}\nabla^2\vec{A} - \frac{\partial^2\vec{A}}{\partial t^2} - \left(\frac{\sigma}{\varepsilon} + \frac{\sigma_m}{\mu}\right)\frac{\partial\vec{A}}{\partial t} - \frac{\sigma\sigma_m}{\varepsilon\mu}\vec{A} = -\frac{\vec{J}^{i}}{\varepsilon} \tag{4.13}$$

which is the wave equation in the time domain (WETD) for general lossy homogeneous media.

In the case of general lossy inhomogeneous media, since in reality no d.c. magnetic losses exist, i.e. $\sigma_m = 0$, the equation (4.9) may be reduced to

$$\vec{E}^{A} = -\frac{\partial\vec{A}}{\partial t} - \nabla\Phi \tag{4.14}$$

and it is substituted into (4.6), followed by imposing the Lorenz' gauge (4.12), so that the WETD becomes:

$$\frac{\partial^2 \vec{A}}{\partial t^2}+\frac{\sigma}{\varepsilon}\frac{\partial \vec{A}}{\partial t}-\frac{1}{\mu\varepsilon}\nabla^2\vec{A}-\nabla\left(\frac{1}{\mu\varepsilon}\right)\nabla\cdot\vec{A}+\frac{1}{\varepsilon}\nabla\left(\frac{1}{\mu}\right)\times\nabla\times\vec{A}-\Phi\nabla\left(\frac{\sigma}{\varepsilon}\right)=\frac{\vec{J}^i}{\varepsilon} \quad (4.15)$$

In a similar fashion, the field vectors can be expressed in terms of the electric vector potential $\vec{F}$ only:

$$\begin{cases}\varepsilon\dfrac{\partial \vec{E}^F}{\partial t}=\nabla\times\vec{H}^F-\sigma\vec{E}^F\\ \mu\dfrac{\partial \vec{H}^F}{\partial t}=-\nabla\times\vec{E}^F-\sigma_m\vec{H}^F-\vec{J}_m^i\end{cases} \quad (4.16)$$

Define

$$\vec{E}^F=-\frac{1}{\varepsilon}\nabla\times\vec{F} \quad (4.17)$$

and therefore

$$\vec{D}^F=\varepsilon\vec{E}=-\nabla\times\vec{F}\ \Rightarrow\ \nabla\cdot\vec{D}=0 \quad (4.18)$$

So the EM field due to the electric vector potential $\vec{F}$ has a divergence-free $\vec{D}^F$ vector and therefore it can have only magnetic type sources (magnetic currents $\vec{J}_m^i$ and magnetic charges ρ_m).

Substitute (4.17) in Maxwell's equations (4.16) to obtain:

$$\begin{cases}\nabla\times\dfrac{\partial \vec{F}}{\partial t}=-\nabla\times\vec{H}^F-\dfrac{\sigma}{\varepsilon}\nabla\times\vec{F}\\ \mu\dfrac{\partial \vec{H}^F}{\partial t}=\nabla\times\left(\dfrac{1}{\varepsilon}\nabla\times\vec{F}\right)-\sigma_m\vec{H}^F-\vec{J}_m^i\end{cases} \quad (4.19)$$

In the case of no dielectric inhomogeneities, $\nabla(\sigma/\varepsilon)=0$ and $\nabla(1/\varepsilon)=0$, after imposing Lorenz' gauge

$$\mu\varepsilon\frac{\partial\Psi}{\partial t}+\varepsilon\sigma_m\Psi=-\nabla\cdot\vec{F} \tag{4.20}$$

the WETD in terms of the electric vector potential is obtained for general lossy homogeneous media:

$$\frac{1}{\mu\varepsilon}\nabla^2\vec{F}-\frac{\partial^2\vec{F}}{\partial t^2}-\left(\frac{\sigma}{\varepsilon}+\frac{\sigma_m}{\mu}\right)\frac{\partial\vec{F}}{\partial t}-\frac{\sigma\sigma_m}{\varepsilon\mu}\vec{F}=-\frac{\vec{J}_m^{\,i}}{\mu} \tag{4.21}$$

where the magnetic field vector has been expressed as:

$$\vec{H}^F=-\partial_t\vec{F}-\frac{\sigma}{\varepsilon}\vec{F}-\nabla\Psi \tag{4.22}$$

In the general case of lossy inhomogeneous media, two separate cases exist:

A. When the gradient $\nabla(\sigma/\varepsilon)$ is zero or it is parallel to $\vec{F}$, then the expression for the magnetic field (4.22) holds. Recalling that in reality no d.c. magnetic losses exist, i.e. $\sigma_m=0$, the Lorenz' gauge is simplified to the form:

$$\frac{\partial\Psi}{\partial t}=-\frac{1}{\mu\varepsilon}\nabla\cdot\vec{F} \tag{4.23}$$

Using (4.22), (4.23) and also the expression for the electric field (4.17), the following WE is obtained:

$$\frac{\partial^2\vec{F}}{\partial t^2}+\frac{\sigma}{\varepsilon}\frac{\partial\vec{F}}{\partial t}-\frac{1}{\mu\varepsilon}\nabla^2\vec{F}-\nabla\left(\frac{1}{\mu\varepsilon}\right)\nabla\cdot\vec{F}+\frac{1}{\mu}\nabla\left(\frac{1}{\varepsilon}\right)\times\nabla\times\vec{F}=\frac{\vec{J}_m^{\,i}}{\mu} \tag{4.24}$$

B. In points if inhomogeneity, when the gradient $\nabla(\sigma/\varepsilon)$ is not zero and it is not parallel to $\vec{F}$, the magnetic field vector cannot be expressed explicitly

from the first equation in (4.19). In that case, however, the first equation in (4.19) can be written in the form:

$$\nabla \times \vec{H}^F = -\nabla \times \left[\frac{\partial \vec{F}}{\partial t} - \nabla \Psi \right] - \frac{\sigma}{\varepsilon} \nabla \times \vec{F}$$

Then a time derivative of that first equation and a curl of the second equation in (4.19) can be taken:

$$\left| \begin{array}{l} \nabla \times \dfrac{\partial \vec{H}^F}{\partial t} = -\nabla \times \left[\dfrac{\partial^2 \vec{F}}{\partial t^2} - \nabla \left(\dfrac{\partial \Psi}{\partial t} \right) \right] - \dfrac{\sigma}{\varepsilon} \nabla \times \dfrac{\partial \vec{F}}{\partial t} \\ \nabla \times \dfrac{\partial \vec{H}^F}{\partial t} = \nabla \times \left[\dfrac{1}{\mu} \nabla \times \left(\dfrac{1}{\varepsilon} \nabla \times \vec{F} \right) \right] - \nabla \times \left(\dfrac{\vec{J}_m^i}{\mu} \right) \end{array} \right. \tag{4.25}$$

Equating the right-hand sides of the equations in (4.25) and imposing Lorenz' gauge (4.23), leads to the WE in its most general form:

$$\begin{aligned} \nabla \times \left[\frac{\partial^2 \vec{F}}{\partial t^2} + \frac{\sigma}{\varepsilon} \frac{\partial \vec{F}}{\partial t} - \frac{1}{\mu\varepsilon} \nabla^2 \vec{F} - \nabla \left(\frac{1}{\mu\varepsilon} \right) \nabla \cdot \vec{F} + \frac{1}{\mu} \nabla \left(\frac{1}{\varepsilon} \right) \times \nabla \times \vec{F} - \frac{\vec{J}_m^i}{\mu} \right] \\ -\nabla \left(\frac{\sigma}{\varepsilon} \right) \times \frac{\partial \vec{F}}{\partial t} = 0 \end{aligned} \tag{4.26}$$

In the case of lossless media, equations (4.13) and (4.21) are simplified to:

$$\nabla^2 \vec{A} - \mu\varepsilon \frac{\partial^2 \vec{A}}{\partial t^2} = -\mu \vec{J}^i \tag{4.27}$$

and

$$\nabla^2 \vec{F} - \mu\varepsilon \frac{\partial^2 \vec{F}}{\partial t^2} = -\varepsilon \vec{J}_m^i \tag{4.28}$$

4.3 Boundary conditions for the WETD

According to the uniqueness theorem for Maxwell's equations, the electromagnetic field in a given region is uniquely defined if all sources are specified inside the region and if the tangential field components are specified at the boundary. In order to derive the boundary conditions (BCs) for the components of the magnetic vector potential $\vec{A}$, first the expressions for all field components in Cartesian coordinates are presented below:

$$\frac{\partial E_x}{\partial t} = -\frac{\partial^2 A_x}{\partial t^2} - \frac{\sigma_m}{\mu}\frac{\partial A_x}{\partial t} - \frac{\partial^2 \Phi}{\partial x \partial t} \tag{4.29}$$

$$\frac{\partial E_y}{\partial t} = -\frac{\partial^2 A_y}{\partial t^2} - \frac{\sigma_m}{\mu}\frac{\partial A_y}{\partial t} - \frac{\partial^2 \Phi}{\partial y \partial t} \tag{4.30}$$

$$\frac{\partial E_z}{\partial t} = -\frac{\partial^2 A_z}{\partial t^2} - \frac{\sigma_m}{\mu}\frac{\partial A_z}{\partial t} - \frac{\partial^2 \Phi}{\partial z \partial t} \tag{4.31}$$

$$H_x = \frac{1}{\mu}\left(\frac{\partial A_z}{\partial y} - \frac{\partial A_y}{\partial z}\right) \tag{4.32}$$

$$H_y = \frac{1}{\mu}\left(\frac{\partial A_x}{\partial z} - \frac{\partial A_z}{\partial x}\right) \tag{4.33}$$

$$H_z = \frac{1}{\mu}\left(\frac{\partial A_y}{\partial x} - \frac{\partial A_x}{\partial y}\right) \tag{4.34}$$

Since in reality, as mentioned before, $\sigma_m = 0$, Lorenz' gauge is:

$$\mu\varepsilon\frac{\partial \Phi}{\partial t} = -\nabla \cdot \vec{A} \tag{4.35}$$

Then equations (4.29) to (4.31) can be further simplified by substitution of (4.35) in them:

$$\frac{\partial E_x}{\partial t} = -\frac{\partial^2 A_x}{\partial t^2} + \frac{1}{\mu\varepsilon}\left(\frac{\partial^2 A_x}{\partial x^2} + \frac{\partial^2 A_y}{\partial x \partial y} + \frac{\partial^2 A_z}{\partial x \partial z}\right) \tag{4.36}$$

$$\frac{\partial E_y}{\partial t} = -\frac{\partial^2 A_y}{\partial t^2} + \frac{1}{\mu\varepsilon}\left(\frac{\partial^2 A_x}{\partial x \partial y} + \frac{\partial^2 A_y}{\partial y^2} + \frac{\partial^2 A_z}{\partial y \partial z}\right) \tag{4.37}$$

$$\frac{\partial E_z}{\partial t} = -\frac{\partial^2 A_z}{\partial t^2} + \frac{1}{\mu\varepsilon}\left(\frac{\partial^2 A_x}{\partial x \partial z} + \frac{\partial^2 A_y}{\partial y \partial z} + \frac{\partial^2 A_z}{\partial z^2}\right) \tag{4.38}$$

Three types of interfaces will be considered here, as they will be encountered in the simulations presented later.

1. Electric wall.

A typical example is the infinite ground plane of microstrip structure, or metallic walls of a waveguide. The vanishing tangential components of the electric field dictate that:

$$\frac{\partial A_n}{\partial n} = 0 \tag{4.39}$$

$$A_\xi = 0 \tag{4.40}$$

Here n denotes the direction that is normal to the electric wall surface and ξ denotes the tangential components of $\vec{A}$. This is equivalent to setting the value of the electric scalar potential Φ to a constant at the ground plane:

$$\frac{\partial \Phi_0}{\partial t} = -\frac{1}{\mu\varepsilon}\nabla \cdot \vec{A}_0 = 0$$

2. Magnetic wall.

This boundary condition is used when the structure (including the excitation) is symmetric with respect to a given plane. It is equivalent to setting

the tangential components of the magnetic field $\vec{H}$ equal to zero. Therefore, the boundary conditions for $\vec{A}_0$ in this case are defined as:

$$A_n = 0 \tag{4.41}$$

$$\frac{\partial A_\xi}{\partial \xi} = 0 \tag{4.42}$$

3. Dielectric-to dielectric interface.

The dielectric media are considered to have no magnetic properties ($\mu_{r_1} = \mu_{r_2} = 1$). The continuity of all three components of the $\vec{H}$ field implies the following boundary conditions at the interface:

$$A_n^{(1)} = A_n^{(2)} \tag{4.43}$$

$$A_\xi^{(1)} = A_\xi^{(2)};\ \frac{\partial A_\xi^{(1)}}{\partial n} = \frac{\partial A_\xi^{(2)}}{\partial n} \tag{4.44}$$

It is clear that equations (4.44) are enough to define uniquely the tangential $\vec{A}$ components. However, the normal component A_n cannot be calculated by the single relation (4.43). Here an additional continuity relation will be used – the continuity of the scalar potential Φ which follows from the continuity of the tangential $\vec{E}$ components and the first of equations (4.44):

$$\frac{1}{\mu_0 \varepsilon_1}\left(\frac{\partial A_n^{(1)}}{\partial n} + \frac{\partial A_{\xi_1}^{(1)}}{\partial \xi_1} + \frac{\partial A_{\xi_2}^{(1)}}{\partial \xi_2}\right) = \frac{1}{\mu_0 \varepsilon_2}\left(\frac{\partial A_n^{(2)}}{\partial n} + \frac{\partial A_{\xi_1}^{(2)}}{\partial \xi_1} + \frac{\partial A_{\xi_2}^{(2)}}{\partial \xi_2}\right) \tag{4.45}$$

Since the tangential components are continuous, i.e. $A_{\xi_i}^{(1)} = A_{\xi_i}^{(2)};\ i = 1,2$, the second relation for the A_n component is thus obtained:

$$\varepsilon_2 \frac{\partial A_n^{(1)}}{\partial n} - \varepsilon_1 \frac{\partial A_n^{(2)}}{\partial n} = (\varepsilon_1 - \varepsilon_2)\left(\frac{\partial A_{\xi_1}}{\partial \xi_1} - \frac{\partial A_{\xi_2}}{\partial \xi_2} \right) \tag{4.46}$$

Equations (4.43) and (4.46) define completely the value of A_n at the interface. Here it can be noted that the presence of dielectric-to-dielectric interface couples the normal component of $\vec{A}$ with its tangential components. Naturally, the components are uncoupled if $\varepsilon_1 = \varepsilon_2$, and in such case every component simply obeys its wave equation.

4.4 Outline of the time-domain wave-potentials (TDWP) technique

Georgieva and Rickard (1999), (2000) showed recently the first applications of a pair of collinear vector potentials (VPs) of fixed direction, such that the wave equations only for two scalar wave potentials (WPs) were necessary to solve. The first finite-difference implementation showed that general inhomogeneous problems could be solved in terms of two scalar quantities. The theoretical estimate of the CPU-time and memory requirements of the time-domain wave-potential (TDWP) algorithm in comparison with Yee's FDTD algorithm gives a reduction of at least 1/3 in the *general* case, which is due to the reduced number of unknowns. These first applications, however, revealed several

problems. The choice of the direction of the VPs was crucial when dielectric interfaces were present, especially between regions, whose dielectric constants would differ significantly or when corners and edges were present. The formulation of the boundary conditions for the VPs and the conditions for the direction change of the collinear pair of wave potentials are thoroughly studied by Georgieva (2001). In the following, only the outline of the derivation of the wave equations for the time-domain wave potentials (TDWP) technique will be presented. This will be enough to serve the objective of this research, which is to develop PML ABC for the wave equation in the time domain (WETD).

First, the magnetic VP $\vec{A}$ and the electric VP $\vec{F}$ are introduced in the classic way, as in (4.3) and (4.17). As mentioned above, $\vec{H}^A$ is the magnetic field vector of a field associated with electric sources only ($\nabla \cdot \vec{B}^A = 0$). The $\vec{E}^F$ vector is the electric field associated with magnetic sources only ($\nabla \cdot \vec{D}^F = 0$). Their counterparts, $\vec{E}^A$ and $\vec{H}^F$, are found by substitution in Maxwell's equations. The total field is a superposition of $(\vec{E}^A, \vec{H}^A)$ and $(\vec{E}^F, \vec{H}^F)$. Note that this implies linear media. The next step is to substitute (4.3) and (4.17) in Maxwell's equations:

$$\left|\begin{aligned}
&-\nabla\times\frac{\partial\vec{F}}{\partial t}+\varepsilon\frac{\partial\vec{E}^{A}}{\partial t}=\nabla\times\nabla\times\frac{\vec{A}}{\mu}-\nabla\times\left[\left(\nabla\frac{1}{\mu}\right)\times\vec{A}\right]\\
&\qquad+\nabla\times\vec{H}^{F}-\sigma\vec{E}^{A}+\nabla\times\left(\frac{\sigma}{\varepsilon}\vec{F}\right)-\left(\nabla\frac{\sigma}{\varepsilon}\right)\times\vec{F}-\vec{J}^{i}\\
&\nabla\times\frac{\partial\vec{A}}{\partial t}+\mu\frac{\partial\vec{H}^{F}}{\partial t}=\nabla\times\nabla\times\frac{\vec{F}}{\varepsilon}-\nabla\times\left[\left(\nabla\frac{1}{\varepsilon}\right)\times\vec{F}\right]\\
&\qquad-\nabla\times\vec{E}^{A}-\sigma_m\vec{H}^{F}-\nabla\times\left(\frac{\sigma_m}{\mu}\vec{A}\right)+\left(\nabla\frac{\sigma_m}{\mu}\right)\times\vec{A}-\vec{J}_m^{i}
\end{aligned}\right. \tag{4.47}$$

and split them into two systems of equations as shown below:

$$\left|\begin{aligned}
&\nabla\times\vec{H}^{F}=-\nabla\times\frac{\partial\vec{F}}{\partial t}-\nabla\times\left(\frac{\sigma}{\varepsilon}\vec{F}\right)+\nabla\times\left[\left(\nabla\frac{1}{\mu}\right)\times\vec{A}\right]\\
&\mu\frac{\partial\vec{H}^{F}}{\partial t}=\nabla\times\nabla\times\frac{\vec{F}}{\varepsilon}-\sigma_m\vec{H}^{F}+\left(\nabla\frac{\sigma_m}{\mu}\right)\times\vec{A}-\vec{J}_m^{i}
\end{aligned}\right. \tag{4.48}$$

$$\left|\begin{aligned}
&\varepsilon\frac{\partial\vec{E}^{A}}{\partial t}=\nabla\times\nabla\times\frac{\vec{A}}{\mu}-\sigma\vec{E}^{A}-\left(\nabla\frac{\sigma}{\varepsilon}\right)\times\vec{F}-\vec{J}^{i}\\
&\nabla\times\vec{E}^{A}=-\nabla\times\frac{\partial\vec{A}}{\partial t}-\nabla\times\left[\left(\nabla\frac{1}{\varepsilon}\right)\times\vec{F}\right]-\nabla\times\left(\frac{\sigma_m}{\mu}\vec{A}\right)
\end{aligned}\right. \tag{4.49}$$

In the above transformations, the following identity has been used:

$$\nabla\times\left(\frac{1}{\chi}\nabla\times\vec{v}\right)=\nabla\times\left[\nabla\times\left(\frac{\vec{v}}{\chi}\right)-\nabla\left(\frac{1}{\chi}\right)\times\vec{v}\right],\quad(\vec{v},\chi)\equiv(\vec{A},\mu)\ \text{ or }\ (\vec{F},\varepsilon)$$

From the first equation in (4.48), it follows that

$$\vec{H}^{F}=-\frac{\partial\vec{F}}{\partial t}-\frac{\sigma}{\varepsilon}\vec{F}-\nabla\Psi+\left(\nabla\frac{1}{\mu}\right)\times\vec{A} \tag{4.50}$$

and, from the second equation in (4.49), it follows that

$$\vec{E}^{A}=-\frac{\partial\vec{A}}{\partial t}-\frac{\sigma_m}{\mu}\vec{A}-\nabla\Phi-\left(\nabla\frac{1}{\varepsilon}\right)\times\vec{F} \tag{4.51}$$

Here, Ψ and Φ are the magnetic scalar potential and the electric scalar potential, respectively. Note the cross coupling between the *F*-field and the *A*-potential and the *A*-field and the *F*-potential due to the non-zero gradients of the constitutive parameters of the medium in (4.50) and (4.51). This cross coupling appears also in the governing equations of the VPs given below. If Lorenz' gauges to the potentials $\vec{A}_\mu = \vec{A}/\mu$ and $\vec{F}_\varepsilon = \vec{F}/\varepsilon$ are defined as:

$$-\nabla\cdot\vec{A}_\mu = \varepsilon\frac{\partial\Phi}{\partial t} + \sigma\Phi; \quad -\nabla\cdot\vec{F}_\varepsilon = \mu\frac{\partial\Psi}{\partial t} + \sigma_m\Psi \tag{4.52}$$

then the general wave equations in time domain (WETD) become:

$$\begin{aligned} &-\nabla^2\vec{A}_\mu + \mu\varepsilon\frac{\partial^2\vec{A}_\mu}{\partial t^2} + (\varepsilon\sigma_m + \mu\sigma)\frac{\partial\vec{A}_\mu}{\partial t} + \sigma\sigma_m\vec{A}_\mu \\ &\quad -(\nabla\varepsilon)\frac{\partial\Phi}{\partial t} - (\nabla\sigma)\Phi - \nabla\varepsilon\times\frac{\partial\vec{F}_\varepsilon}{\partial t} - \nabla\sigma\times\vec{F}_\varepsilon = \vec{J}^i \end{aligned} \tag{4.53}$$

$$\begin{aligned} &-\nabla^2\vec{F}_\varepsilon + \mu\varepsilon\frac{\partial^2\vec{F}_\varepsilon}{\partial t^2} + (\mu\sigma + \varepsilon\sigma_m)\frac{\partial\vec{F}_\varepsilon}{\partial t} + \sigma\sigma_m\vec{F}_\varepsilon \\ &\quad -(\nabla\mu)\frac{\partial\Psi}{\partial t} - (\nabla\sigma_m)\Psi + \nabla\mu\times\frac{\partial\vec{A}_\mu}{\partial t} + \nabla\sigma_m\times\vec{A}_\mu = \vec{J}_m^i \end{aligned} \tag{4.54}$$

To complete the analysis, the components of the total field $(\vec{E},\vec{H})$ will be expressed in terms of the potentials $\vec{A}_\mu$ and $\vec{F}_\mu$. The construction of solutions in terms of VPs is based on the superposition of both fields: $(\vec{E}^A,\vec{H}^A)$ and $(\vec{E}^F,\vec{H}^F)$. Making use of equations (4.3), (4.17), (4.50) and (4.51), the following field-potential relations are obtained:

$$\begin{aligned}\vec{E} &= \vec{E}^A + \vec{E}^F = -\mu\frac{\partial \vec{A}_\mu}{\partial t} - \sigma_m A_\mu - \nabla\Phi - \nabla\times\vec{F}_\varepsilon \\ \vec{H} &= \vec{H}^A + \vec{H}^F = -\varepsilon\frac{\partial \vec{F}_\varepsilon}{\partial t} - \sigma\vec{F}_\varepsilon - \nabla\Psi + \nabla\times\vec{A}_\mu\end{aligned} \tag{4.55}$$

Alternatively, equations (4.3), (4.17), the second equation in (4.48) and the first equation in (4.49) can be used, to derive the equivalent relations:

$$\begin{aligned}\varepsilon\frac{\partial \vec{E}}{\partial t} + \sigma\vec{E} &= \nabla\times(\nabla\times\vec{A}_\mu - \sigma\vec{F}_\varepsilon - \varepsilon\frac{\partial \vec{F}_\varepsilon}{\partial t}) - \vec{J}^i \\ \mu\frac{\partial \vec{H}}{\partial t} + \sigma_m\vec{H} &= \nabla\times(\nabla\times\vec{F}_\varepsilon + \sigma_m\vec{A}_\mu + \mu\frac{\partial \vec{A}_\mu}{\partial t}) - \vec{J}_m^i\end{aligned} \tag{4.56}$$

Equations (4.55) can be cast in a form similar to that of (4.56):

$$\begin{aligned}\varepsilon\frac{\partial \vec{E}}{\partial t} + \sigma\vec{E} &= \nabla\nabla\cdot\vec{A}_\mu - \mu\varepsilon\frac{\partial^2 \vec{A}_\mu}{\partial t^2} - (\mu\sigma + \varepsilon\sigma_m)\frac{\partial \vec{A}_\mu}{\partial t} - \sigma\sigma_m\vec{A}_\mu \\ &\quad + \frac{\partial\Phi}{\partial t}\nabla\varepsilon + \Phi\nabla\sigma - \varepsilon\nabla\times\frac{\partial \vec{F}_\varepsilon}{\partial t} - \sigma\nabla\times\vec{F}_\varepsilon \\ \mu\frac{\partial \vec{H}}{\partial t} + \sigma_m\vec{H} &= \nabla\nabla\cdot\vec{F}_\varepsilon - \mu\varepsilon\frac{\partial^2 \vec{F}_\varepsilon}{\partial t^2} - (\mu\sigma + \varepsilon\sigma_m)\frac{\partial \vec{F}_\varepsilon}{\partial t} - \sigma\sigma_m\vec{F}_\varepsilon \\ &\quad + \frac{\partial\Psi}{\partial t}\nabla\mu + \Psi\nabla\sigma_m + \mu\nabla\times\frac{\partial \vec{A}_\mu}{\partial t} + \sigma_m\nabla\times\vec{A}_\mu\end{aligned} \tag{4.57}$$

The following important conclusions follow from equations (4.53) and (4.54).

1. Collinear VPs, which are normal to dielectric/magnetic/loss interfaces, are not mutually coupled. The scattering of the VP pair at an interface, orthogonal to the direction of the VP pair, can be fully described by two scalar quantities: the magnitudes of the VPs.

2. In addition, further analysis shows that the boundary conditions at conducting edges of a pair of VPs, which are tangential to the conducting edge, are well posed. Homogeneous Dirichlet condition is imposed on the magnetic VP, $A_\tau = 0$, regardless of the direction from which the edge is approached. A homogeneous Neumann condition is imposed on the electric VP, $\partial F_\tau / \partial n = 0$, where $\hat{n}$ is *any* direction normal to the edge; for further details see Georgieva (2001).

3. Therefore, in practical applications, the computational domain is to be divided into domains of constant direction of the VP pairs in such a way that mode coupling is avoided, that is, the direction of the VP pair changes according to the direction of the gradient of the constitutive parameters of the medium. A seamless transition between orthogonal VP pairs at the mutual boundaries of neighboring domains can be carried out using the field-vectors' longitudinal components, which depend on a single potential; thus the wave potentials of a VP pair at the boundary of any domain are calculated independently from each other.

Chapter 5

Improved Absorbing Boundary Condition for the Wave Equation in the Time Domain (WETD)

5.1 Introduction

An improved three-dimensional (3-D) algorithm with PML ABC for the scalar wave equation in the time-domain (WETD) is presented in this Chapter for general inhomogeneous lossy or loss-free problems. The proposed PML ABC is applicable to finite difference schemes treating the time-domain wave equation, such as the time-domain wave-potential (TDWP) technique and the time-domain scalar wave equation approaches to the analysis of optical structures. The modified time-domain wave equation for lossy media is expressed in terms of stretched coordinate variables. Modified PML conductivity profiles are developed and optimized for use with the second order wave equation, which offer lower reflections in a wider frequency band in comparison with the commonly used (in FDTD algorithms) profiles. The effect of new types of termination walls on the overall PML performance is studied and the best choices are singled out.

Berenger's PML in the time domain has been used mainly in conjunction with the FDTD algorithm to the solution of Maxwell's equations, as well as with the finite element time-domain (FETD) method.

PML ABCs have been also developed for most of the frequency-domain techniques, such as the finite element method (FEM) as in Tang *et al.* (1998) and Stupfel and Mittra (1996), the finite-difference frequency-domain (FDFD) method as in Marengo *et al.* (1999), or the frequency-domain beam propagation method (BPM) as in Huang *et al.* (1996) and Cuccinotta *et al.* (1999).

Recent trends in computational electrodynamics include the development of scalar or vector wave equation techniques for applications in numerical algorithms, not only for optical waveguides and devices but also in the microwave and millimetre-wave structure analysis. The time-domain vector-potential technique, as outlined in Section 4.2, is based on the solution of the vector wave equation for the magnetic vector potential $\vec{A}$. The time-domain wave-potential (TDWP) approach as outlined in Section 4.4, uses two scalar quantities, the magnitudes of a pair of collinear vector potentials $(A, F)\hat{\xi}$, in order to analyze an EM problem in a region of distinguished axis $\hat{\xi}$ parallel to the vector potentials. The propagation of the two potential functions is also governed by the 3-D scalar wave equation.

In photonics, approaches based on the time domain wave equations are used to analyze optical waveguide problems. Among those, the most widely used are the methods based on the time-domain scalar or semi-vectorial finite-

difference wave equation [see, for example, Huang *et al.* (1991a), (1991b), (1993)]; as well as the time-domain beam propagation method (BPM) [see for example Koshiba *et al.* (2000)]. These techniques typically reduce the 3-D problem to a set of 2-D scalar wave equations, where one of the dimensions is along the direction of propagation.

These new algorithms require a reliable and efficient ABC, which can handle both open problems (i.e. radiation and scattering) and problems involving port terminations (high-frequency circuit problems). It will become clear from the derivations to follow that the IPML ABC proposed here is not limited to electromagnetic problems only. It can be applied to any physical phenomenon modeled by the general lossy 3-D scalar wave equation, which requires reflection-free boundaries.

Recently, a one-directional PML ABC has been applied to terminate one of the ports in a dielectric-slab waveguide problem solved in terms of the two-dimensional (2-D) scalar wave equation in the time domain, see Zhou *et al.* (2001). In this thesis, the method proposed by Zhou *et al.* (2001) is extended to a general 3-dimensional PML for the 3-D wave equation in the time domain in loss-free or lossy media. To the authors' knowledge, this is the first PML ABC developed and successfully implemented in conjunction with the 3-D wave equation in the time domain. The derivation of the PML equations is based on the well-known stretched-coordinate approach proposed by Chew and Weedon (1994) for the FDTD solution to Maxwell's equations.

This Chapter contains three main contributions.

1. The IPML formulas of the 3-D scalar wave equation absorber are derived and discretized according to the requirements of a finite-difference time domain scheme.

2. Modified profiles of the IPML variables are defined, so that a superior performance is obtained (lower reflections in a broader frequency band) in comparison with commonly used PML profiles when applied to the wave equation absorber. The proposed modification adds a new degree of freedom in the algorithm and is a problem-independent approach to the optimization of the PML performance.

3. New types of lossy termination walls for the IPML medium are derived and discretized by modifying known lossless single-layer ABCs, according to the requirements of a finite-difference time domain scheme.

5.2 Derivation of the IPML equations

5.2.1 IPML for the WETD in homogeneous lossy media

Consider the wave equation in the time domain (WETD) governing the behaviour of the vector potential $\vec{A}$, as obtained in Chapter 4. In the case of a homogeneous lossy medium it is re-written here for convenience:

$$\nabla^2 \vec{A} - \mu\varepsilon \frac{\partial^2 \vec{A}}{\partial t^2} - \left(\sigma_m \varepsilon + \mu\sigma\right) \frac{\partial \vec{A}}{\partial t} - \sigma\sigma_m \vec{A} = -\mu \vec{J} \tag{5.1}$$

Here σ and σ_m denote the specific electric and magnetic conductivities of the medium, respectively. Recall that the equation for the electric vector potential $\vec{F}$ is the same, except for the source term $\mu\vec{J}$, which is replaced by $\varepsilon\vec{J}_m$, with $\vec{J}_m$ being the magnetic current density. Using the stretched coordinate approach of Chew and Weedon (1994) outlined in Section 3.4.1, the complex stretching variables s_x, s_y, s_z along the three Cartesian coordinates are introduced in the Laplacian:

$$\nabla_s^2 = \frac{1}{s_x}\frac{\partial}{\partial x}\left(\frac{1}{s_x}\frac{\partial}{\partial x}\right)+\frac{1}{s_y}\frac{\partial}{\partial y}\left(\frac{1}{s_y}\frac{\partial}{\partial y}\right)+\frac{1}{s_z}\frac{\partial}{\partial z}\left(\frac{1}{s_z}\frac{\partial}{\partial z}\right) \tag{5.2}$$

where $s_\xi = \alpha_\xi + \sigma_\xi/(j\omega\varepsilon)$, $\xi = x, y, z$. The WE in (5.1) is then mapped into the frequency domain:

$$\nabla_s^2\tilde{\tilde{A}} - \mu\varepsilon(j\omega)^2\tilde{\tilde{A}} - (\mu\sigma+\varepsilon\sigma_m)j\omega\tilde{\tilde{A}} - \sigma\sigma_m\tilde{\tilde{A}} = -\mu\tilde{\tilde{J}} \tag{5.3}$$

Six auxiliary variables are introduced in a fashion similar to that proposed by Zhou *et al.* (2001):

$$\begin{aligned}
j\omega\tilde{\tilde{X}}_1 &= \frac{1}{s_x}\frac{\partial\tilde{\tilde{A}}}{\partial x}; \quad j\omega\tilde{\tilde{X}}_2 = \frac{1}{s_x}\frac{\partial\left(j\omega\tilde{\tilde{X}}_1\right)}{\partial x} \\
j\omega\tilde{\tilde{Y}}_1 &= \frac{1}{s_y}\frac{\partial\tilde{\tilde{A}}}{\partial y}; \quad j\omega\tilde{\tilde{Y}}_2 = \frac{1}{s_y}\frac{\partial\left(j\omega\tilde{\tilde{Y}}_1\right)}{\partial y} \\
j\omega\tilde{\tilde{Z}}_1 &= \frac{1}{s_z}\frac{\partial\tilde{\tilde{A}}}{\partial z}; \quad j\omega\tilde{\tilde{Z}}_2 = \frac{1}{s_z}\frac{\partial\left(j\omega\tilde{\tilde{Z}}_1\right)}{\partial z}
\end{aligned} \tag{5.4}$$

The mapped frequency-domain WE now becomes:

$$\mu\varepsilon(j\omega)^2\tilde{\tilde{A}}+(\mu\sigma+\varepsilon\sigma_m)j\omega\tilde{\tilde{A}}+\sigma\sigma_m\tilde{\tilde{A}}=j\omega\tilde{\tilde{X}}_2+j\omega\tilde{\tilde{Y}}_2+j\omega\tilde{\tilde{Z}}_2+\mu\tilde{\tilde{J}} \tag{5.5}$$

which can be mapped back into the time domain as:

$$\mu\varepsilon\frac{\partial^2\vec{A}}{\partial t^2}+\left(\varepsilon\sigma_m+\mu\sigma\right)\frac{\partial\vec{A}}{\partial t}+\sigma\sigma_m\vec{A}=\frac{\partial\vec{X}_2}{\partial t}+\frac{\partial\vec{Y}_2}{\partial t}+\frac{\partial\vec{Z}_2}{\partial t}+\mu\vec{J} \tag{5.6}$$

The auxiliary variables in the time domain are calculated according to the equations in (5.4), which are also mapped back into the time domain:

$$\begin{aligned}
&\alpha_x\frac{\partial\vec{X}_1}{\partial t}+\frac{\sigma_x}{\varepsilon}\vec{X}_1=\frac{\partial\vec{A}}{\partial x};\ \ \alpha_x\frac{\partial\vec{X}_2}{\partial t}+\frac{\sigma_x}{\varepsilon}\vec{X}_2=\frac{\partial^2\vec{X}_1}{\partial x\partial t}\\
&\alpha_y\frac{\partial\vec{Y}_1}{\partial t}+\frac{\sigma_y}{\varepsilon}\vec{Y}_1=\frac{\partial\vec{A}}{\partial y};\ \ \alpha_y\frac{\partial\vec{Y}_2}{\partial t}+\frac{\sigma_y}{\varepsilon}\vec{Y}_2=\frac{\partial^2\vec{Y}_1}{\partial y\partial t}\\
&\alpha_z\frac{\partial\vec{Z}_1}{\partial t}+\frac{\sigma_z}{\varepsilon}\vec{Z}_1=\frac{\partial\vec{A}}{\partial z};\ \ \alpha_z\frac{\partial\vec{Z}_2}{\partial t}+\frac{\sigma_z}{\varepsilon}\vec{Z}_2=\frac{\partial^2\vec{Z}_1}{\partial z\partial t}
\end{aligned} \tag{5.7}$$

Equations (5.6) and (5.7) are the basis of the proposed 3-D wave equation IPML ABC.

5.2.2 IPML for the WETD in inhomogeneous lossless media

Since by definition for lossless media

$$\vec{H}=\frac{1}{\mu}\nabla\times\vec{A};\qquad \vec{E}=-\frac{\partial\vec{A}}{\partial t}-\nabla\Phi\ , \tag{5.8}$$

from Maxwell's equations, the WE in inhomogeneous lossless media is obtained as:

$$-\frac{\partial^2\vec{A}}{\partial t^2}-\nabla\frac{\partial\Phi}{\partial t}=\frac{1}{\varepsilon}\nabla\times\left(\frac{1}{\mu}\nabla\times\vec{A}\right)-\frac{1}{\varepsilon}\vec{J}^i \tag{5.9}$$

where Φ is the scalar potential for which Lorenz' gauge holds:

$$\frac{\partial \Phi}{\partial t} = -\frac{1}{\mu\varepsilon}\nabla \cdot \vec{A} \tag{5.10}$$

Lorenz' gauge (5.10) ensures the uniqueness of the magnetic vector potential.

Upon substituting it in the WE and also using the vector identity:

$$\nabla \times \nabla \times \vec{A} = \nabla\left(\nabla \cdot \vec{A}\right) - \nabla^2 \vec{A}$$

the WE is reduced to the form:

$$-\frac{\partial^2 \vec{A}}{\partial t^2} - \nabla\left(-\frac{1}{\mu\varepsilon}\nabla \cdot \vec{A}\right) = \frac{1}{\varepsilon}\nabla \times \left(\frac{1}{\mu}\nabla \times \vec{A}\right) - \frac{1}{\varepsilon}\vec{J}^i \tag{5.11}$$

Now in the case when no magnetic inhomogeneities are present, $\nabla\mu = 0$, $\mu = \mu_0\mu_r$, the WE can be further simplified:

$$-\frac{\partial^2 \vec{A}}{\partial t^2} + \frac{1}{\mu_0\mu_r\varepsilon_0}\nabla\left(\frac{1}{\varepsilon_r}\nabla \cdot \vec{A}\right) = \frac{1}{\mu_0\varepsilon_0\mu_r\varepsilon_r}\left[\nabla\left(\nabla \cdot \vec{A}\right) - \nabla^2 \vec{A}\right] - \frac{1}{\varepsilon}\vec{J}^i \tag{5.12}$$

or,

$$-\frac{\partial^2 \vec{A}}{\partial t^2} + \frac{1}{\mu_0\varepsilon_0\mu_r}\nabla\left(\frac{1}{\varepsilon_r}\right)\left(\nabla \cdot \vec{A}\right) + \frac{1}{\mu_0\varepsilon_0\mu_r\varepsilon_r}\nabla^2 \vec{A} = -\frac{1}{\varepsilon}\vec{J}^i \tag{5.13}$$

The component wise WE for $\vec{J}^i = 0$ is therefore:

$$\frac{\partial^2 A_x}{\partial t^2} = \frac{c^2}{\mu_r}\frac{\partial}{\partial x}\left(\frac{1}{\varepsilon_r}\right)\left(\nabla \cdot \vec{A}\right) + \frac{c^2}{\mu_r\varepsilon_r}\left[\frac{\partial^2 A_x}{\partial x^2} + \frac{\partial^2 A_x}{\partial y^2} + \frac{\partial^2 A_x}{\partial z^2}\right] \tag{5.14}$$

$$\frac{\partial^2 A_y}{\partial t^2} = \frac{c^2}{\mu_r}\frac{\partial}{\partial y}\left(\frac{1}{\varepsilon_r}\right)\left(\nabla \cdot \vec{A}\right) + \frac{c^2}{\mu_r\varepsilon_r}\left[\frac{\partial^2 A_y}{\partial x^2} + \frac{\partial^2 A_y}{\partial y^2} + \frac{\partial^2 A_y}{\partial z^2}\right] \tag{5.15}$$

$$\frac{\partial^2 A_z}{\partial t^2} = \frac{c^2}{\mu_r}\frac{\partial}{\partial z}\left(\frac{1}{\varepsilon_r}\right)\left(\nabla \cdot \vec{A}\right) + \frac{c^2}{\mu_r\varepsilon_r}\left[\frac{\partial^2 A_z}{\partial x^2} + \frac{\partial^2 A_z}{\partial y^2} + \frac{\partial^2 A_z}{\partial z^2}\right] \tag{5.16}$$

In the setting of the stretched coordinate approach, the definition and the discretization equations for the auxiliary variables will remain unchanged since the Laplacian remains unchanged, that is, in the case of $\vec{A} = A_z \hat{z}$, equations (5.7) hold. Therefore, the basis of the proposed 3-D wave equation IPML ABC in lossless inhomogeneous media are equations (5.7) and (5.16). Note that in this case it is necessary to calculate explicitly the divergence of the vector potential in the form:

$$div\vec{A} = \alpha_x \frac{\partial X_{1x}}{\partial t} + \frac{\sigma_x}{\varepsilon} X_{1x} + \alpha_y \frac{\partial Y_{1y}}{\partial t} + \frac{\sigma_y}{\varepsilon} Y_{1y} + \alpha_z \frac{\partial Z_{1z}}{\partial t} + \frac{\sigma_z}{\varepsilon} Z_{1z} \tag{5.17}$$

It should be noted that in the important and frequently met case of layered dielectrics, where all the interfaces of media with different permittivities share the same normal, say a normal in the *z*-direction, only the *z*-component of the vector potential $\vec{A} = A_z \hat{z}$ will be enough to describe the problem. In that case the above set of equations (5.14) to (5.16) for the vector potential will be reduced to the last equation only, which can be simplified to the following form:

$$\frac{\partial^2 A_z}{\partial t^2} = \frac{c^2}{\mu_r \varepsilon_r}\left[\frac{\partial^2 A_z}{\partial x^2} + \frac{\partial^2 A_z}{\partial y^2} + \varepsilon_r \frac{\partial}{\partial z}\left(\frac{1}{\varepsilon_r}\frac{\partial A_z}{\partial z}\right)\right] \tag{5.18}$$

since

$$\frac{c^2}{\mu_r}\frac{\partial}{\partial z}\left(\frac{1}{\varepsilon_r}\right)\left(\nabla \cdot \vec{A}\right) + \frac{c^2}{\mu_r \varepsilon_r}\frac{\partial^2 A_z}{\partial z^2} = \frac{c^2}{\mu_r}\frac{\partial}{\partial z}\left(\frac{1}{\varepsilon_r}\right)\left(\frac{\partial A_z}{\partial z}\right) + \frac{c^2}{\mu_r \varepsilon_r}\frac{\partial^2 A_z}{\partial z^2}$$
$$= \frac{c^2}{\mu_r}\left[\frac{\partial}{\partial z}\left(\frac{1}{\varepsilon_r}\frac{\partial A_z}{\partial z}\right)\right]$$

and the divergence of the vector potential is no longer calculated explicitly.

In this particular case, in the setting of stretched coordinates approach, from the definitions of the auxiliary variables (5.7), it follows that the equations for the auxiliary variables X_{1z}, X_{2z}, Y_{1z}, Y_{2z} will remain unchanged, as in the case of homogeneous medium, but the equations for the auxiliary variables Z_{1z}, Z_{2z} should be accordingly modified:

$$\begin{aligned} \frac{1}{\varepsilon_r}\frac{\partial Z_{1z}}{\partial t} &= -\frac{1}{\varepsilon_r}\frac{\sigma_z}{\varepsilon\alpha_z}Z_{1z} + \frac{1}{\alpha_z}\left(\frac{1}{\varepsilon_r}\frac{\partial A_z}{\partial z}\right) \\ \frac{\partial Z_{2z}}{\partial t} &= -\frac{\sigma_z}{\varepsilon\alpha_z}Z_{2z} + \frac{\varepsilon_r}{\alpha_z}\frac{1}{\varepsilon_r}\frac{\partial^2 Z_{1z}}{\partial z\partial t} \end{aligned} \tag{5.19}$$

or,

$$\begin{aligned} \frac{\partial}{\partial t}\left(\frac{Z_{1z}}{\varepsilon_r}\right) &= -\frac{\sigma_z}{\varepsilon\alpha_z}\left(\frac{Z_{1z}}{\varepsilon_r}\right) + \frac{1}{\alpha_z}\frac{1}{\varepsilon_r}\frac{\partial A_z}{\partial z} \\ \frac{\partial Z_{2z}}{\partial t} &= -\frac{\sigma_z}{\varepsilon\alpha_z}Z_{2z} + \frac{\varepsilon_r}{\alpha_x}\frac{\partial^2}{\partial z\partial t}\left(\frac{Z_{1z}}{\varepsilon_r}\right) \end{aligned} \tag{5.20}$$

5.2.3 IPML for the WETD in lossy inhomogeneous media

In Chapter 4 the general WETD in lossy inhomogeneous media is obtained as:

$$\frac{\partial^2\vec{A}}{\partial t^2} + \frac{\sigma}{\varepsilon}\frac{\partial\vec{A}}{\partial t} - \frac{1}{\mu\varepsilon}\nabla^2\vec{A} - \nabla\left(\frac{1}{\mu\varepsilon}\right)\nabla\cdot\vec{A} + \frac{1}{\varepsilon}\nabla\left(\frac{1}{\mu}\right)\times\nabla\times\vec{A} - \Phi\nabla\left(\frac{\sigma}{\varepsilon}\right) = \frac{\vec{J}^i}{\varepsilon} \tag{5.21}$$

and clearly the scalar potential has to be explicitly calculated from Lorenz' gauge:

$$\mu\varepsilon\frac{\partial\Phi}{\partial t} + \mu\sigma\Phi = -\nabla\cdot\vec{A} \tag{5.22}$$

as well as the divergence of the magnetic vector potential. Since in that case the Laplacian remains unchanged, the definitions, discretizations and calculations of the auxiliary variables will remain unchanged, as in the case of homogeneous media; the divergence of $\vec{A}$ will be calculated in the form (5.17).

5.3 Discretization

5.3.1 IPML for the WETD in homogeneous lossy media

All the equations are discretized using central finite differences. The auxiliary variables $\vec{X}_1$, $\vec{Y}_1$ and $\vec{Z}_1$ are positioned half a cell "after" the locations of $\vec{A}$ in the direction of the *x*-, *y*-, and *z*-axis, respectively; and $\vec{X}_2$, $\vec{Y}_2$, $\vec{Z}_2$ are at the same locations as $\vec{A}$ (see Fig. 5.1).

Since a non-uniform grid is used, the spatial increments Δx, Δy, Δz are expressed in terms of the minimal spatial step:

$$\Delta l_{\min} = \min_{\substack{1\le i\le n_{x\max} \\ 1\le j\le n_{y\max} \\ 1\le k\le n_{z\max}}} \left(\Delta x(i), \Delta y(j), \Delta z(k)\right) \tag{5.23}$$

Thus the spatial increments can be expressed through the dimensionless coefficients $h_x(i)$, $h_y(j)$, $h_z(k)$ as:

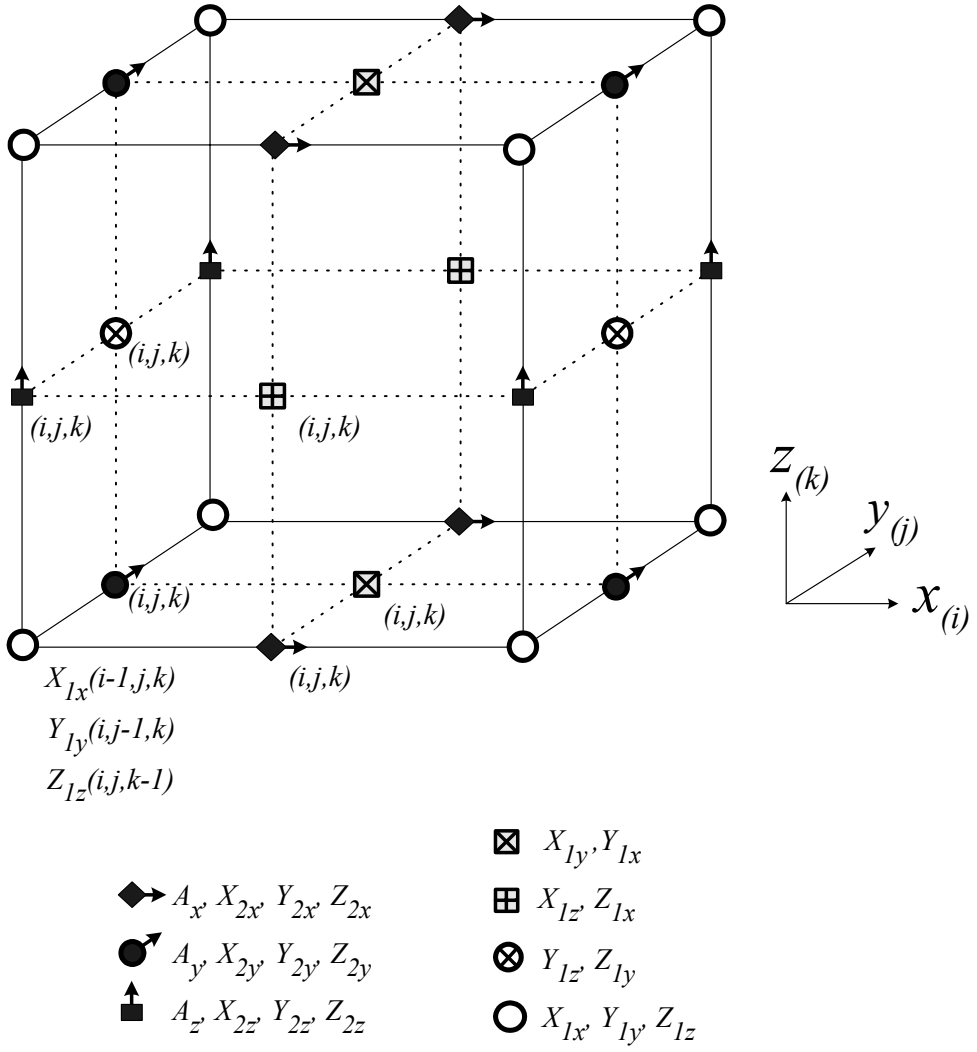

Fig. 5.1. A discretization cell showing the spatial locations of the components of the vector potential and the corresponding auxiliary variables.

$$\begin{aligned} \Delta x(i) &= h_x(i)\Delta l_{\min}; \quad h_x(i) \geq 1,\ 1 \leq i \leq n_{x\max} \\ \Delta y(j) &= h_y(j)\Delta l_{\min};\ h_y(j) \geq 1,\ 1 \leq j \leq n_{y\max} \\ \Delta z(k) &= h_z(k)\Delta l_{\min};\ h_z(k) \geq 1,\ 1 \leq k \leq n_{z\max} \end{aligned} \tag{5.24}$$

For numerical stability, it can be shown rigorously that the step size with respect to time, Δt, has to meet the same Courant's stability condition as the one for the leapfrog scheme used in the discretization of Maxwells' equations, see e.g. Taflove (1995) or Strikwerda (1989):

$$\Delta t \leq \frac{1}{c}\min_{i,j,k}\frac{1}{\sqrt{\left(\frac{1}{\Delta x(i)}\right)^2+\left(\frac{1}{\Delta y(j)}\right)^2+\left(\frac{1}{\Delta z(k)}\right)^2}}$$

In the applications here, it is set to $\Delta t = \Delta l_{\min}/(2c)$ where c is the highest velocity of light in the analyzed structure.

Since, in general, $\vec{A} = A_x\hat{x} + A_y\hat{y} + A_z\hat{z}$, there are three scalar WETD for the three Cartesian components of $\vec{A}$.

Here follows the discretization of the IPML equations (5.6) and (5.7) using the A_z potential. The auxiliary variables have also their corresponding z-components: X_{1z}, Y_{1z}, Z_{1z}, X_{2z}, Y_{2z}, Z_{2z}. For convenience the following numerical constants are defined:

$$r_\xi = \frac{\sigma_\xi \Delta t}{2\varepsilon\alpha_\xi},\ \xi = x, y, z \tag{5.25}$$

The equations for the calculation of the auxiliary variables are obtained using central finite differences as shown below:

$$X_{1z}^{(n+1/2)}(i,j,k)=\left(\frac{1-r_x}{1+r_x}\right)X_{1z}^{(n-1/2)}(i,j,k) + \frac{1}{2c\left(1+r_x\right)\alpha_x h_x(i)}\left[A_z^{(n)}(i+1,j,k)-A_z^{(n)}(i,j,k)\right] \tag{5.26}$$

$$Y_{1z}^{(n+1/2)}(i,j,k)=\left(\frac{1-r_y}{1+r_y}\right)Y_{1z}^{(n-1/2)}(i,j,k) + \frac{1}{2c\left(1+r_y\right)\alpha_y h_y(j)}\left[A_z^{(n)}(i,j+1,k)-A_z^{(n)}(i,j,k)\right] \tag{5.27}$$

$$Z_{1z}^{(n+1/2)}(i,j,k)=\left(\frac{1-r_z}{1+r_z}\right)Z_{1z}^{(n-1/2)}(i,j,k) + \frac{1}{2c\left(1+r_z\right)\alpha_z h_z(k)}\left[A_z^{(n)}(i,j,k+1)-A_z^{(n)}(i,j,k)\right] \tag{5.28}$$

$$X_{2z}^{(n+1/2)}(i,j,k)=\left(\frac{1-r_x}{1+r_x}\right)X_{2z}^{(n-1/2)}(i,j,k)+\frac{1}{\left(1+r_x\right)\alpha_x h_x(i-1)\Delta l_{\min}}\cdot \left[X_{1z}^{(n+1/2)}(i,j,k)-X_{1z}^{(n+1/2)}(i-1,j,k) -X_{1z}^{(n-1/2)}(i,j,k)+X_{1z}^{(n-1/2)}(i-1,j,k)\right] \tag{5.29}$$

$$Y_{2z}^{(n+1/2)}(i,j,k)=\left(\frac{1-r_y}{1+r_y}\right)Y_{2z}^{(n+1/2)}(i,j,k)+\frac{1}{\left(1+r_y\right)\alpha_y h_y(j-1)\Delta l_{\min}}\cdot \left[Y_{1z}^{(n+1/2)}(i,j,k)-Y_{1z}^{(n+1/2)}(i,j-1,k) -Y_{1z}^{(n-1/2)}(i,j,k)+Y_{1z}^{(n-1/2)}(i,j-1,k)\right] \tag{5.30}$$

$$Z_{2z}^{(n+1/2)}(i,j,k)=\left(\frac{1-r_z}{1+r_z}\right)Z_{2z}^{(n-1/2)}(i,j,k)+\frac{1}{\left(1+r_z\right)\alpha_z h_z(k-1)\Delta l_{\min}}\cdot \left[Z_{1z}^{(n+1/2)}(i,j,k)-Z_{1z}^{(n+1/2)}(i,j,k-1) -Z_{1z}^{(n-1/2)}(i,j,k)+Z_{1z}^{(n-1/2)}(i,j,k-1)\right] \tag{5.31}$$

Equation (5.6) is discretized in a similar manner, which leads to the following finite-difference expression:

$$D_t A_z^{(n+1/2)}(i,j,k) = \left(\frac{1-r_0}{1+r_0}\right) D_t A_z^{(n-1/2)}(i,j,k) + \frac{\Delta l_{\min}^2}{4\mu_r \varepsilon_r (1+r_0)} \cdot \left[\frac{1}{\Delta t}\mathcal{L}\{A_z\}^{(n)} - \sigma\sigma_m \cdot A_z^{(n)}(i,j,k) + \mu J_z\right] \tag{5.32}$$

where:

$$\mathcal{L}\{A_z\}^{(n)} = \left[X_{2z}^{(n+1/2)}(i,j,k) - X_{2z}^{(n-1/2)}(i,j,k) + Y_{2z}^{(n+1/2)}(i,j,k) - Y_{2z}^{(n-1/2)}(i,j,k) + Z_{2z}^{(n+1/2)}(i,j,k) - Z_{2z}^{(n-1/2)}(i,j,k)\right] \tag{5.33}$$

is the analog of the finite-difference Laplacian operator applied to A_z;

$r_0 = \frac{\Delta t}{2}\left(\frac{\sigma_m}{\mu} + \frac{\sigma}{\varepsilon}\right)$ is a numerical constant; and

$D_t A_z^{(n+1/2)}(i,j,k) = A_z^{(n+1)}(i,j,k) - A_z^{(n)}(i,j,k)$ is a first-order finite-difference operator in time.

It should be pointed out that sources are unlikely to exist in a practical PML region and, therefore, the term μJ_z in (5.32) may be set to zero. Note also that the material constants σ, σ_m, $\varepsilon = \varepsilon_0 \varepsilon_r$ and $\mu = \mu_0 \mu_r$ are those of the analyzed volume terminated with the IPML; in other words, they are not associated with the anisotropic IPML constants defined in (5.25).

Finally, the update equation for the vector potential is:

$$A_z^{(n+1)}(i,j,k) = A_z^{(n)}(i,j,k) + D_t A_z^{(n+\frac{1}{2})}(i,j,k) \tag{5.34}$$

5.3.2 IPML for the WETD in inhomogeneous lossless media

In the setting of the stretched-coordinate approach, the discretization equations for the auxiliary variables will remain unchanged since the Laplacian remains unchanged; that is, equations (5.26) to (5.31) hold. However, the update equation for the finite-difference expression for the vector-potential first-order time derivative $D_t A_z^{(n+1/2)}(i,j,k) = A_z^{(n+1)}(i,j,k) - A_z^{(n)}(i,j,k)$, will be changed, as follows:

$$\begin{aligned} D_t A_z^{(n+\frac{1}{2})}(i,j,k) = D_t A_z^{(n-\frac{1}{2})}(i,j,k) + \frac{\Delta l_{\min}^2}{4\mu_r\varepsilon_r}\cdot\left[\frac{1}{\Delta t}\mathcal{L}\{A_z\}^{(n)} + \mu J_z\right] \\ + \frac{\Delta l_{\min}}{8} M_{\mu\varepsilon}^{(n)}(i,j,k) - \frac{c}{4\varepsilon_r(i,j,k)} N_{\mu}^{(n)}(i,j,k) \end{aligned} \tag{5.35}$$

Here the divergence of the vector potential has to be calculated explicitly as:

$$\begin{aligned} divA^{(n)}(i,j,k) = \frac{1}{\Delta t}\Bigg\{ & (\alpha_x + \frac{\sigma_x \Delta t}{2\varepsilon}) X_{1x}^{(n+\frac{1}{2})}(i-1,j,k) + (-\alpha_x + \frac{\sigma_x \Delta t}{2\varepsilon}) X_{1x}^{(n-\frac{1}{2})}(i-1,j,k) \\ & + (\alpha_y + \frac{\sigma_y \Delta t}{2\varepsilon}) Y_{1y}^{(n+\frac{1}{2})}(i,j-1,k) + (-\alpha_y + \frac{\sigma_y \Delta t}{2\varepsilon}) Y_{1y}^{(n-\frac{1}{2})}(i,j-1,k) \\ & + (\alpha_z + \frac{\sigma_z \Delta t}{2\varepsilon}) Z_{1z}^{(n+\frac{1}{2})}(i,j,k-1) + (-\alpha_z + \frac{\sigma_z \Delta t}{2\varepsilon}) Z_{1z}^{(n-\frac{1}{2})}(i,j,k-1) \Bigg\} \end{aligned} \tag{5.36}$$

and the expressions for $N_{\mu}^{(n)}(i,j,k)$ and $M_{\mu\varepsilon}^{(n)}(i,j,k)$ are as follows:

$$\begin{aligned} & M_{\mu\varepsilon}^{(n)}(i,j,k) = \\ & \frac{divA^{(n)}(i,j,k)}{h_z(k-1)}\left[\frac{1}{\mu_r(i,j,k)\varepsilon_r(i,j,k)} - \frac{1}{\mu_r(i,j,k-1)\varepsilon_r(i,j,k-1)}\right] \\ & + \frac{divA^{(n)}(i,j,k+1)}{h_z(k)}\left[\frac{1}{\mu_r(i,j,k+1)\varepsilon_r(i,j,k+1)} - \frac{1}{\mu_r(i,j,k)\varepsilon_r(i,j,k)}\right] \end{aligned} \tag{5.37}$$

$$N_{\mu}^{(n)}(i,j,k)=\left\{\left[\frac{1}{\mu_r(i+1,j,k)}-\frac{1}{\mu_r(i,j,k)}\right]\frac{1}{h_x(i)}\times\right.$$
$$\left[Z_{1x}^{(n+\frac{1}{2})}(i,j,k)-Z_{1x}^{(n-\frac{1}{2})}(i,j,k)+X_{1z}^{(n+\frac{1}{2})}(i,j,k)-X_{1z}^{(n-\frac{1}{2})}(i,j,k)\right]$$
$$+\left[\frac{1}{\mu_r(i,j,k)}-\frac{1}{\mu_r(i-1,j,k)}\right]\frac{1}{h_x(i-1)}\times$$
$$\left[Z_{1x}^{(n+\frac{1}{2})}(i-1,j,k)-Z_{1x}^{(n-\frac{1}{2})}(i-1,j,k)+X_{1z}^{(n+\frac{1}{2})}(i-1,j,k)-X_{1z}^{(n-\frac{1}{2})}(i-1,j,k)\right]$$
$$-\left[\frac{1}{\mu_r(i,j+1,k)}-\frac{1}{\mu_r(i,j,k)}\right]\frac{1}{h_y(j)}\times$$
$$\left[Y_{1z}^{(n+\frac{1}{2})}(i,j,k)-Y_{1z}^{(n-\frac{1}{2})}(i,j,k)+Z_{1y}^{(n+\frac{1}{2})}(i,j,k)-Z_{1y}^{(n-\frac{1}{2})}(i,j,k)\right]$$
$$-\left[\frac{1}{\mu_r(i,j,k)}-\frac{1}{\mu_r(i,j-1,k)}\right]\frac{1}{h_y(j-1)}\times$$
$$\left.\left[Y_{1z}^{(n+\frac{1}{2})}(i,j-1,k)-Y_{1z}^{(n-\frac{1}{2})}(i,j-1,k)+Z_{1y}^{(n+\frac{1}{2})}(i,j-1,k)-Z_{1y}^{(n-\frac{1}{2})}(i,j-1,k)\right]\right\} \quad (5.38)$$

The divergence is located at the bottom left corner of the discretization cell in Fig. 5.1. The permittivity is always defined at the same locations as the components of the vector potential itself.

In the special case of layered dielectrics sharing the same normal, say in the *z*-direction, the divergence of the vector potential may not be calculated explicitly. The update equations (5.26), (5.27), (5.29) and (5.30) will remain unchanged, but equations (5.28) and (5.31) will have the form:

$$Z_{1z}^{(n+1/2)}(i,j,k)=\left(\frac{1-r_z}{1+r_z}\right)Z_{1z}^{(n-1/2)}(i,j,k)+\frac{1}{2c(1+r_z)\alpha_z h_z(k)}\cdot\frac{2}{\left[\varepsilon_r(i,j,k+1)+\varepsilon_r(i,j,k)\right]}\times\left[A_z^{(n)}(i,j,k+1)-A_z^{(n)}(i,j,k)\right] \tag{5.39}$$

$$Z_{2z}^{(n+1/2)}(i,j,k)=\left(\frac{1-r_z}{1+r_z}\right)Z_{2z}^{(n-1/2)}(i,j,k)+\frac{\varepsilon_r(i,j,k)}{(1+r_z)\alpha_z h_z(k-1)\Delta l_{\min}}\times\left[Z_{1z}^{(n+1/2)}(i,j,k)-Z_{1z}^{(n+1/2)}(i,j,k-1)-Z_{1z}^{(n-1/2)}(i,j,k)+Z_{1z}^{(n-1/2)}(i,j,k-1)\right] \tag{5.40}$$

The update equation for the finite-difference expression of the vector-potential first-order time derivative will be reduced to:

$$D_t A_z^{(n+\frac{1}{2})}(i,j,k)=D_t A_z^{(n-\frac{1}{2})}(i,j,k)+\frac{\Delta l_{\min}^2}{4\mu_r\varepsilon_r}\cdot\left[\frac{1}{\Delta t}\mathcal{L}\{A_z\}^{(n)}+\mu J_z\right] \tag{5.41}$$

5.3.3 IPML for the WETD in lossy inhomogeneous media

In the general case of lossy inhomogeneous medium, the auxiliary variables are calculated as in the case of homogeneous medium, through equations (5.26) to (5.31). The update equation for the finite-difference expression for the vector-potential first-order time derivative, $D_t A_z^{(n+1/2)}(i,j,k)=A_z^{(n+1)}(i,j,k)-A_z^{(n)}(i,j,k)$, will be changed to the form:

$$
\begin{aligned}
D_t A_z^{(n+\frac{1}{2})}(i,j,k) = & \left(\frac{1-r_0}{1+r_0}\right) D_t A_z^{(n-\frac{1}{2})}(i,j,k) + \\
& \frac{\Delta l_{\min}^2}{4\mu_r \varepsilon_r (1+r_0)} \cdot \left[\frac{1}{\Delta t}\mathcal{L}\{A_z\}^{(n)} + \mu J_z\right] \\
& + \frac{\Delta l_{\min}}{8(1+r_0)} M_{\mu\varepsilon}^{(n)}(i,j,k) \\
& + \frac{\Delta l_{\min}\mu_0}{8(1+r_0)} \left\{ \frac{\Phi^{(n)}(i,j,k)}{h_z(k-1)} \left[\frac{\sigma(i,j,k)}{\varepsilon_r(i,j,k)} - \frac{\sigma(i,j,k-1)}{\varepsilon_r(i,j,k-1)}\right] \right. \\
& \left. + \frac{\Phi^{(n)}(i,j,k+1)}{h_z(k)} \left[\frac{\sigma(i,j,k+1)}{\varepsilon_r(i,j,k+1)} - \frac{\sigma(i,j,k)}{\varepsilon_r(i,j,k)}\right] \right\} \\
& - \frac{c}{4(1+r_0)\varepsilon_r(i,j,k)} N_{\mu}^{(n)}(i,j,k)
\end{aligned}
\tag{5.42}
$$

where

$\mathcal{L}\{A_z\}^{(n)}$ is defined in (5.33);

$r_0 = \dfrac{\sigma\Delta t}{2\varepsilon}$ is a numerical constant.

The divergence $divA$ is calculated as in equation (5.36); $M_{\mu\varepsilon}^{(n)}(i,j,k)$ and $N_{\mu}^{(n)}(i,j,k)$ as in (5.37) and (5.38), respectively. The scalar potential has the following update equation:

$$
\Phi^{(n)}(i,j,k) = \frac{1-r}{1+r}\Phi^{(n-1)}(i,j,k) - \frac{1}{\mu\varepsilon(1+r)} divA^{(n)}(i,j,k) \tag{5.43}
$$

It is calculated at points located at the bottom left corner of the discretization cell in Fig. 5.1, same as the location of the divergence $divA$. In equation (5.43), the constant r is $r = \dfrac{\sigma\Delta t}{2\varepsilon}$.

Here it is again reminded that in equations (5.42) and (5.43) the constitutive parameters σ, μ and ε are those of the lossy inhomogeneous medium, and they are not associated with the IPML variables.

5.4 Exponential time stepping

As already mentioned in Chapter 3, in high-loss media such as the PML, the above standard time-stepping scheme can be replaced by the exponential time stepping algorithm, proposed by Holland (1994). Below, that concept is developed and applied in the setting of the coordinate-stretching approach to the case of IPML for the WETD.

As before, the update equation for any of the variables is regarded as a first order ODE with respect to time, for example take the first of the equations (5.7):

$$\frac{\partial X_{1z}}{\partial t} = -\frac{\sigma_x}{\varepsilon\alpha_x} X_{1z} + \frac{1}{\alpha_x}\frac{\partial A_z}{\partial x} \tag{5.44}$$

Its homogeneous part is considered to be the result of the right-hand side contribution over the previous time steps, excluding the contribution of the spatial derivative of the present time step:

$$X_{1z_{(\text{hom})}} = Ce^{-\frac{\sigma_x t}{\varepsilon\alpha_x}} \tag{5.45}$$

Therefore the decay during the last time step is:

$$X_{1z_{(\text{hom})}}^{\left(n+\frac{1}{2}\right)} = e^{-\frac{\sigma_x \Delta t}{\varepsilon\alpha_x}} X_{1z_{(\text{hom})}}^{\left(n-\frac{1}{2}\right)} \tag{5.46}$$

The particular solution is considered to be the result of the right-hand side contribution of the spatial derivative during the present time step, which for the auxiliary variables starts half a time step before the time step for the vector potential. The time t' is measured from its beginning, so that for $0 \le t' \le \Delta t$:

$$X_{1z_{(part)}}(t') = \left[\frac{1}{\alpha_x} \frac{\partial A_z}{\partial x} \int e^{\int \frac{\sigma_x dt'}{\varepsilon \alpha_x}} dt' + C \right] e^{-\int \frac{\sigma_x dt'}{\varepsilon \alpha_x}} \tag{5.47}$$

From (5.47) the constant C can be evaluated at time $t' = 0$. Finally, the general solution at the end of the present time step will be a sum of the homogeneous and the particular solution where the spatial derivative is taken as an average value at the middle of the time step:

$$X_{1z}^{(n+\frac{1}{2})} = e^{-\frac{\sigma_x \Delta t}{\varepsilon \alpha_x}} X_{1z}^{(n-\frac{1}{2})} + \frac{\varepsilon [1 - e^{-\frac{\sigma_x \Delta t}{\varepsilon \alpha_x}}]}{\sigma_x \Delta x(i)} \left[A_z^{(n)}(i+1, j, k) - A_z^{(n)}(i, j, k) \right] \tag{5.48}$$

Similarly, following the same steps as above, the exponential time-stepping formula for the second auxiliary variable X_{2z} is obtained:

$$\begin{aligned} X_{2z}^{(n+\frac{1}{2})} = e^{-\frac{\sigma_x \Delta t}{\varepsilon \alpha_x}} X_{2z}^{(n-\frac{1}{2})} + \frac{\varepsilon [1 - e^{-\frac{\sigma_x \Delta t}{\varepsilon \alpha_x}}]}{\sigma_x \Delta x(i-1) \Delta t} \cdot \\ \left[X_{1z}^{(n+1/2)}(i, j, k) - X_{1z}^{(n+1/2)}(i-1, j, k) \right. \\ \left. - X_{1z}^{(n-1/2)}(i, j, k) + X_{1z}^{(n-1/2)}(i-1, j, k) \right] \end{aligned} \tag{5.49}$$

5.5 Modified IPML variable profiles

The performance of the numerical absorber depends crucially on the growth profile of the PML variables: the PML conductivity σ_ξ and the PML loss factor α_ξ ($\xi = x, y, z$), which takes care of the evanescent mode attenuation. It also depends on other parameters, like the user-defined reflection coefficient, the material parameters of the medium, etc. Initially, a variety of profiles already available in the literature were implemented, such as those given by Berenger (1994), B. Chen *et al.* (1995) and J. Fang *et al.* (1996). However, the PML is now integrated with the wave equation, which is a second-order PDE. The conventional PML profiles did not perform well and they had to be modified and optimized. It is well known that greater rates of attenuation can be attained by choosing larger increments in the values of the PML parameters σ_ξ and α_ξ. Larger attenuation means decreased thickness of the PML absorber, and, therefore, less computational load. However, a larger attenuation rate gives rise to spurious numerical reflections. A compromise must be reached between insufficient and excessive attenuation. It has been observed that the first few PMLs cause the greatest numerical reflections (due to the stepwise PML conductivity jumps in the discrete space). That is why the increments in the conductivity in the first few PMLs have to be small. However, in order to reach sufficient attenuation, the PML conductivity has to increase significantly towards the final layer. If a broadband performance is a necessity, the rate of attenuation

has to be decreased in comparison to the case of the narrow-band requirements. The number of PMLs is in direct relation with the rate of conductivity increase. The slower the conductivity rises, the thicker the absorber must be to ensure broadband performance.

To meet these competing requirements, the best performance, in terms of low reflections in a broad frequency band, was achieved when *a new degree of freedom* was incorporated in the definition of the PML variable profiles. As mentioned in section 3.3.2, to the author's knowledge, this has never been considered before and represents a problem-independent approach to the improvement and optimization of the PML performance. Namely, the PML conductivity σ_ξ is now proposed to increase by an order β faster than the order of the PML loss factor α_ξ :

$$\sigma_\xi(\rho) = \sigma_{\max}\left(\frac{\rho}{\delta_\xi}\right)^{n+\beta}, \quad \beta \in [1,3], \quad \xi = x, y, z \tag{5.50}$$

$$\alpha_\xi(\rho) = 1 + \varepsilon_{\max}\left(\frac{\rho}{\delta_\xi}\right)^{n}, \quad \rho \in [0, \delta_\xi], \quad \xi = x, y, z \tag{5.51}$$

Here, β is the user-defined new degree of freedom added to the order n of increase of the PML conductivity σ_ξ, whose optimal values in all experiments are shown to be between 1 and 3; δ_ξ is the PML thickness in the ξ-direction; ρ is the depth in PML; R_0 is the chosen reflection coefficient at normal incidence,

and $\varepsilon_{\max}$ is a chosen constant, generally between 0 and 5. The theoretical reflection coefficient at normal incidence is (see Chapter 3):

$$R_0 = \exp\left(-\frac{2}{\varepsilon_0 \varepsilon_r c} \int_0^{\delta} \sigma(\rho)\, d\rho \right) \tag{5.52}$$

From (5.52) the PML conductivity parameter $\sigma_{\max}$ as a function of the user defined R_0 is easily obtained as:

$$\sigma_{\max} = \frac{(n+\beta+1)\varepsilon_0 \varepsilon_r c \;\; \ln\left(R_0^{-1}\right)}{2\delta}, \;\; \beta \in [1,3] \tag{5.53}$$

In Chapter 6 it will be shown that increasing the power rate of the PML conductivity σ_{ξ} by one ($\beta = 1$), while keeping the power rate of α_{ξ} the same, has the effect of broadening the frequency band in which the reflections are below -60 dB. An increase in the power rate of σ_{ξ} by two ($\beta = 2$) reduces the number of PMLs by additional 4 or 5 cells while the reflections can be still kept at the prescribed level, which is usually below -60 dB (corresponding to 0.1 % of the magnitude of the incident wave).

Note that a simultaneous increase in the power rate *n* of both σ_{ξ} and α_{ξ}, as it is done in most PML absorbers, does not improve the bandwidth. It has the effect of increasing the spurious numerical reflections, thereby degrading the absorber's performance. An extensive comparison between the proposed IPML variable profile and the conventional PML profiles is provided in Chapter 6.

The PML conductivity and PML loss factor participate in the coefficients r_i, $i = x, y, z$, see equations (5.26) to (5.31). In Fig. 5.2 these coefficients with the proposed IPML conductivity and loss factor profiles are shown for $\beta = 1$ and $\beta = 2$, together with the PML conductivity profiles of Berenger (1994) and GPML of J. Fang *et al.* (1995). All other PML parameters are maintained the same for the three absorbers: the PML thickness is 10 cells, $R_0 = 10^{-4}$, $n = 2$.

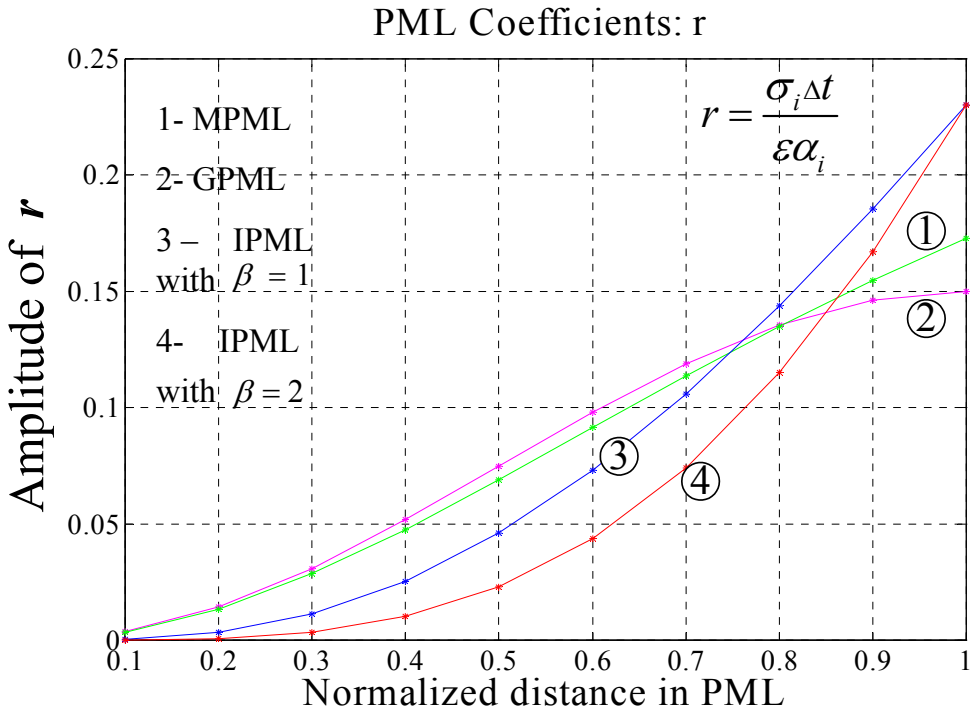

Fig. 5.2. The PML conductivity profiles: 1 – GPML, 2 – Berenger, 3 – current profile $\beta = 1$, 4 – current profile $\beta = 2$. In all cases, $N_{PML} = 10$, $R_0 = 10^{-4}$, $n = 2$.

From the example in Fig. 5.2 the reason for the better performance of the proposed IPML can be seen; namely, the proposed coefficients increase more gradually in the first layers in the absorber, which contributes to less numerical reflections, while their values become greater at the end of it, which means less electromagnetic energy reaches the end of the absorber and is reflected back.

5.6 Modified IPML terminations

Another means to improve the PML performance is to replace the perfect electric conductor (PEC) wall that usually terminates the PML medium, with a low-cost simple ABC, which will be referred to as *a single-layer ABC*. In this work, three types of single-layer absorbers have been investigated to terminate the perfectly matched layer.

First, the lossy one-way wave equation first-order ABC was implemented. Rappaport (1996) first reported the improvement of PML absorbers with this termination.

Second, a lossy version of Mur's second-order ABC was developed, to be used as an efficient PML termination [the lossless original version is in Mur (1981)].

The third PML termination, which is developed and investigated in this research, is a lossy version of Litva's second-order dispersive boundary condition (DBC) [Bi *et al.* (1992)].

The choice of these termination layers has been dictated by the following considerations:

1. The simplicity of implementation,
2. The minimal additional computational overhead, and
3. The discretization possible with no additional memory requirements.

Here, a unified approach will be described to the derivation of lossy PML terminations from existing single-layer ABCs, which were originally designed to terminate loss-free computational domains. The EM potential wave equation (5.1) inside the PML region has its EM constitutive parameters such that they must satisfy the constraint for reflection-free propagation; see e.g. Berenger (1994):

$$\frac{\sigma}{\varepsilon} = \frac{\sigma_m}{\mu} = \frac{1}{\tau} \tag{5.54}$$

where τ is the dielectric (and magnetic) relaxation constant. Having (5.54) in mind, equation (5.1) can be written in the factored form:

$$(L^2 - \mu\varepsilon\nabla^2)\{\vec{A}\} = 0 \tag{5.55}$$

where $L = \partial/\partial t + \tau^{-1}$. In (5.55) it is implied that there are no sources present in the PML region. Equation (5.55) is the basis for all first and second order lossy ABCs considered here.

In the direction of propagation (and absorption), say the ξ-direction ($\xi = x,\ y,\ z$), the 1-D version of equation (5.55) is:

$$L^+ L^- \{\vec{A}\} = 0 \tag{5.56}$$

where the wave operators L^+ and L^-, corresponding to forward and backward propagation, respectively, are defined as:

$$L^+ = L + v_\xi \partial / \partial \xi \tag{5.57}$$

$$L^- = L - v_\xi \partial / \partial \xi \tag{5.58}$$

Here, v_ξ is the velocity of propagation in the ξ-direction. Taking only the operator in (5.57), which describes the forward (one-way) propagating wave, one obtains the lossy one-way wave equation ABC, proposed first by Rappaport (1995):

$$\frac{1}{v_\xi}\left(\frac{\partial \vec{A}}{\partial t} + \frac{\vec{A}}{\tau}\right) + \frac{\partial \vec{A}}{\partial \xi} = 0 \tag{5.59}$$

in which the first order approximation of the velocity of propagation in the ξ-direction is used, namely $v_\xi = v = 1/\sqrt{\mu\varepsilon}$.

To derive the lossy version of Mur's second order ABC, the general procedure given by Mur (1981) is followed, while substituting the $\partial / \partial t$ derivative by the lossy operator $(\partial / \partial t + \tau^{-1})$ in (5.55). First, the second order approximation of the propagation velocity v_ξ in ξ-direction is expressed through the propagation velocities in the other two directions v_η, v_ζ and the propagation velocity in the structure v, as follows:

$$\frac{1}{v_\xi^2}+\frac{1}{v_\eta^2}+\frac{1}{v_\zeta^2}=\frac{1}{v^2}\ \Rightarrow$$

$$\frac{1}{v_\xi}=\frac{1}{v}\sqrt{1-\left(\frac{v}{v_\eta}\right)^2-\left(\frac{v}{v_\zeta}\right)^2}\approx\frac{1}{v}\left\{1-\frac{1}{2}\left[\left(\frac{v}{v_\eta}\right)^2+\left(\frac{v}{v_\zeta}\right)^2\right]\right\} \tag{5.60}$$

From (5.60) $v_\eta,\ v_\zeta$ are expressed as:

$$\frac{1}{v_\eta^2}+\frac{1}{v_\zeta^2}=\frac{2}{v}\left(\frac{1}{v}-\frac{1}{v_\xi}\right) \tag{5.61}$$

The WETD (5.55) is then expanded in the form:

$$\left[\frac{1}{v^2}\left(\frac{\partial}{\partial t}+\frac{1}{\tau}\right)^2-\left(\frac{\partial^2}{\partial\xi^2}+\frac{\partial^2}{\partial\eta^2}+\frac{\partial^2}{\partial\zeta^2}\right)\right]\vec{A}=0\ \Rightarrow$$

$$\left[\left(\frac{1}{v_\xi^2}+\frac{1}{v_\eta^2}+\frac{1}{v_\zeta^2}\right)\left(\frac{\partial}{\partial t}+\frac{1}{\tau}\right)^2-\left(\frac{\partial^2}{\partial\xi^2}+\frac{\partial^2}{\partial\eta^2}+\frac{\partial^2}{\partial\zeta^2}\right)\right]\vec{A}=0\ \Rightarrow \tag{5.62}$$

$$\left[\frac{1}{v_\xi^2}\left(\frac{\partial}{\partial t}+\frac{1}{\tau}\right)^2-\frac{\partial^2}{\partial\xi^2}\right]\vec{A}=0=-\left[\left(\frac{1}{v_\eta^2}+\frac{1}{v_\zeta^2}\right)\left(\frac{\partial}{\partial t}+\frac{1}{\tau}\right)^2-\left(\frac{\partial^2}{\partial\eta^2}+\frac{\partial^2}{\partial\zeta^2}\right)\right]\vec{A}$$

where (5.56) is also used. From here, after substituting (5.61) in the right-hand side of (5.62), the following equation is obtained:

$$\left[\frac{2}{v}\left(\frac{1}{v}-\frac{1}{v_\xi}\right)\left(\frac{\partial}{\partial t}+\frac{1}{\tau}\right)^2-\left(\frac{\partial^2}{\partial\eta^2}+\frac{\partial^2}{\partial\zeta^2}\right)\right]\vec{A}=0 \tag{5.63}$$

Next, from the one-way WE (5.59):

$$\frac{1}{v_\xi}\left(\frac{\partial\vec{A}}{\partial t}+\frac{\vec{A}}{\tau}\right)=-\frac{\partial\vec{A}}{\partial\xi} \tag{5.64}$$

After substitution of (5.64) into (5.63) and dividing by 2, the second-order approximation of the lossy one-way WE is obtained:

$$\left[\frac{1}{v^2}\left(\frac{\partial}{\partial t}+\frac{1}{\tau}\right)^2-\frac{1}{2}\left(\frac{\partial^2}{\partial\eta^2}+\frac{\partial^2}{\partial\zeta^2}\right)+\frac{1}{v}\frac{\partial}{\partial\xi}\left(\frac{\partial}{\partial t}+\frac{1}{\tau}\right)\right]\vec{A}=0 \tag{5.65}$$

Thus, this termination is obtained by expanding (5.65) as:

$$\frac{\partial^2\vec{A}}{\partial t^2}=-\frac{2}{\tau}\frac{\partial\vec{A}}{\partial t}-v\frac{\partial^2\vec{A}}{\partial\xi\partial t}-\frac{v}{\tau}\frac{\partial\vec{A}}{\partial x}-\frac{1}{\tau^2}\vec{A}+\frac{v^2}{2}\left(\frac{\partial^2\vec{A}}{\partial\eta^2}+\frac{\partial^2\vec{A}}{\partial\zeta^2}\right) \tag{5.66}$$

where $v=(\mu\varepsilon)^{-1/2}$, and (η,ζ) are the transverse with respect to ξ coordinates.

Similarly, from the original second order DBC of Bi *et al.* (1992),

$$\left(\frac{1}{v_{1\xi}}\frac{\partial}{\partial t}+\frac{\partial}{\partial\xi}\right)\left(\frac{1}{v_{2\xi}}\frac{\partial}{\partial t}+\frac{\partial}{\partial\xi}\right)\{\vec{A}\}=0 \tag{5.67}$$

its lossy version is obtained as follows:

$$\left[\frac{1}{v_{1\xi}}\left(\frac{\partial}{\partial t}+\frac{1}{\tau}\right)+\frac{\partial}{\partial\xi}\right]\left[\frac{1}{v_{2\xi}}\left(\frac{\partial}{\partial t}+\frac{1}{\tau}\right)+\frac{\partial}{\partial\xi}\right]\{\vec{A}\}=0 \tag{5.68}$$

This last equation is expanded in a similar way as above to give the lossy second order DBC:

$$\frac{\partial^2\vec{A}}{\partial t^2}=-\frac{2}{\tau}\frac{\partial\vec{A}}{\partial t}-\left(v_{1\xi}+v_{2\xi}\right)\frac{\partial^2\vec{A}}{\partial\xi\partial t}-\frac{\left(v_{1\xi}+v_{2\xi}\right)}{\tau}\frac{\partial\vec{A}}{\partial x}-\frac{1}{\tau^2}\vec{A}+v_{1\xi}v_{2\xi}\frac{\partial^2\vec{A}}{\partial\xi^2} \tag{5.69}$$

where $v_{1\xi}$ and $v_{2\xi}$ are the velocities in the direction of propagation (absorption), corresponding to two different frequencies in the band of interest.

Below, the discretized forms of the three single-layer PML terminations will be shown in the case of $\xi = x$ for the A_ζ component of the potential, where $\zeta = x, y, z$.

5.6.1 One-way wave equation (WE) termination

From the lossy one-way wave equation (5.59) used to terminate the PML medium, say in the *x*-direction, its discretized version is obtained in a similar way as in Rappaport (1996):

$$A_\zeta^{(n+1)}(i+1,j,k) = \frac{1-r_x-r_{0x}}{1+r_x} A_\zeta^{(n)}(i+1,j,k) + \frac{r_{0x}}{1+r_x} A_\zeta^{(n)}(i,j,k) \tag{5.70}$$

where the following constants are used:

$$r_x = \frac{\sigma_x \Delta t}{2\varepsilon\alpha_x};\ r_{0x} = \frac{v\ \Delta t}{\Delta x\sqrt{\alpha_x}};\ v = \frac{1}{\sqrt{\mu\varepsilon}} \tag{5.71}$$

5.6.2 Mur's second order ABC termination

The lossy version of Mur's second order ABC from (5.66) is discretized without averaging with respect to spatial location in the second order spatial derivatives in the transverse plane, since the numerical experiments show no significant improvement in the results if averaging is used. No previous time step values are necessary to store in the proposed version:

$$
\begin{aligned}
D_t A_\zeta^{(n+\frac{1}{2})}(i+1,j,k) = {} & \frac{1-r_{0x}}{1+r_x+r_{0x}} D_t A_\zeta^{(n-\frac{1}{2})}(i+1,j,k) \\
& + \frac{r_{0x}}{1+r_x+r_{0x}} D_t A_\zeta^{(n+\frac{1}{2})}(i,j,k) \\
& - \frac{r_x r_{0x}+r_x^2}{1+r_x+r_{0x}} A_\zeta^{(n)}(i+1,j,k) + \frac{r_x r_{0x}}{1+r_x+r_{0x}} A_\zeta^{(n)}(i,j,k) \\
& + \frac{\Delta t^2 v^2}{2\Delta y^2\left(1+r_x+r_{0x}\right)} \times \\
& \left[A_\zeta^{(n)}(i+1,j+1,k) - 2A_\zeta^{(n)}(i+1,j,k) + A_\zeta^{(n)}(i+1,j-1,k) \right] \\
& + \frac{\Delta t^2 v^2}{2\Delta z^2\left(1+r_x+r_{0x}\right)} \times \\
& \left[A_\zeta^{(n)}(i+1,j,k+1) - 2A_\zeta^{(n)}(i+1,j,k) + A_\zeta^{(n)}(i+1,j,k-1) \right]
\end{aligned}
\tag{5.72}
$$

In equation (5.72) the coefficients r_x and r_{0x} are the same as in (5.71). The potential itself is calculated as:

$$
A_\zeta^{(n+1)}(i+1,j,k) = A_\zeta^{(n)}(i+1,j,k) + D_t A_\zeta^{(n+\frac{1}{2})}(i+1,j,k) \tag{5.73}
$$

5.6.3 Second order DBC termination

The DBC equation (5.69), written for propagation/absorption in the *x*-direction is:

$$
\begin{aligned}
\frac{\partial^2 A_\zeta}{\partial t^2} = {} & -\frac{2}{\tau}\frac{\partial A_\zeta}{\partial t} - \left(v_{1x}+v_{2x}\right)\frac{\partial^2 A_\zeta}{\partial x \partial t} - \frac{\left(v_{1x}+v_{2x}\right)}{\tau}\frac{\partial A_\zeta}{\partial x} \\
& - \frac{1}{\tau^2} A_\zeta - v_{1x} v_{2x} \frac{\partial^2 A_\zeta}{\partial x^2}
\end{aligned}
\tag{5.74}
$$

From here, the discretized version of this second order DBC (5.74) is easily obtained as:

$$
\begin{aligned}
D_t A_\zeta^{(n+\frac{1}{2})}(i+1,j,k) = {} & \frac{1-r_{Dx}}{1+r_x+r_{Dx}} D_t A_\zeta^{(n-\frac{1}{2})}(i+1,j,k) \\
& + \frac{r_{Dx}}{1+r_x+r_{Dx}} D_t A_\zeta^{(n+\frac{1}{2})}(i,j,k) \\
& - \frac{r_x r_{Dx}+r_x^2}{1+r_x+r_{Dx}} A_\zeta^{(n)}(i+1,j,k) \\
& + \frac{r_x r_{Dx}}{1+r_x+r_{Dx}} A_\zeta^{(n)}(i,j,k) + \frac{v_{1x} v_{2x} \Delta t^2}{\alpha \Delta x^2 \left(1+r_x+r_{Dx}\right)} \times \\
& \left[A_\zeta^{(n)}(i+1,j,k) - 2A_\zeta^{(n)}(i,j,k) + A_\zeta^{(n)}(i-1,j,k) \right]
\end{aligned}
\tag{5.75}
$$

where for convenience the following coefficients have been defined:

$$
r_x = \frac{\sigma \Delta t}{2\varepsilon \alpha_x}; \quad r_{Dx} = \frac{\left(v_{1x}+v_{2x}\right)\Delta t}{\Delta x \sqrt{\alpha_x}}
$$

Finally, the potential is calculated as:

$$
A_\zeta^{(n+1)}(i+1,j,k) = A_\zeta^{(n)}(i+1,j,k) + D_t A_\zeta^{(n+\frac{1}{2})}(i+1,j,k) \tag{5.76}
$$

Chapter 6

Validation and Discussion

The numerical algorithms developed here use only one set of update equations to handle all computational regions, no matter if they are regular FDTD/WETD or PML regions. A 3-dimensional non-uniform rectangular grid pattern is determined, depending on the specific structure to save computational resources, while maintaining satisfactory (prescribed) accuracy. In particular, the algorithms can characterize different material regions by simply assigning different material parameters to the corresponding grid points. The constitutive parameters are always defined at the respective locations of the field/potential components. At material interfaces, an average of the constitutive parameters is used.

The experiments will show that the proposed modified profiles of the PML variables offer superior performance (lower reflections in a broader frequency band) in comparison with commonly used PML profiles both for the case of the FDTD solution to Maxwell's equations, and for the case of the time-domain wave equation for the vector potentials. The influence of new types

termination walls of the PML on its overall performance is investigated and the best options available are singled out.

6.1 Normalization of the split-field components for the IPML-FDTD

For numerical stability, it is always beneficial if the program variables are of the same order of magnitude; and preferably dimensionless wherever possible. Therefore a normalization of the E-field components is performed:

$$E_{(original)} = \sqrt{\frac{\mu_0}{\varepsilon_0}} \hat{E}_{(program)} \tag{6.1}$$

No normalization is necessary for the H-field components, i.e.:

$$H_{(original)} = \hat{H}_{(program)} \tag{6.2}$$

Next, the spatial increments Δx, Δy, Δz are expressed in terms of the minimal spatial increment Δl_{min}:

$$\Delta l_{\min} = \min_{\substack{1 \le i \le n_{x\max} \\ 1 \le j \le n_{y\max} \\ 1 \le k \le n_{z\max}}} \left(\Delta x(i), \Delta y(j), \Delta z(k) \right) \tag{6.3}$$

and the dimensionless quantities $h_x(i)$, $h_y(j)$, $h_z(k)$ as:

$$\begin{aligned} \Delta x(i) &= h_x(i) \Delta l_{\min}; \quad h_x(i) \ge 1, \ 1 \le i \le n_{x\max} \\ \Delta y(j) &= h_y(j) \Delta l_{\min}; \ h_y(j) \ge 1, \ 1 \le j \le n_{y\max} \\ \Delta z(k) &= h_z(k) \Delta l_{\min}; \ h_z(k) \ge 1, \ 1 \le k \le n_{z\max} \end{aligned} \tag{6.4}$$

The time step is chosen in accordance with Courant's stability condition as

$$\Delta t = \Delta l_{\min} / 2c;\ \ c = 1/\sqrt{\mu_0 \varepsilon_0} \tag{6.5}$$

The procedure to derive an update normalized IPML-FDTD equation will be shown for one of the split-field components, say E_{xy}. The application of the normalization (6.1), (6.2) in the defining equation for E_{xy}, results in the normalized equation:

$$\frac{\partial \hat{E}_{xy}}{\partial t} + \frac{\sigma_y}{\varepsilon_0 \alpha_y} \hat{E}_{xy} = \frac{c}{\alpha_y} \frac{\partial \left(\hat{H}_{zx} + \hat{H}_{zy} \right)}{\partial y} \tag{6.6}$$

The discretized version of (6.6) is obtained as follows (see details in Section 3.4.1). The homogeneous solution is:

$$\hat{E}^{(n+1)}_{xy_{(\text{hom})}} = e^{-\frac{\sigma_y \Delta t}{\varepsilon_0 \alpha_y}} \hat{E}^{(n)}_{xy_{(\text{hom})}} \tag{6.7}$$

and the particular solution is

$$\begin{aligned} \hat{E}_{xy_{(part)}}(t') &= \left[\frac{c}{\alpha_y} \frac{\partial \left(\hat{H}_{zx} + \hat{H}_{zy} \right)}{\partial y} \int e^{\int \frac{\sigma_y}{\varepsilon_0 \alpha_y} dt'} dt' + C \right] e^{-\int \frac{\sigma_y}{\varepsilon_0 \alpha_y} dt'} \\ &= \frac{c \varepsilon_0}{\sigma_y} \frac{\partial \left(\hat{H}_{zx} + \hat{H}_{zy} \right)}{\partial y} + C e^{-\frac{\sigma_y t'}{\varepsilon_0 \alpha_y}} \end{aligned} \tag{6.8}$$

where the time t' is measured from the beginning of the n^{th} step. Evaluate (6.8) at $t' = 0$ to obtain C:

$$C = -\frac{c \varepsilon_0}{\sigma_y} \frac{\partial \left(\hat{H}_{zx} + \hat{H}_{zy} \right)}{\partial y}$$

and then the particular solution

$$\hat{E}_{xy_{(part)}}(t') = \frac{c\varepsilon_0}{\sigma_y}\frac{\partial\left(\hat{H}_{zx}+\hat{H}_{zy}\right)}{\partial y}\left(1-e^{-\frac{\sigma_y t'}{\varepsilon_0\alpha_y}}\right) \tag{6.9}$$

Now (6.9) is evaluated at $t' = \Delta t$ to obtain $\hat{E}^{n+1}_{xy_{(part)}}$ and the update normalized equation as a sum of the homogeneous and the particular solutions:

$$\hat{E}^{n+1}_{xy}(i,j,k) = e^{-\frac{\sigma_y(j)\Delta t}{\varepsilon_0\alpha_y(j)}}\hat{E}^{n}_{xy}(i,j,k) + \frac{c\varepsilon_0\left[1-e^{-\frac{\sigma_y(j)\Delta t}{\varepsilon_0\alpha_y(j)}}\right]}{\sigma_y(j)\Delta l_{\min}}\times \tag{6.10}$$
$$\left[\frac{\hat{H}^{n+\frac{1}{2}}_{zx}(i,j,k)-\hat{H}^{n+\frac{1}{2}}_{zx}(i,j-1,k)}{h_{y_H}(j)}+\frac{\hat{H}^{n+\frac{1}{2}}_{zy}(i,j,k)-\hat{H}^{n+\frac{1}{2}}_{zy}(i,j-1,k)}{h_{y_H}(j)}\right]$$

where

$$h_{y_H}(j) = \frac{h_y(j)+h_y(j+1)}{2}$$

For convenience, define:

$$r_y(j) = \frac{\sigma_y(j)\Delta t}{\varepsilon_0\alpha_y(j)}$$
$$= \frac{\left(n+\beta+1\right)\varepsilon_0 c\cdot\ln\left(\frac{1}{R(0)}\right)\left(\frac{\rho(j)}{\delta_y}\right)^{n+\beta}}{2\delta_y}\cdot\frac{\Delta l_{\min}}{2c\varepsilon_0\left[1+\varepsilon_{\max}\left(\frac{\rho(j)}{\delta_y}\right)^{n}\right]}$$
$$= \frac{\left(n+\beta+1\right)\cdot\ln\left(\frac{1}{R(0)}\right)\left(\frac{\rho(j)}{\delta_y}\right)^{n+\beta}}{4\left(\frac{\delta_y}{\Delta l_{\min}}\right)\left[1+\varepsilon_{\max}\left(\frac{\rho(j)}{\delta_y}\right)^{n}\right]} \tag{6.11}$$

and rearrange the coefficient before the spatial derivative:

$$\frac{c\varepsilon_0\left(1-e^{-\frac{\sigma_y(j)\Delta t}{\varepsilon_0\alpha_y(j)}}\right)}{\sigma_y(j)\Delta l_{min}} = \frac{c\varepsilon_0\left(1-e^{-\frac{\sigma_y(j)\Delta t}{\varepsilon_0\alpha_y(j)}}\right)}{\sigma_y(j)2c\Delta t}$$
$$= \frac{\varepsilon_0\left(1-e^{-\frac{\sigma_y(j)\Delta t}{\varepsilon_0\alpha_y(j)}}\right)\frac{\sigma_y(j)}{\varepsilon_0\alpha_y(j)}}{2\sigma_y(j)\left(\frac{\sigma_y(j)\Delta t}{\varepsilon_0\alpha_y(j)}\right)} \tag{6.12}$$
$$= \frac{1-e^{-r_y(j)}}{r_y(j)}\frac{1}{2\alpha_y(j)}$$

Finally, with the notation (6.11) and (6.12), when a grid point is in IPML, the normalized update equation (6.10) becomes:

$$\hat{E}_{xy}^{n+1}(i,j,k) = e^{-r_y(j)}\hat{E}_{xy}^{n}(i,j,k) + \frac{1-e^{-r_y(j)}}{2\alpha_y(j)r_y(j)}\times \tag{6.13}$$
$$\left[\frac{\hat{H}_{zx}^{n+\frac{1}{2}}(i,j,k)-\hat{H}_{zx}^{n+\frac{1}{2}}(i,j-1,k)}{h_{y_H}(j)} + \frac{\hat{H}_{zy}^{n+\frac{1}{2}}(i,j,k)-\hat{H}_{zy}^{n+\frac{1}{2}}(i,j-1,k)}{h_{y_H}(j)}\right]$$

Two important conclusions can be drawn here.

1. From equation (6.13) it becomes obvious that the same update equation can be used both inside and outside of IPML, simply by postulating for grid points outside of IPML that

$$r_i = 0;\ \alpha_i = 1;\ i = x,y,z \tag{6.14}$$

since the latter reduces (6.13) to the original Yee's discretization. (Here L'Hopitalle's rule is used: $\lim_{r_y\to 0}\frac{1-e^{-r_y}}{r_y} = \lim_{r_y\to 0}\frac{e^{-r_y}}{1} = 1$.)

2. It should be noted that in the case when a dielectric material ends in the IPML medium, the permittivity of the free space should be replaced by the permittivity of that material; namely, the *H*-field derivatives are to be divided by the local relative dielectric constant ε_r in the update equations for the *E*-field components. The derivation follows the same routine as for the case of free space, with the free-space permittivity ε_0 replaced by the local dielectric material permittivity $\varepsilon = \varepsilon_0 \varepsilon_r$. Therefore, the update equation (6.13) becomes:

$$\hat{E}_{xy}^{n+1}(i,j,k) = e^{-r_y(j)} \hat{E}_{xy}^{n}(i,j,k) + \frac{1-e^{-r_y(j)}}{2\alpha_y(j) r_y(j) \varepsilon_r(i,j,k)} \times \left[\frac{\hat{H}_{zx}^{n+\frac{1}{2}}(i,j,k) - \hat{H}_{zx}^{n+\frac{1}{2}}(i,j-1,k)}{h_{y_H}(j)} + \frac{\hat{H}_{zy}^{n+\frac{1}{2}}(i,j,k) - \hat{H}_{zy}^{n+\frac{1}{2}}(i,j-1,k)}{h_{y_H}(j)} \right] \tag{6.15}$$

where the local dielectric constant $\varepsilon_r(i,j,k)$ is defined at the same locations as the *E*-field component. For the case when the *E*-field component lies on the interface of two dielectric materials of different dielectric constants, an average dielectric constant is to be used.

Equation (6.15) is to be used for the case when the same update equation is used throughout the whole computational region, both inside and outside of IPML, and there is a presence of dielectric materials of permittivity different from that of free-space.

The normalized update equations for the *H*-field components may be derived in a similar fashion. For example, to derive the update equation for the

component H_{xy}, one starts with the split-field equation, followed by the normalization (6.1), (6.2):

$$\mu_0\kappa_y\frac{\partial\hat{H}_{xy}}{\partial t}+\sigma_y^m\hat{H}_{xy}=-\frac{\partial\left(\sqrt{\frac{\mu_0}{\varepsilon_0}}\hat{E}_{zx}+\sqrt{\frac{\mu_0}{\varepsilon_0}}\hat{E}_{zy}\right)}{\partial y} \tag{6.16}$$

Then the IPML parameters in (6.16) are substituted using $\kappa_y=\alpha_y$ and $\sigma_y^m=\frac{\mu_0}{\varepsilon_0}\sigma_y$, to produce:

$$\frac{\partial\hat{H}_{xy}}{\partial t}+\frac{\sigma_y}{\varepsilon_0\alpha_y}\hat{H}_{xy}=-\frac{c}{\alpha_y}\frac{\partial\left(\hat{E}_{zx}+\hat{E}_{zy}\right)}{\partial y} \tag{6.17}$$

Equation (6.17) is discretized exactly in the same manner as the equation for the *E*-field components, leading to the update equation:

$$\hat{H}_{xy}^{n+\frac{1}{2}}(i,j,k)=e^{-r_y(j)}\hat{H}_{xy}^{n-\frac{1}{2}}(i,j,k)-\frac{1-e^{-r_y(j)}}{2\alpha_y(j)r_y(j)}\cdot \tag{6.18}$$
$$\left[\frac{\hat{E}_{zx}^n(i,j+1,k)-\hat{E}_{zx}^n(i,j,k)}{h_y(j)}+\frac{\hat{E}_{zy}^n(i,j+1,k)-\hat{E}_{zy}^n(i,j,k)}{h_y(j)}\right]$$

Fig. 6.1 shows a comparison of the coefficients $a_i=e^{-r_i}$ and $b_i=\frac{1-e^{-r_i}}{2\alpha_i r_i}$ for different PML variable profiles – the MPML of B. Chen et al (1995), the GPML of J. Fang et al (1996) and the current profiles for $\beta=1$ and $\beta=2$. It can be immediately seen that the coefficients before the spatial derivative are practically the same for all PMLs; but a better overall performance can be expected from the new profiles since the profile of the coefficient *a* is changing more gradually in

the first PMLs and reaches greater values towards the end of PML in comparison to MPML and GPML.

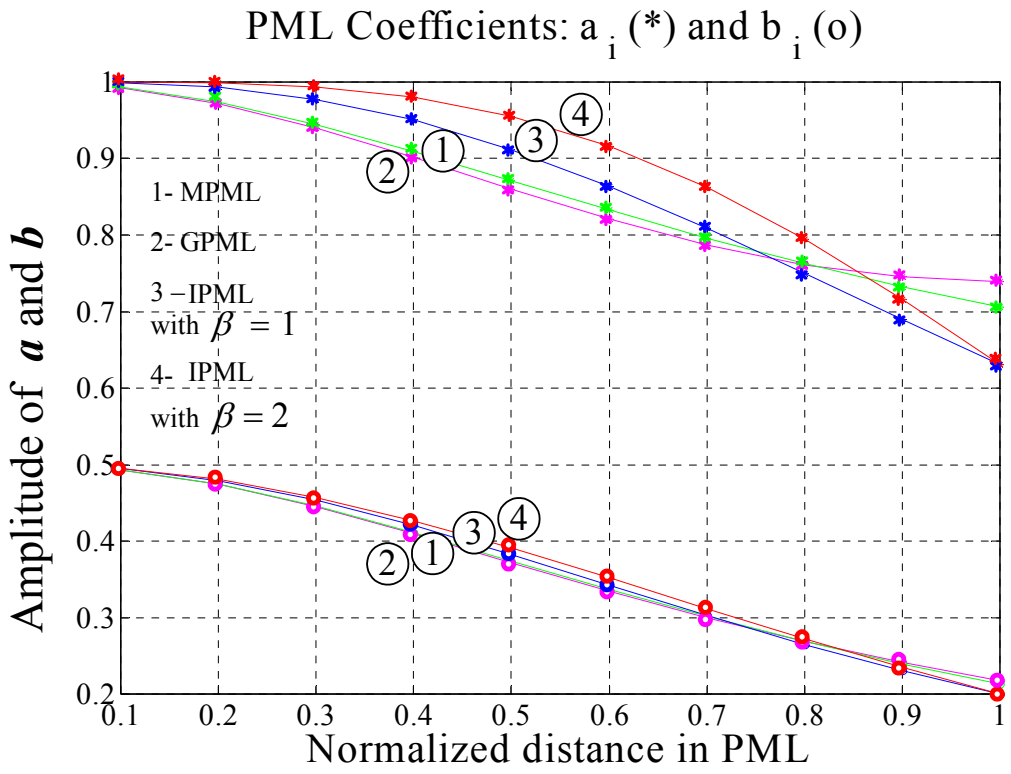

Fig. 6.1. PML coefficients comparison: 1 – MPML, 2 – GPML, 3 – IPML with $\beta = 1$; 4 – IPML with $\beta = 2$. With circles – the coefficients before the old value to be updated; with stars – the coefficients before the spatial derivative. In all cases, $R_0 = 10^{-4}$; $n = 2$; $N_{PML} = 10$.

6.2. Normalization of the components for the IPML-WETD

For stability purposes, the auxiliary variables are normalized and the following quantities are actually calculated:

$$\begin{aligned} \vec{x}_1 &= \vec{X}_1 \frac{\Delta l_{\min}}{\Delta t};\ \vec{x}_2 = \vec{X}_2 \frac{\Delta l_{\min}^2}{\Delta t} \\ \vec{y}_1 &= \vec{Y}_1 \frac{\Delta l_{\min}}{\Delta t};\ \vec{y}_2 = \vec{Y}_2 \frac{\Delta l_{\min}^2}{\Delta t} \\ \vec{z}_1 &= \vec{Z}_1 \frac{\Delta l_{\min}}{\Delta t};\ \vec{z}_2 = \vec{Z}_2 \frac{\Delta l_{\min}^2}{\Delta t} \end{aligned} \tag{6.19}$$

Here, $\Delta l_{\min}$ is the minimal spatial step in the non-uniform grid, as defined in (6.3) and the time step defined in (6.5) is chosen so that Courant's stability condition is satisfied, c is the highest velocity of light in the analyzed structure. Thus the spatial increments are expressed through the dimensionless coefficients $h_x(i)$, $h_y(j)$, $h_z(k)$ as in (6.4). As in Chapter 5, the following quantities are defined:

$$r_\xi = \frac{\sigma_\xi \Delta t}{2\varepsilon \alpha_\xi},\ \xi = x, y, z \tag{6.20}$$

From the discretizations obtained in Chapter 5, after the inclusion of the normalization (6.19), the update equations for the normalized auxiliary variables are derived as shown below:

$$\begin{aligned} x_{1z}^{(n+1/2)}(i,j,k) = &\left(\frac{1-r_x}{1+r_x}\right) x_{1z}^{(n-1/2)}(i,j,k) + \frac{1}{(1+r_x)\alpha_x h_x(i)} \\ &\times\left[A_z^{(n)}(i+1,j,k) - A_z^{(n)}(i,j,k)\right] \end{aligned} \tag{6.21}$$

$$y_{1z}^{(n+1/2)}(i,j,k)=\left(\frac{1-r_y}{1+r_y}\right)y_{1z}^{(n-1/2)}(i,j,k)+\frac{1}{\left(1+r_y\right)\alpha_y h_y(j)} \times\left[A_z^{(n)}(i,j+1,k)-A_z^{(n)}(i,j,k)\right] \tag{6.22}$$

$$z_{1z}^{(n+1/2)}(i,j,k)=\left(\frac{1-r_z}{1+r_z}\right)z_{1z}^{(n-1/2)}(i,j,k)+\frac{1}{\left(1+r_z\right)\alpha_z h_z(k)} \times\left[A_z^{(n)}(i,j,k+1)-A_z^{(n)}(i,j,k)\right] \tag{6.23}$$

$$x_{2z}^{(n+1/2)}(i,j,k)=\left(\frac{1-r_x}{1+r_x}\right)x_{2z}^{(n-1/2)}(i,j,k)+\frac{1}{\left(1+r_x\right)\alpha_x h_x(i-1)}\cdot \times\left[x_{1z}^{(n+1/2)}(i,j,k)-x_{1z}^{(n+1/2)}(i-1,j,k) -x_{1z}^{(n-1/2)}(i,j,k)+x_{1z}^{(n-1/2)}(i-1,j,k)\right] \tag{6.24}$$

$$y_{2z}^{(n+1/2)}(i,j,k)=\left(\frac{1-r_y}{1+r_y}\right)y_{2z}^{(n+1/2)}(i,j,k)+\frac{1}{\left(1+r_y\right)\alpha_y h_y(j-1)}\cdot \times\left[y_{1z}^{(n+1/2)}(i,j,k)-y_{1z}^{(n+1/2)}(i,j-1,k) -y_{1z}^{(n-1/2)}(i,j,k)+y_{1z}^{(n-1/2)}(i,j-1,k)\right] \tag{6.25}$$

$$z_{2z}^{(n+1/2)}(i,j,k)=\left(\frac{1-r_z}{1+r_z}\right)z_{2z}^{(n-1/2)}(i,j,k)+\frac{1}{\left(1+r_z\right)\alpha_z h_z(k-1)}\cdot \times\left[z_{1z}^{(n+1/2)}(i,j,k)-z_{1z}^{(n+1/2)}(i,j,k-1) -z_{1z}^{(n-1/2)}(i,j,k)+z_{1z}^{(n-1/2)}(i,j,k-1)\right] \tag{6.26}$$

Using the normalized variables, the following finite-difference expressions for the WETD are obtained:

1. Case of homogeneous lossy medium:

$$D_t A_z^{(n+1/2)}(i,j,k) = \left(\frac{1-r_0}{1+r_0}\right) D_t A_z^{(n-1/2)}(i,j,k) + \frac{1}{4\mu_r \varepsilon_r (1+r_0)} \cdot \left[\mathcal{L}\{A_z\}^{(n)} - \sigma\sigma_m \Delta l_{\min}^2 \cdot A_z^{(n)}(i,j,k) + \Delta l_{\min}^2 \cdot \mu J_z \right] \tag{6.27}$$

where as before, $r_0 = \frac{\Delta t}{2}\left(\frac{\sigma_m}{\mu} + \frac{\sigma}{\varepsilon}\right)$ is a numerical constant;

$\mathcal{L}\{A_z\}^{(n)} = x_{2z}^{(n+1/2)}(i,j,k) - x_{2z}^{(n-1/2)}(i,j,k) + y_{2z}^{(n+1/2)}(i,j,k) - y_{2z}^{(n-1/2)}(i,j,k) + z_{2z}^{(n+1/2)}(i,j,k) - z_{2z}^{(n-1/2)}(i,j,k)$ is the analog of the finite-difference Laplacian operator applied to A_z; and

$D_t A_z^{(n+1/2)}(i,j,k) = A_z^{(n+1)}(i,j,k) - A_z^{(n)}(i,j,k)$ is the first-order finite-difference operator in time.

2. Case of inhomogeneous lossless medium:

$$D_t A_z^{(n+1/2)}(i,j,k) = D_t A_z^{(n-1/2)}(i,j,k) + \frac{1}{4\mu_r(i,j,k)\varepsilon_r(i,j,k)} \mathcal{L}\{A_z\}^{(n)} + \frac{1}{8} \hat{M}_{\mu\varepsilon}^{(n)}(i,j,k) + \frac{1}{8\varepsilon_r(i,j,k)} \hat{N}_{\mu}^{(n)}(i,j,k) \tag{6.28}$$

where the normalization for the divergence of the vector potential is:

$$divA_{(original)} = \frac{1}{\Delta l_{min}} div\hat{A}_{(program)} \tag{6.29}$$

and is located at the bottom left corner of the discretization cell (see Fig. 5.1). Note that the permittivity is always defined at the same locations as the components of the vector potential itself.

The update equation for the normalized divergence is therefore:

$$
\begin{aligned}
div\hat{A}^{(n)}(i,j,k) = \Bigg\{ & \alpha_x [x_{1x}^{(n+\frac{1}{2})}(i-1,j,k) - x_{1x}^{(n-\frac{1}{2})}(i-1,j,k)] \\
& + \frac{\sigma_x \Delta t}{2\varepsilon} [x_{1x}^{(n+\frac{1}{2})}(i-1,j,k) + x_{1x}^{(n-\frac{1}{2})}(i-1,j,k)] \\
& + \alpha_y [y_{1y}^{(n+\frac{1}{2})}(i,j-1,k) - y_{1y}^{(n-\frac{1}{2})}(i,j-1,k)] \\
& + \frac{\sigma_y \Delta t}{2\varepsilon} [y_{1y}^{(n+\frac{1}{2})}(i,j-1,k) + y_{1y}^{(n-\frac{1}{2})}(i,j-1,k)] \\
& + \alpha_z [z_{1z}^{(n+\frac{1}{2})}(i,j,k-1) - z_{1z}^{(n-\frac{1}{2})}(i,j,k-1)] \\
& + \frac{\sigma_z \Delta t}{2\varepsilon} [z_{1z}^{(n+\frac{1}{2})}(i,j,k-1) + z_{1z}^{(n-\frac{1}{2})}(i,j,k-1)] \Bigg\}
\end{aligned}
\tag{6.30}
$$

The last two terms in equation (6.28) are

$$
\begin{aligned}
\hat{N}_{\mu}^{(n)}(i,j,k) = & \left\{ \left[\frac{1}{\mu_r(i+1,j,k)} - \frac{1}{\mu_r(i,j,k)} \right] \frac{1}{h_x(i)} \times \right. \\
& \left[z_{1x}^{(n+\frac{1}{2})}(i,j,k) - z_{1x}^{(n-\frac{1}{2})}(i,j,k) + x_{1z}^{(n+\frac{1}{2})}(i,j,k) - x_{1z}^{(n-\frac{1}{2})}(i,j,k) \right] \\
& + \left[\frac{1}{\mu_r(i,j,k)} - \frac{1}{\mu_r(i-1,j,k)} \right] \frac{1}{h_x(i-1)} \times \\
& \left[z_{1x}^{(n+\frac{1}{2})}(i-1,j,k) - z_{1x}^{(n-\frac{1}{2})}(i-1,j,k) + x_{1z}^{(n+\frac{1}{2})}(i-1,j,k) - x_{1z}^{(n-\frac{1}{2})}(i-1,j,k) \right] \\
& - \left[\frac{1}{\mu_r(i,j+1,k)} - \frac{1}{\mu_r(i,j,k)} \right] \frac{1}{h_y(j)} \times \\
& \left[y_{1z}^{(n+\frac{1}{2})}(i,j,k) - y_{1z}^{(n-\frac{1}{2})}(i,j,k) + z_{1y}^{(n+\frac{1}{2})}(i,j,k) - z_{1y}^{(n-\frac{1}{2})}(i,j,k) \right] \\
& - \left[\frac{1}{\mu_r(i,j,k)} - \frac{1}{\mu_r(i,j-1,k)} \right] \frac{1}{h_y(j-1)} \times \\
& \left. \left[y_{1z}^{(n+\frac{1}{2})}(i,j-1,k) - y_{1z}^{(n-\frac{1}{2})}(i,j-1,k) + z_{1y}^{(n+\frac{1}{2})}(i,j-1,k) - z_{1y}^{(n-\frac{1}{2})}(i,j-1,k) \right] \right\}
\end{aligned}
\tag{6.31}
$$

$$\hat{M}_{\mu\varepsilon}^{(n)}(i,j,k)=$$
$$\left\{\frac{div\hat{A}^{(n)}(i,j,k+1)}{h_z(k)}\left[\frac{1}{\mu_r(i,j,k+1)\varepsilon_r(i,j,k+1)}-\frac{1}{\mu_r(i,j,k)\varepsilon_r(i,j,k)}\right]\right. \tag{6.32}$$
$$\left.+\frac{div\hat{A}^{(n)}(i,j,k)}{h_z(k-1)}\left[\frac{1}{\mu_r(i,j,k)\varepsilon_r(i,j,k)}-\frac{1}{\mu_r(i,j,k-1)\varepsilon_r(i,j,k-1)}\right]\right.$$

3. *Case of lossy inhomogeneous medium:*

$$D_tA_z^{(n+1/2)}(i,j,k)=\frac{1-r_0}{1+r_0}D_tA_z^{(n-1/2)}(i,j,k)$$
$$+\frac{1}{4\mu_r(i,j,k)\varepsilon_r(i,j,k)(1+r_0)}\mathcal{L}\{A_z\}^{(n)}$$
$$+\frac{\hat{\Phi}^{(n)}(i,j,k+1)}{h_z(k)}\left[\frac{\sigma(i,j,k+1)}{\varepsilon_0\varepsilon_r(i,j,k+1)}-\frac{\sigma(i,j,k)}{\varepsilon_0\varepsilon_r(i,j,k)}\right] \tag{6.33}$$
$$+\frac{\hat{\Phi}^{(n)}(i,j,k)}{h_z(k-1)}\left[\frac{\sigma(i,j,k)}{\varepsilon_0\varepsilon_r(i,j,k)}-\frac{\sigma(i,j,k-1)}{\varepsilon_0\varepsilon_r(i,j,k-1)}\right]\Bigg\}$$
$$+\frac{1}{8(1+r_0)}\hat{M}_{\mu\varepsilon}^{(n)}(i,j,k)+\frac{1}{8(1+r_0)\varepsilon_r(i,j,k)}\hat{N}_{\mu}^{(n)}(i,j,k)$$

where the divergence is normalized as in (6.29) and calculated as in (6.30); $\hat{M}_{\mu\varepsilon}^{(n)}(i,j,k)$ and $\hat{N}_{\mu}^{(n)}(i,j,k)$ are calculated as in (6.31) and (6.32), respectively; the constant r_0 is $r_0=\frac{\sigma_{\Delta}t}{2\varepsilon}$. Here the scalar potential is normalized as

$$\Phi_{(original)}=\frac{1}{\mu_0\varepsilon_{0\Delta}l_{min}}\hat{\Phi}_{(program)} \tag{6.34}$$

and explicitly calculated as follows:

$$\hat{\Phi}^{(n)}(i,j,k)=\frac{1-r}{1+r}\hat{\Phi}^{(n-1)}(i,j,k)-\frac{1}{\mu_r\varepsilon_r(1+r)}div\hat{A}^{(n)}(i,j,k) \tag{6.35}$$

In equation (6.35) the notation $r=\frac{\sigma\Delta t}{2\varepsilon}$ is used for convenience. The scalar potential and the divergence are calculated at points located at the bottom left corner of the discretization cell, see Fig. 5.1.

4. Special case of layered dielectrics sharing the same normal

Let the unit normal to the interfaces of inhomogeneity of all dielectric layers be in the *z*-direction.

From the equations for the auxiliary variables along the *z*-direction:

$$\frac{\partial}{\partial t}\left(\frac{Z_{1z}}{\varepsilon_r}\right)=-\frac{\sigma_z}{\varepsilon\alpha_z}\left(\frac{Z_{1z}}{\varepsilon_r}\right)+\frac{1}{\alpha_z}\frac{1}{\varepsilon_r}\frac{\partial A_z}{\partial z}$$

$$\frac{\partial Z_{2z}}{\partial t}=-\frac{\sigma_z}{\varepsilon\alpha_z}Z_{2z}+\frac{\varepsilon_r}{\alpha_x}\frac{\partial^2}{\partial z\partial t}\left(\frac{Z_{1z}}{\varepsilon_r}\right)$$

it becomes clear that the following change in the normalization of Z_{1z} is needed:

$$Z_{1z(original)}=\frac{\Delta t\ \varepsilon_r}{\Delta l_{\min}}z_{1z(program)}$$

Thus, the normalized variables are related as:

$$\frac{\partial z_{1z}}{\partial t}=-\frac{\sigma_z}{\varepsilon\alpha_z}z_{1z}+\frac{1}{\alpha_z}\left(\frac{1}{\varepsilon_r}\frac{\partial A_z}{\partial z}\right)$$

$$\frac{\partial z_{2z}}{\partial t}=-\frac{\sigma_z}{\varepsilon\alpha_z}z_{2z}+\frac{\varepsilon_r}{\alpha_z}\frac{\partial^2 z_{1z}}{\partial z\partial t}$$

Finally, for completeness, the discretization formulas for the case of layered dielectrics with a common normal to their interfaces in the *z*-direction, are shown:

$$x_{1z}^{(n+1/2)}(i,j,k)=\frac{1-r_x}{1+r_x}x_{1z}^{(n-1/2)}(i,j,k)+\frac{1}{\alpha_x\left(1+r_x\right)h_x(i)}\left[A_z^{(n)}(i+1,j,k)-A_z^{(n)}(i,j,k)\right]$$

$$x_{2z}^{(n+1/2)}(i,j,k)=\frac{1-r_x}{1+r_x}x_{2z}^{(n-1/2)}(i,j,k)+\frac{1}{\alpha_x\left(1+r_x\right)h_x(i-1)}\left[x_{1z}^{(n+1/2)}(i,j,k)-x_{1z}^{(n+1/2)}(i-1,j,k)-x_{1z}^{(n-1/2)}(i,j,k)+x_{1z}^{(n-1/2)}(i-1,j,k)\right]$$

$$y_{1z}^{(n+1/2)}(i,j,k)=\frac{1-r_y}{1+r_y}y_{1z}^{(n-1/2)}(i,j,k)+\frac{1}{\alpha_y\left(1+r_y\right)h_y(j)}\left[A_z^{(n)}(i,j+1,k)-A_z^{(n)}(i,j,k)\right]$$

$$y_{2z}^{(n+1/2)}(i,j,k)=\frac{1-r_y}{1+r_y}y_{2z}^{(n-1/2)}(i,j,k)+\frac{1}{\alpha_y\left(1+r_y\right)h_y(j-1)}\left[y_{1z}^{(n+1/2)}(i,j,k)-y_{1z}^{(n+1/2)}(i,j-1,k)-y_{1z}^{(n-1/2)}(i,j,k)+y_{1z}^{(n-1/2)}(i,j-1,k)\right]$$

$$z_{1z}^{(n+1/2)}(i,j,k)=\frac{1-r_z}{1+r_z}z_{1z}^{(n-1/2)}(i,j,k)+\frac{2}{\varepsilon_r(i,j,k)+\varepsilon_r(i,j,k+1)}\times\frac{1}{\alpha_z\left(1+r_z\right)h_z(k)}\left[A_z^{(n)}(i,j,k+1)-A_z^{(n)}(i,j,k)\right]$$

$$z_{2z}{}^{(n+1/2)}(i,j,k) = \frac{1-r_z}{1+r_z} z_{2z}{}^{(n-1/2)}(i,j,k) + \frac{\varepsilon_r(i,j,k)}{\alpha_z(1+r_z)h_z(k-1)}\Big[z_{1z}{}^{(n+1/2)}(i,j,k) - z_{1z}{}^{(n+1/2)}(i,j,k-1) - z_{1z}{}^{(n-1/2)}(i,j,k) + z_{1z}{}^{(n-1/2)}(i,j,k-1)\Big]$$

$$D_t A_z^{(n+1/2)}(i,j,k) = \frac{1-r_0}{1+r_0} D_t A_z^{(n-1/2)}(i,j,k) + \frac{1}{4\mu_r\varepsilon_r(1+r_0)} \mathcal{L}\{A_z\}^{(n)}$$

where r_0 and $\mathcal{L}\{A_z\}^{(n)}$ are defined above, in the lossy homogeneous case.

As sources are unlikely to exist in a practical PML region, the term μJ_z in (6.27) may be set to zero. Recall also that the EM material constants σ, σ_m, $\varepsilon = \varepsilon_0\varepsilon_r$ and $\mu = \mu_0\mu_r$ are those of the analyzed volume terminated with the PML; in other words, they are not associated with the anisotropic PML constants σ_i and α_i, $i = x, y, z$.

The formulae above are in a form suitable for straightforward implementation. The time-stepping algorithm for the wave equation PML is summarized below:

1. Update the auxiliary variables $x_{1\xi}, y_{1\xi}, z_{1\xi}$, $\xi = x, y, z$, according to equations (6.21) to (6.23).
2. Update the auxiliary variables $x_{2\xi}, y_{2\xi}, z_{2\xi}$, $\xi = x, y, z$, according to equations (6.24) to (6.26).
3. Update the time-derivatives $D_t A_\xi$, $\xi = x, y, z$, according to equation (6.27).

4. Update the potential components A_ξ, $\xi = x, y, z$, using

$$A_\xi^{(n+1)}(i,j,k) = A_\xi^{(n)}(i,j,k) + D_t A_\xi^{(n+1/2)}(i,j,k) \tag{6.36}$$

and if it is a homogeneous medium, go to 1; otherwise go to 5.

5. In the inhomogeneous case, update the divergence of the vector potential using equation (6.30). If it is a lossless medium, go to 1; otherwise go to 6.
6. In the lossy inhomogeneous case, update the scalar potential using equation (6.35) and go to 1.

6.3 Excitation and its frequency characteristics

6.3.1 Gaussian pulse excitation

The excitation pulse in the case of open problems is usually chosen to be a Gaussian pulse in time, propagating in $+\xi$-direction:

$$g(\xi,\eta,\varsigma,t) = \varphi(\eta,\varsigma)\exp[-\alpha(t - t_0 - \frac{\xi - \xi_0}{v_\xi})^2] \tag{6.37}$$

where $\varphi(\eta,\varsigma)$ is the distribution in the transverse plane, v_ξ is the velocity of the pulse in the specific medium and the pulse has its maximum at $\xi = \xi_0$ when $t = t_0$. The main reason for this choice is that the Fourier transform of this pulse is also a Gaussian function (of frequency):

$$G(f) \approx \exp\left[-\frac{\pi^2 f^2}{\alpha}\right] \tag{6.38}$$

Therefore, the frequency band of the pulse can be regulated through the parameter α. This is important for the case when the time domain response of the structure of interest is used to calculate certain frequency-domain characteristics, such as *S*-parameters or far-field patterns (in scattering problems). The choice of α is dictated by two constraints:

1. If frequency data are needed up to a maximum frequency of $f_{\max}$, then the pulse must have a spectrum wide enough to cover the (0 , $f_{\max}$) band. That is, we will require that at $f_{\max}$ the spectrum of the Gaussian pulse is at least 10 % of its maximum value, i.e. G($f_{\max}$)=0.1.
2. The parameter α also has to be a function of the number of time steps, β, from truncation (/start) point to the maximum of the time-domain Gaussian pulse, so that the launch of the pulse is smooth enough.

In order to have a truncation level of approximately –140 dB (corresponding to exp(-16)) at the truncation point, a practical solution is to choose α vary as [see Kunz and Luebbers (1993)]:

$$\alpha = \left(\frac{4}{\beta \Delta t} \right)^2 \tag{6.39}$$

From the first constraint, we can obtain a relation between $f_{\max}$ and β:

$$\beta = \frac{4\sqrt{\ln 10}}{\pi f_{max} \Delta t} \tag{6.40}$$

The time step Δt is determined by the minimal spatial step $\Delta l_{\min}$ and Courant's stability condition ($q = \frac{\Delta l_{\min}}{c\Delta t} \geq \sqrt{3}$). The above equation can be written in terms of the shortest wavelength of interest as:

$$\beta = \frac{4q\sqrt{\ln 10}\sqrt{\mu_r \varepsilon_r}}{\pi}\left(\frac{\lambda_{\min}}{\Delta l_{\min}}\right) \tag{6.41}$$

For proper spatial sampling of the field propagation, the following condition must be satisfied:

$$N_s = \frac{\lambda_{\min}}{\Delta l_{\min}} \geq 8 \tag{6.42}$$

Therefore usually $\Delta l_{\min}$ is determined first and then the pulse width β is calculated. The last equation shows that even for the smallest possible value of $N_s = 8$, in a structure, which does not contain dielectric materials, the pulse width has to be at least $\beta = 32$. Naturally, if the structure contains a dielectric material of relative permittivity ε_r, the pulse width has to be increased $\sqrt{\varepsilon_r}$ times since the cell size and the time steps would be reduced by the same factor, as shown in equation (6.41). One should note that β is not to be increased too much, because this should correspond to a decrease of $\Delta l_{\min}$. Otherwise, increasing β and leaving $\Delta l_{\min}$ unchanged would narrow the spectrum of the pulse below the desired upper frequency limit.

An example of the Gaussian pulse and its frequency characteristics are plotted in Fig.6.2 and Fig.6.3, respectively.

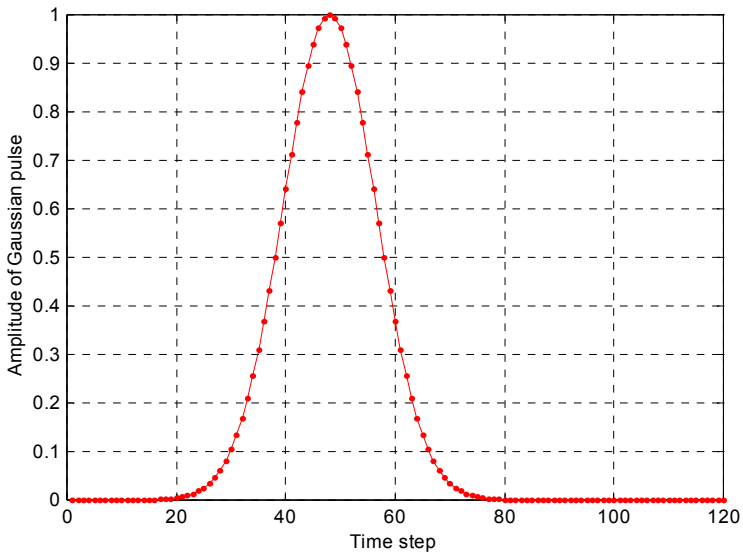

Fig. 6.2. Example of Gaussian pulse excitation, $\beta = 12$, $t_0 = 48\Delta t$, for $\Delta l_{min} = 2.5$ mm.

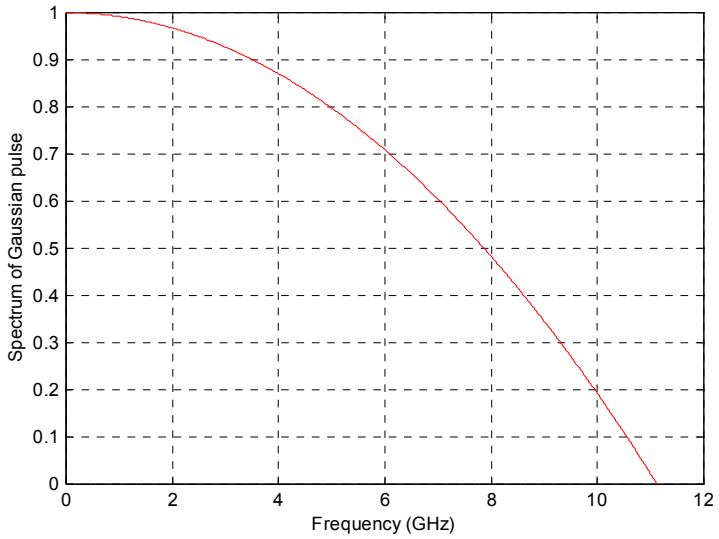

Fig. 6.3. Spectrum of the Gaussian pulse shown in Fig. 6.1 with $\beta = 12$, $t_0 = 48\Delta t$.

6.3.2 The BHW modulated sinusoidal wave excitation

The excitation in the case of waveguide problems is usually a sine wave modulated by Blackman-Harris window (BHW) function, see Harris (1978):

$$
\begin{aligned}
&b(\xi,\eta,\varsigma,t) = \varphi(\eta,\varsigma)\sin(2\pi f_0 t)w(t)\delta(\xi-\xi_0)\\
&w(t) = a_0 - a_1\cos\left(\frac{2\pi t}{T_{BHW}}\right) + a_2\cos\left(\frac{4\pi t}{T_{BHW}}\right) - a_3\cos\left(\frac{6\pi t}{T_{BHW}}\right)\\
&a_0 = 0.35875;\ a_1 = 0.48829;\ a_2 = 0.14128;\ a_3 = 0.01168
\end{aligned}
\tag{6.43}
$$

where f_0 is the central frequency of the excitation, which is located at $\xi = \xi_0$ with a distribution in the transverse plane $\varphi(\eta,\varsigma)$. T_{BHW} is the duration of the Blackman-Harris window function by which one controls the excitation frequency bandwidth.

The window functions are being applied to smoothen the spectral samples, since the amplitude of the harmonic estimate at a given frequency is biased by the accumulated broadband noise included in the bandwidth of the window. The particular window function (BHW function) is chosen for its lowest side-lobe level (-92 dB).

An example of a sine wave modulated by Blackman-Harris window (BHW) function and its frequency characteristics are plotted in Fig. 6.4 and 6.5, respectively.

In summary, in order to have a good resolution during simulations, and avoid frequency components below the cutoff frequency, one has to take into account few factors:

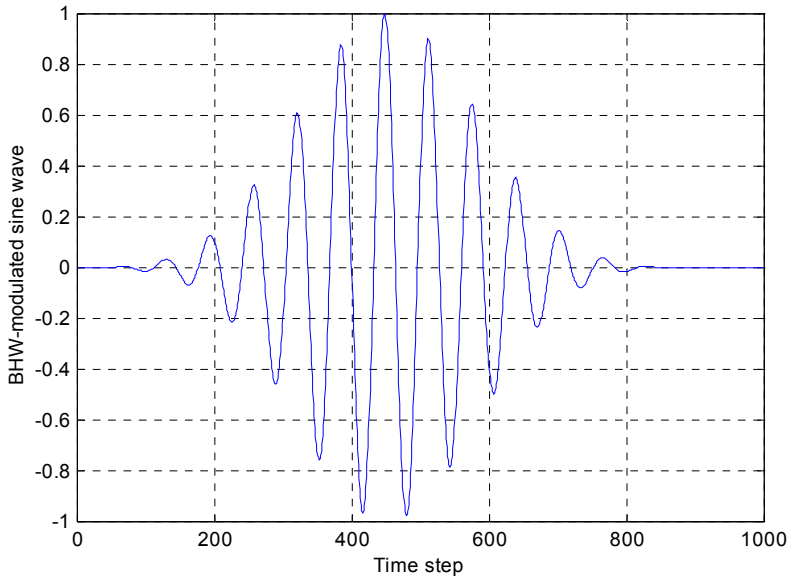

Fig. 6.4. Sine wave modulated by Blackman-Harris window (BHW) function, $f_0 = 4.7\ GHz$, $T_{BHW} = 900\Delta t$; $\Delta t = 3.33357\ ps$

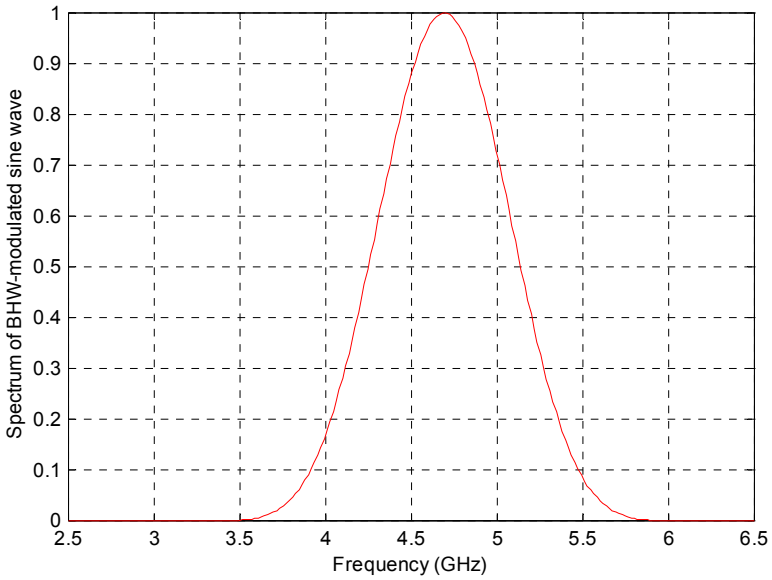

Fig. 6.5. Spectrum of the sine wave modulated by BHW function from Fig.6.3.

1. The minimal spatial step Δl_{min} has to be small enough to represent the structure in sufficient details.
2. The time step Δt has to satisfy the Courant stability criterion.
3. The excitation pulse/window should be narrow enough to cover the frequency band of interest.
4. The pulse should be wide/long enough to contain satisfactory spatial distribution information within it.
5. If the requirements 3 and 4 cannot be met together, choose a smaller spatial step and a corresponding smaller time step.

6.3.3 Calculation of the maximum number of time steps

The number of time steps, required to sample the time domain responses in the sampling planes, should be large enough so that the traveling waves inside the structure of interest are attenuated to negligible amplitude by the end of the simulation. Usually, the following formula is used to calculate the minimal necessary number of time steps in guiding structures:

$$n_{t_{\max}} \geq \left[\kappa \cdot \frac{\Delta l_{\min}}{c\Delta t} \cdot \dim_{\max} + w_{exc} \right] \tag{6.44}$$

where

$\kappa \geq 2;\ \dim_{\max} = \max\left(n_{x_{\max}}, n_{y_{\max}}, n_{z_{\max}}\right)$

w_{exc} is the width of the excitation pulse (expressed in time steps) to the truncation moment.

6.4. Examples of IPML for FDTD

To validate the method proposed in Chapter 3, the improved PML ABC has been applied to both radiation and high-frequency circuit problems solved in terms of the FDTD method to the solution of Maxwell's equations. Here, two examples will be considered: an infinitesimal dipole radiating in open space and a microstrip line.

6.4.1 Infinitesimal dipole in open space

The problem of the *z*-directed infinitesimal dipole, which radiates in open space, is modeled first by Yee's FDTD method. It has a computational domain of dimensions ($120\,\Delta x$, $120\,\Delta y$, $120\,\Delta z$), where $\Delta x = \Delta y = \Delta z = 2.5$ mm. The dipole is excited by the *z*-component of the electric field, which is a Gaussian pulse in time. The reflection is calculated using the ratio of the reflected and the incident *z*-component of the electric field:

$$R_{\mathrm{dB}} = 20\log_{10}\left|\frac{\mathcal{F}\{E_z^{refl}\}}{\mathcal{F}\{E_z^{inc}\}}\right| \tag{6.45}$$

where $\mathcal{F}$ denotes the Fourier transform of the respective time-dependent field component. Two types of PML ABCs are investigated to terminate the computational domain. They have different variable profiles. One of them implements the Berenger's PML conductivity profile as in Berenger (1994). The second absorber is based on the modified PML conductivity profile proposed in

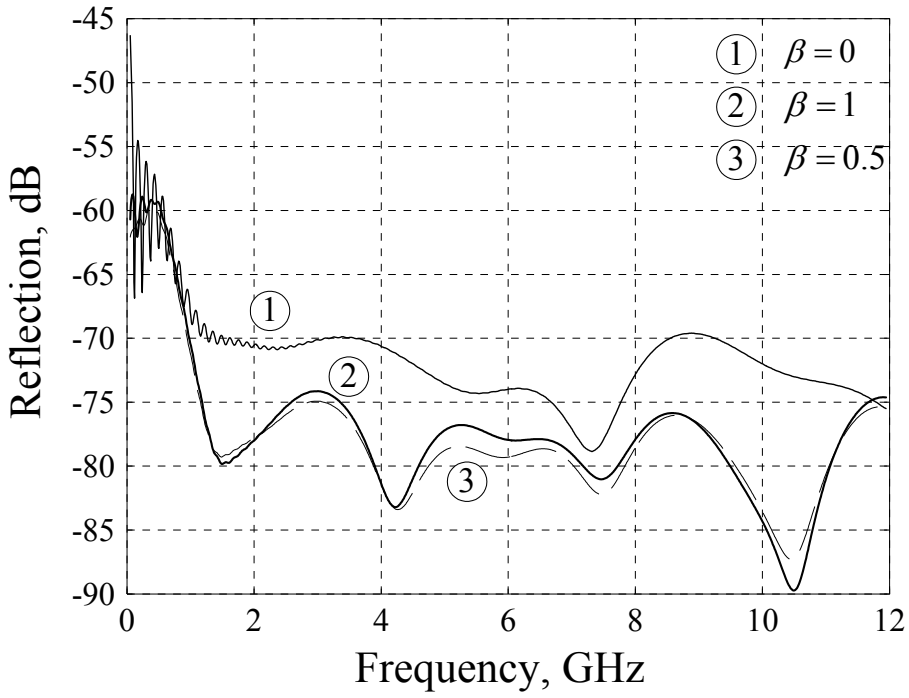

Fig.6.6. Spectrum of the reflection in the dipole radiation problem using two different PML conductivity profiles: 1 – Berenger's PML, 2 – current profiles $\beta = 1$, 3 – current profiles $\beta = 0.5$ ($N_{\text{PML}} = 10$, $R_0 = 10^{-4}$, $\varepsilon_{\max} = 0$, $n = 2$ in all three cases).

Chapter 3, for two values of the constant β, $\beta = 0.5$ and $\beta = 1$. The reflections are calculated by (6.45) and are shown in Fig. 6.6. In all cases the absorbers are 10 cells thick; their theoretical reflection coefficient at normal incidence is chosen to be $R_0 = 10^{-4}$; the constant $\varepsilon_{\max}$ is set as $\varepsilon_{\max} = 0$, and the order of increase of the PML conductivity profile *n* defined in Chapter 3 is set to $n = 2$. Fig. 6.6 shows that the current modification of the PML conductivity profile offers

superior performance in terms of reflection levels in the whole frequency band. In all cases the observation point is in the dipole's H-plane, halfway from the absorber. The reflections are similar for any other observation point.

6.4.2 Microstrip line

The geometry of the microstrip line is shown in Fig. 6.7(a). It is excited by the *z*-component of the electric field, which is launched with equal amplitude in the dielectric under the microstrip line, in a transverse plane, 5 spatial steps after the front-end IPML. The excitation is a Gaussian pulse in time that has its spectrum in the frequency band from 0 GHz to 100 GHz. The amplitude of the E_z component is shown after 1000 time steps in Fig. 6.7(b). The size of the computational domain is ($500\,\Delta x$, $56\,\Delta y$, $26\,\Delta z$), where $\Delta x = \Delta y = \Delta z = 0.1$ mm. The 3-dimensional computational domain was terminated in all directions (except the ground plane) by two types of PML ABCs: the MPML as in B. Chen *et al* (1995), and the proposed in Chapter 3 improved PML with $\beta = 1$ and $\beta = 2$. In all cases, the PML is 10 cells thick, the reflection coefficient is chosen to be $R_0 = 10^{-4}$, the constant $\varepsilon_{\max}$ is set to $\varepsilon_{\max} = 1$, the order of increase of the PML loss factor is set to $n = 3$. The reflections as defined in (6.45) are plotted in Fig. 6.8(a); and the magnitude of the reflections defined as $R_{\text{magn}} = \left| \dfrac{\mathcal{F}\{E_z^{refl}\}}{\mathcal{F}\{E_z^{inc}\}} \right|$ are plotted in Fig. 6.8(b). Lower-reflection broadband performance of the IPML profile is observed

in comparison with the MPML.

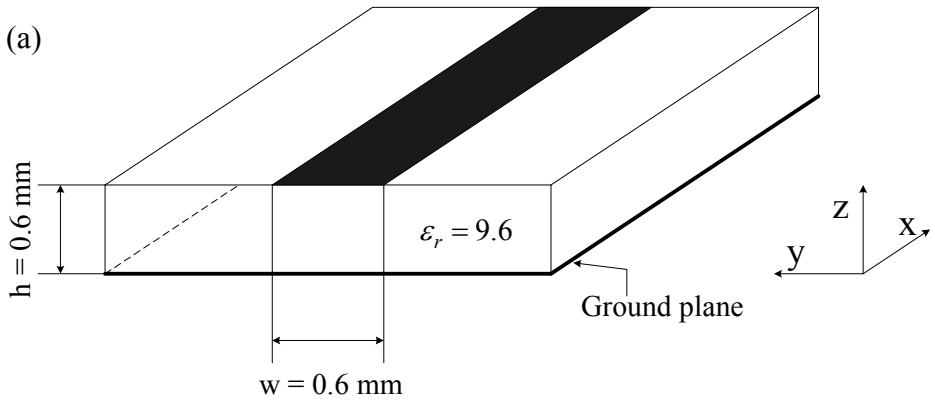

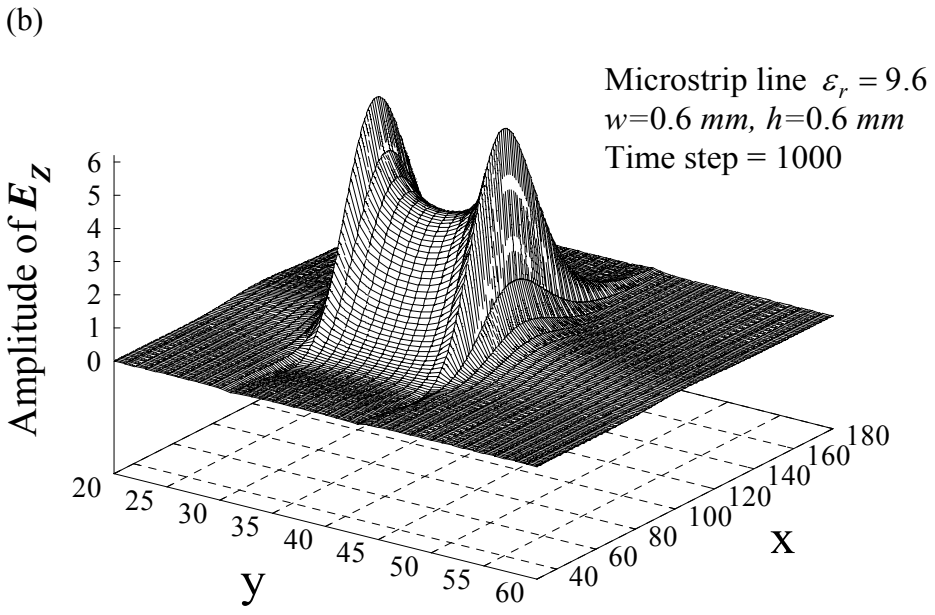

Fig. 6.7. (a) Geometry of the microstrip line; strip width $w = 0.6$ mm, dielectric $\varepsilon_r = 9.6$ of height $h = 0.6$ mm.

(b) Time-domain amplitude of the *z*-component of the electric field propagating along the microstrip line.

(a)

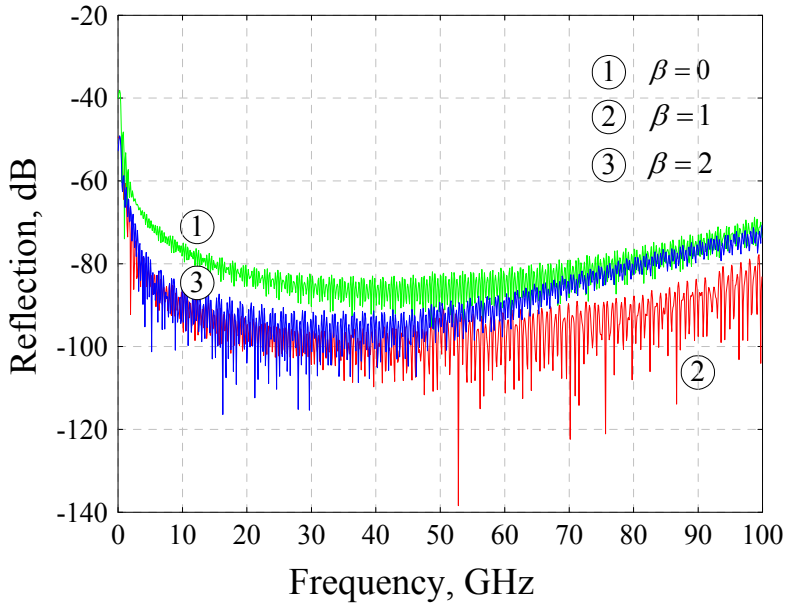

(b)

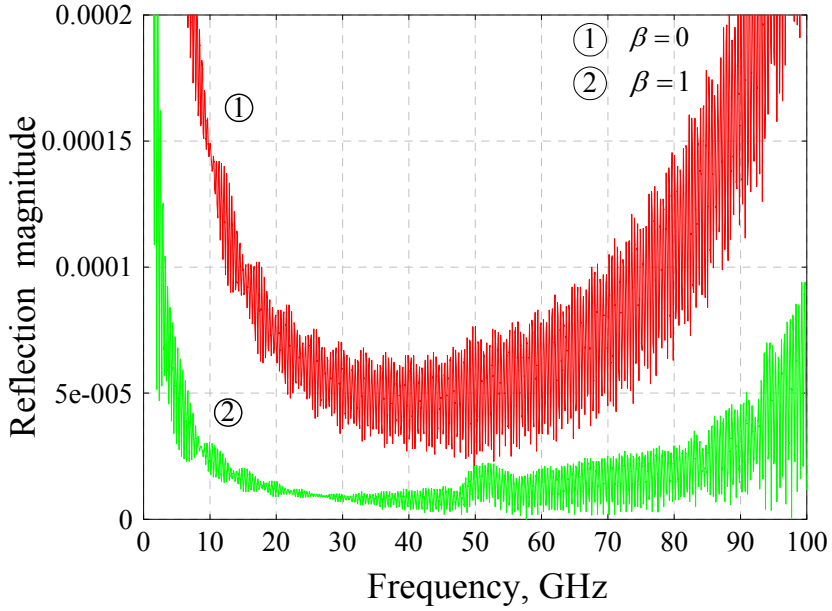

Fig. 6.8. Reflections spectrum in the microstrip problem using two different PMLs: 1 – MPML of Chen *et al.* (1995) corresponding to $\beta = 0$, 2 – IPML $\beta = 1$, 3 – IPML $\beta = 2$ ($N_{\text{PML}} = 10$, $R_0 = 10^{-4}$, $\varepsilon_{\max} = 1$, $n = 3$ in all cases). (a) in dB; (b) dimensionless.

6.5 Examples of IPML for WETD

To validate the PML ABC for the WETD proposed in Chapter 5, the algorithm was applied to both radiation and waveguide problems solved in terms of wave potentials in the time domain. Here, three structures are considered: a dipole in open space, a hollow rectangular waveguide, and a rectangular waveguide partially filled with dielectric. Finally, a 3-dimensional optical structure is considered, the simulation of which requires all three components of the vector potential; namely, a buried optical waveguide terminated by two-layer antireflection coating. The results of its simulation by both the FDTD for Maxwell's equations and by the WETD are presented.

6.5.1 Infinitesimal dipole in open space

The problem of the *z*-directed infinitesimal dipole, which radiates in open space, has two planes of symmetry. Therefore, the computational domain can be the first octant whose dimensions are ($60\Delta x$, $60\Delta y$, $60\Delta z$), where $\Delta x = \Delta y = \Delta z = 2.5$ mm. Proper BCs account for the symmetry: a horizontal PEC wall through the centre of the dipole; and two vertical mutually orthogonal PMC walls through the dipole. The potential A_z is excited by the *z*-directed current of the dipole, which is a Gaussian pulse in time. The reflection is estimated using the ratio of reflected and incident wave potential, which in this case is the *z*-component of the magnetic vector potential, $\vec{A} = \hat{z}A_z$:

$$R_{\mathrm{dB}} = 20\log_{10}\left|\frac{\mathcal{F}\{A_z^{refl}\}}{\mathcal{F}\{A_z^{inc}\}}\right| \tag{6.46}$$

Here, $\mathcal{F}$ denotes the Fourier transform of the respective time-dependent potential.

Three types of PML ABCs are investigated to terminate the computational domain of the time-domain wave equation. They have different variable profiles. The first type implements the MPML conductivity profiles as in B. Chen *et al.* (1995). The performance of two MPML profiles is shown in Fig. 6.9: for the orders n = 3 and n = 5; the second one being chosen to correspond to the case of $n+\beta = 3+2 = 5$. The second type PML has the GPML profile as in J. Fang *et al.* (1996). The third absorber is based on the proposed here profile as described in Chapter 5, when the orders n and β are set as: $n = 3$, $\beta = 2$. All absorbers are 16 cells thick; their theoretical reflection coefficient at normal incidence is chosen to be $R_0 = 10^{-4}$; the constant $\varepsilon_{\max}$ is set as $\varepsilon_{\max} = 4$. All of them are terminated with a PEC wall. The respective reflections are plotted in Fig. 6.9, which shows that the proposed modification of the PML conductivity profile has superior performance in terms of both reflection level and frequency bandwidth. It can be observed that a simple increase of the power rate of the MPML from $n = 3$ to $n = 5$ does not improve the absorption. In fact, it leads to a slight increase of the reflections. In all cases, the observation point is in the dipole's H-plane, halfway between the dipole and the absorber. The results are similar for any other observation point.

Fig. 6.10 compares the performance of the proposed PML absorber with the regular MPML, while varying the value of the power increase parameter β. It is evident that the frequency band becomes wider and the reflections lower with the proposed PML when its power order is increased by $\beta = 1$ or by $\beta = 2$ in comparison with the regular MPML profile, which in fact corresponds to the particular case of $\beta = 0$ in the proposed PML conductivity profile. From all experiments carried out so far, the conclusion can be drawn that the value of $\beta = 2$ provides optimal PML performance for the WETD.

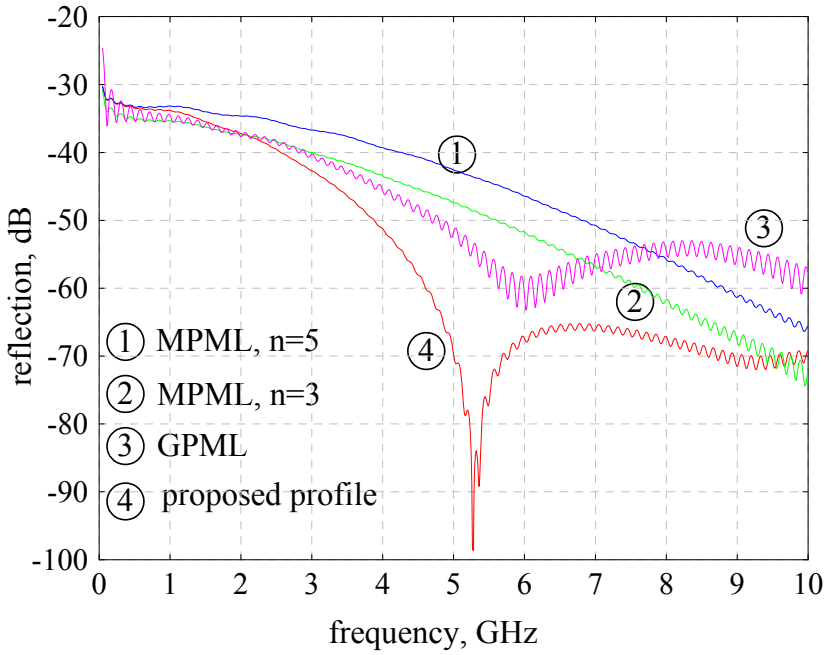

Fig. 6.9. Spectrum of the reflection in the dipole radiation problem using three different PML conductivity profiles: 1 – MPML, n=5; 2 – MPML, n=3; 3 – GPML; 4 – current profile, n=3, $\beta = 2$ ($N_{\mathrm{PML}} = 16$, $R_0 = 10^{-3}$, $\varepsilon_{\max} = 3$ in all four cases).

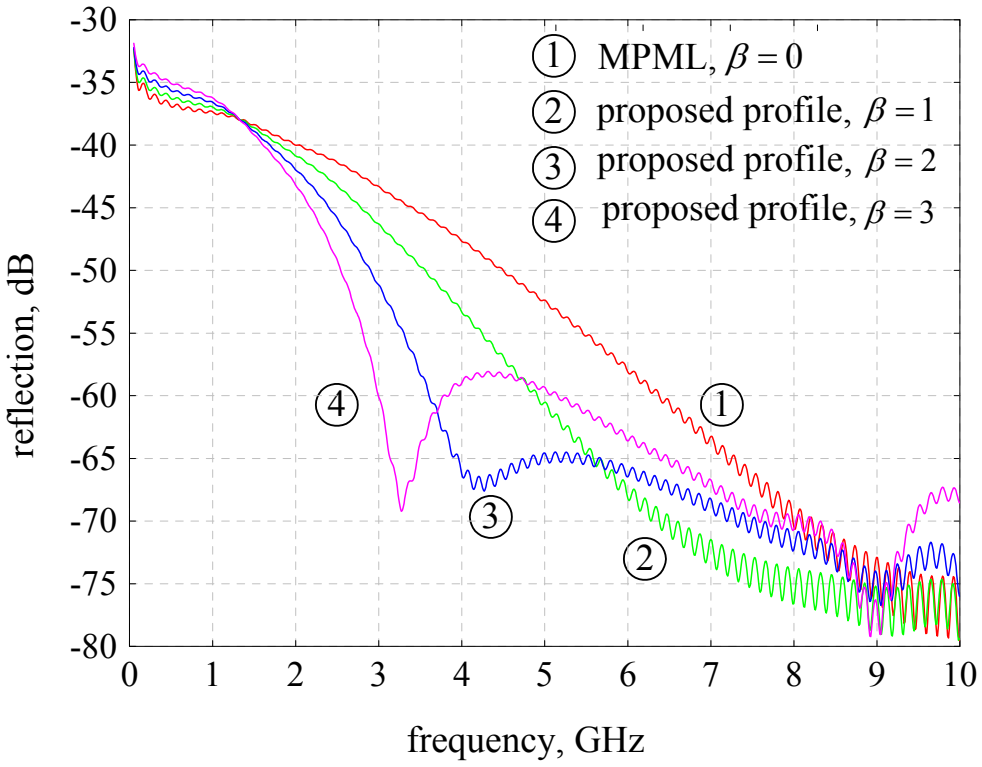

Fig. 6.10. Dependence of the spectrum bandwidth of the reflection in the dipole radiation problem on the PML conductivity parameter β: 1 – MPML, n=3 (corresponding to $\beta = 0$); 2 – current profile, n=3, $\beta = 1$; 3 – current profile, n=3, $\beta = 2$; 4 – current profile, n=3, $\beta = 3$ ($N_{\text{PML}} = 20$, $R_0 = 10^{-4}$, $\varepsilon_{\max} = 4$ in all four cases).

Fig. 6.11 shows the dependence of the frequency bandwidth on the number of cells in the proposed 3-D PML absorber terminating the dipole computational region. Here, it is important to point out that the physical thickness of the absorber, as a percentage of the wavelength, is very important at the lower frequency end. If the physical thickness of PML δ is calculated as a percentage of the wavelength λ, it shows that the reflection level drops below –60dB exactly when δ becomes greater than $\frac{2}{3}\lambda$. That is why a thickness of the PML medium should be recommended of at least 65–70% of the longest wavelength of interest.

Fig. 6.12 shows the dependence of the reflection on the thickness of the PML in the dipole problem at $f = 7$ GHz for $\beta = 1$ and $\beta = 2$ ($R_0 = 10^{-4}$, $\varepsilon_{\max} = 4$, $n = 3$). The reflections at other frequencies have similar behaviour as long as they are in the frequency band for which the PML thickness is larger then 2/3 of the corresponding wavelength. From both Fig. 6.11 and Fig. 6.12 it can be seen that for *open problems* at least 12 to 16 PML cells are necessary to ensure a reflection level below –60 dB. The corresponding number of PMLs in the FDTD solution of Maxwell's equations is *the same* if MPML or GPML are used, i.e. $\varepsilon_{\max} > 0$; but 5-6 layers *less* are enough if the original Berenger's PML is used, i.e. $\varepsilon_{\max} = 0$. It should be underlined that the last statement is valid only for open problems containing no guiding structures, when the relative dielectric constant of the computational domain terminated by PML is that of free space, $\varepsilon_r = 1$.

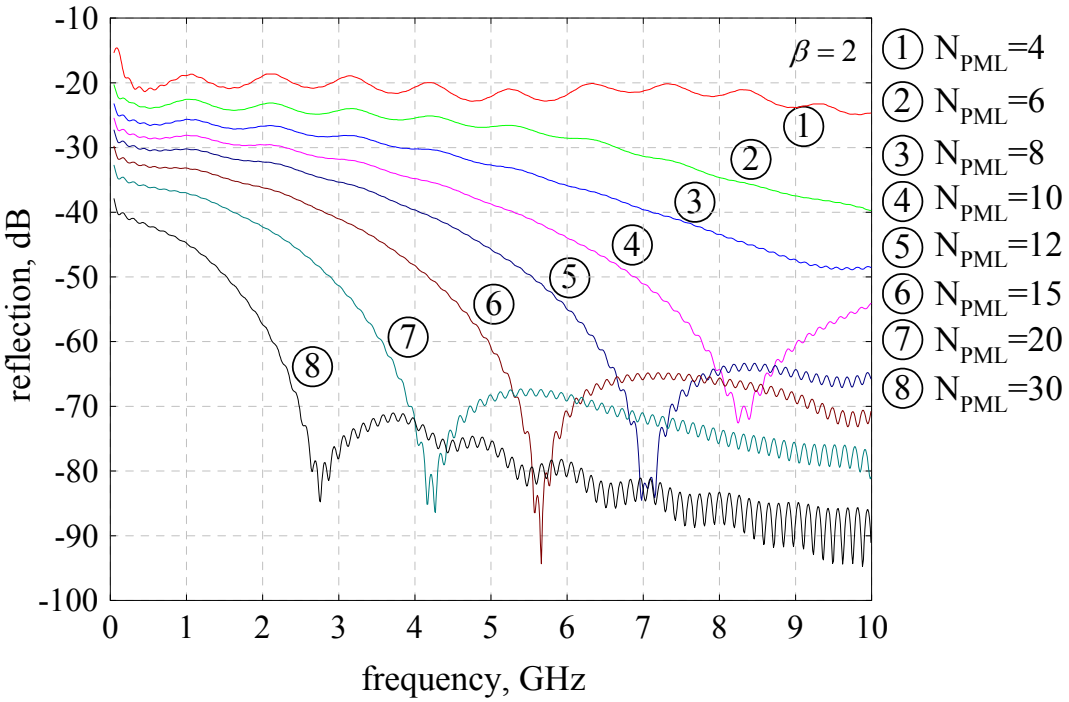

Fig. 6.11. Dependence of the spectrum bandwidth in the dipole radiation problem on the number of cells in the proposed PML absorber: 1 – $N_{\mathrm{PML}}=4$; 2 – $N_{\mathrm{PML}}=6$; 3 – $N_{\mathrm{PML}}=8$; 4 – $N_{\mathrm{PML}}=10$; 5 – $N_{\mathrm{PML}}=12$; 6 – $N_{\mathrm{PML}}=15$; 7 – $N_{\mathrm{PML}}=20$; 8 – $N_{\mathrm{PML}}=30$ ($R_0=10^{-3}$, $\varepsilon_{\max}=3$, n=3, $\beta=2$ in all cases).

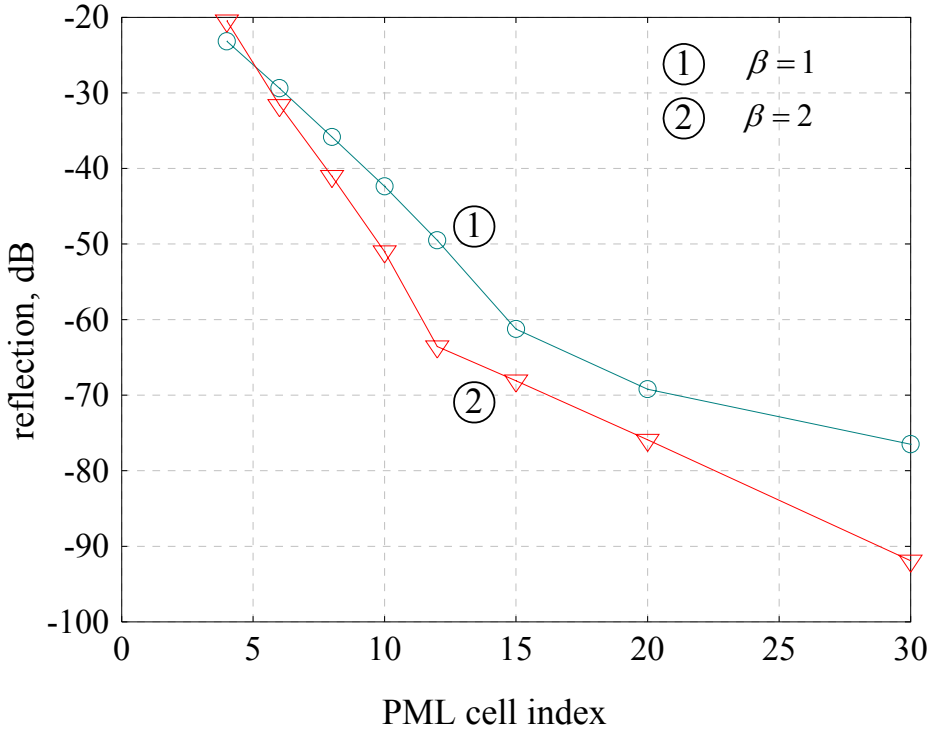

Fig. 6.12. Dependence of the reflection on the thickness of the proposed PML in the dipole problem at $f = 7$ GHz for $\beta = 1$ and $\beta = 2$ ($R_0 = 10^{-4}$, $\varepsilon_{\max} = 4$, $n = 3$).

6.5.2 Hollow rectangular waveguide

The rectangular waveguide has a cross-section of 30 mm by 15 mm, shown in Fig. 6.13. It is excited by a 10 GHz sinusoidal waveform modulated by Blackman-Harris window (BHW) function. The band-limited excitation has its spectrum in the frequency band from 7.5 GHz to 12.5 GHz. The size of the

computational domain is ($350\,\Delta x$, $30\,\Delta y$, $15\,\Delta z$), where $\Delta x = \Delta y = \Delta z = 1\,\text{mm}$. The ports were terminated by the same three types of PML ABCs as described above and by Mur's second order ABC. The PML is 8 cells thick, and $R_0 = 10^{-4}$, $\varepsilon_{\max} = 1$, $n = 2$. The reflections as defined in (6.46) are plotted in Fig. 6.14. Again low-reflection broadband performance of the proposed modified PML profile is observed.

The dependence of the reflection in the hollow waveguide on the thickness of the PML at 10 GHz is shown in Fig. 6.15 for $R_0 = 10^{-4}$, $\varepsilon_{\max} = 1$, $n = 2$. It can be observed that here, as in the case of the FDTD solution to Maxwell's equations, problems with guiding structures require much lower PML thickness when compared to the case of open problems.

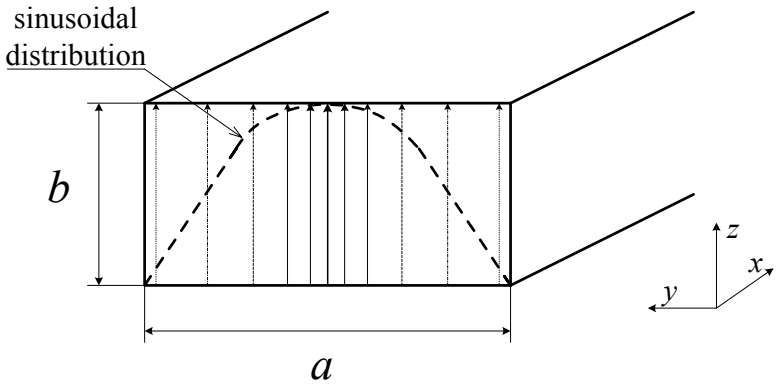

Fig. 6.13. Field distribution of the TE_{10} mode in the hollow rectangular waveguide, $a = 30\,\text{mm}$, $b = 15\,\text{mm}$.

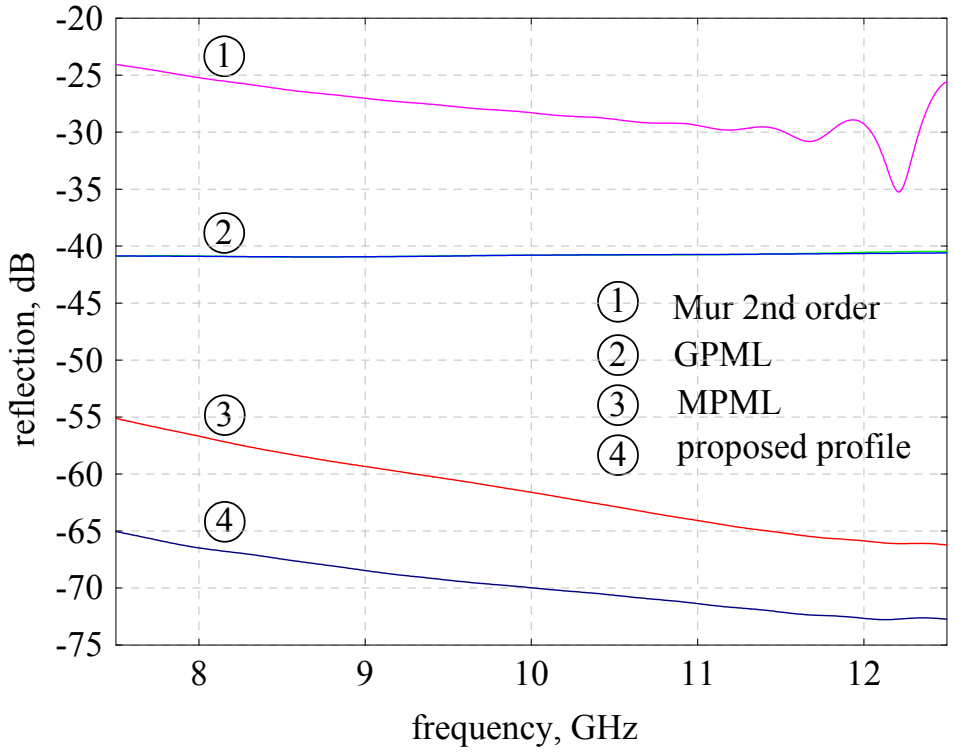

Fig. 6.14. Spectrum of the reflection in the waveguide problem with different PML conductivity profiles compared to Mur's second order ABC: 1 – Mur's second order ABC, 2 – GPML, 3 – MPML, 4 – current profiles ($N_{\mathrm{PML}} = 8$, $R_0 = 10^{-4}$, $\varepsilon_{\max} = 1$, $n = 2$ in all three PML cases).

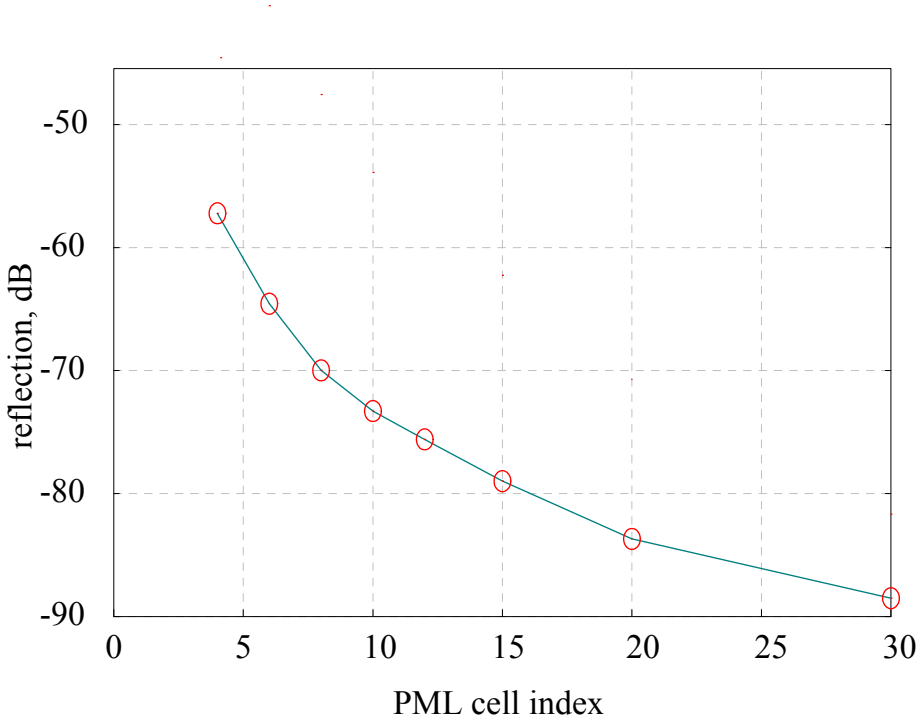

Fig. 6.15. Dependence of the reflection in the hollow waveguide on the thickness of the PML at 10 GHz ($R_0 = 10^{-4}$, $\varepsilon_{\max} = 1$, $n = 2$).

6.5.3 Partially filled with dielectric rectangular waveguide

This rectangular waveguide has a cross-section of 40 mm by 18 mm. It is half-filled with a dielectric layer parallel to its wide side (the dielectric constant is $\varepsilon_r = 2.45$). Its geometry is seen in Fig. 6.16. It is excited by a 4.7 GHz sinusoidal waveform modulated by Blackman-Harris window (BHW) function, shown in Fig. 6.16. The time-domain sample of the reflections is given in Fig. 6.17 for the case of twelve-cell thick PML with $R_0 = 10^{-5}$, $\varepsilon_{\max} = 1$, $n = 2$, $\beta = 2$. The band-limited excitation of the waveguide has its spectrum in the frequency band from

3.9 GHz to 5.5 GHz shown in Fig. 6.5. The transverse profile of the excitation corresponds to the dominant TM_{z10} mode, which requires a magnetic vector potential $\vec{A}$ with a z-component only, see Harrington (1961). The size of the computational domain is ($500\,\Delta x$, $20\,\Delta y$, $10\,\Delta z$), where $\Delta x = \Delta y = \Delta z$=2 mm.

To compare the performance of various absorbers with the proposed PML in a typical waveguide port termination problem, the reflection as defined in (6.46) was computed for five types of ABCs. The first two are single-layer absorbers: Mur's second order ABC, and the second-order dispersive boundary condition (DBC). The other three are PML ABCs and they are the same as those used in the case of the dipole: GPML, MPML, and the proposed IPML profile. All three PML absorbers have the following common parameters: the thickness is 10 cells, $R_0 = 10^{-4}$, $\varepsilon_{\max} = 1$, $n = 2$, their PML termination is a one-way lossy wave equation. The results are plotted in Fig. 6.18. The superior performance of the PML absorbers over the single-layer ABCs is obvious. Of all PML absorbers, the proposed modification in the PML profile results in the lowest reflections in the frequency band of the excitation pulse: the IPML reflections are at least one order of magnitude lower than the reflections from any other ABC.

The dependence of the reflection level on the number of layers in the absorber was investigated for both the dipole and the waveguide problem. The purpose was to come up with a recommendation for the minimum number of layers in the absorber, which would ensure a reflection level below -60 dB in the

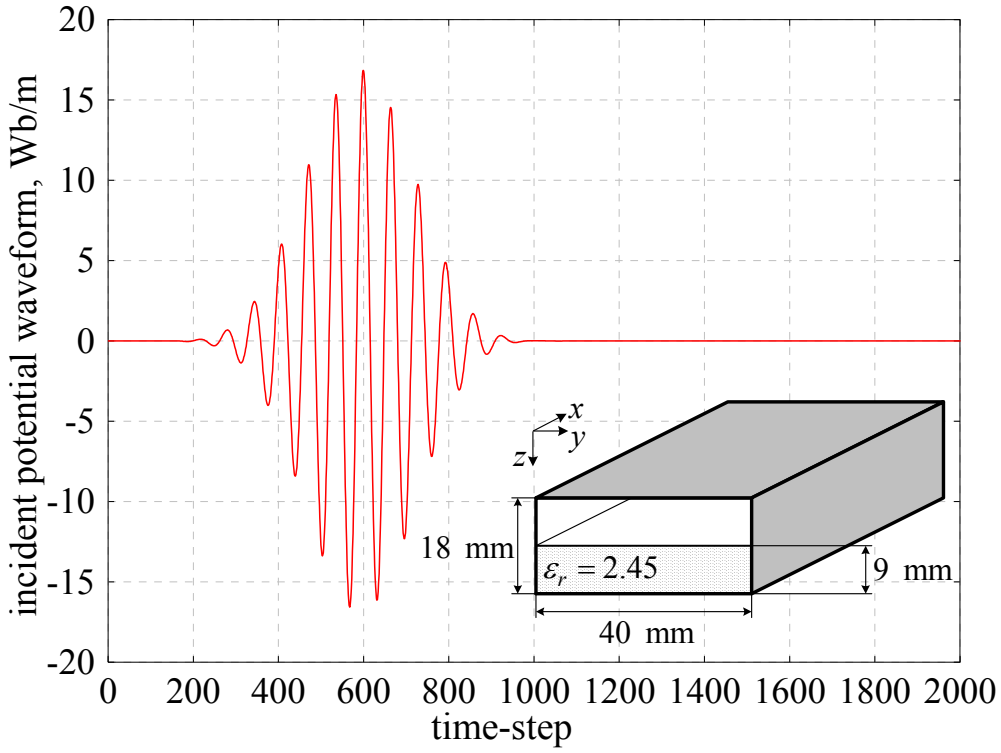

Fig. 6.16. A time sample of the incident potential in the partially filled rectangular waveguide, which is exciting the structure in the frequency band from 3.9 to 5.5 GHz.

frequency band of the excitation. Fig. 6.12 shows this dependence in the 3-D PML absorber of the dipole radiation example at $f = 7$ GHz when $R_0 = 10^{-4}$, $\varepsilon_{\max} = 4$, $n = 3$ for $\beta = 1$ and $\beta = 2$. Fig. 6.15 shows the dependence of the reflection on the PML thickness for the hollow waveguide for the central frequency of 10 GHz, when $R_0 = 10^{-4}$, $\varepsilon_{\max} = 1$, $n = 2$.

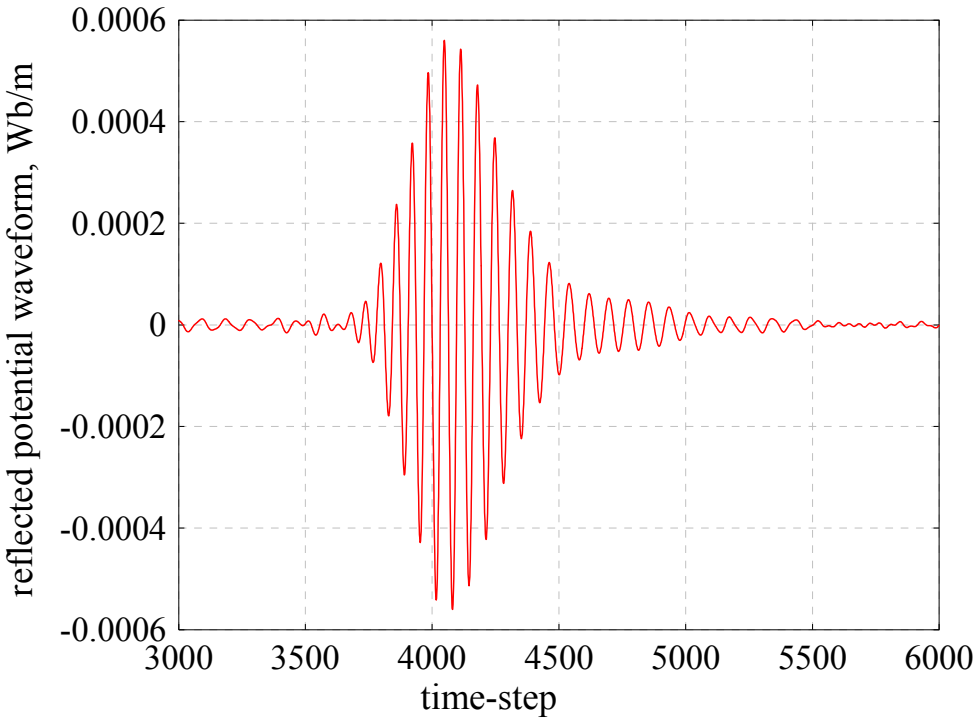

Fig. 6.17. A (later) time sample of the reflected potential in the partially filled rectangular waveguide, whose incident potential waveform is shown in Fig. 6.16. ($N_{\mathrm{PML}} = 12$, $R_0 = 10^{-5}$, $\varepsilon_{\max} = 1$, $n = 2$).

In Fig. 6.19, the dependence of the reflection on the PML thickness in the partially-filled waveguide port termination is shown at the central excitation frequency of 4.7 GHz, when $\varepsilon_{\max} = 1$, $n = 2$ and for different reflection coefficients, $R_0 = 10^{-3}, R_0 = 10^{-4}$, $R_0 = 10^{-5}$. The curves in all examples are very representative of the reflection dependence on the PML thickness in the whole frequency band of the respective source.

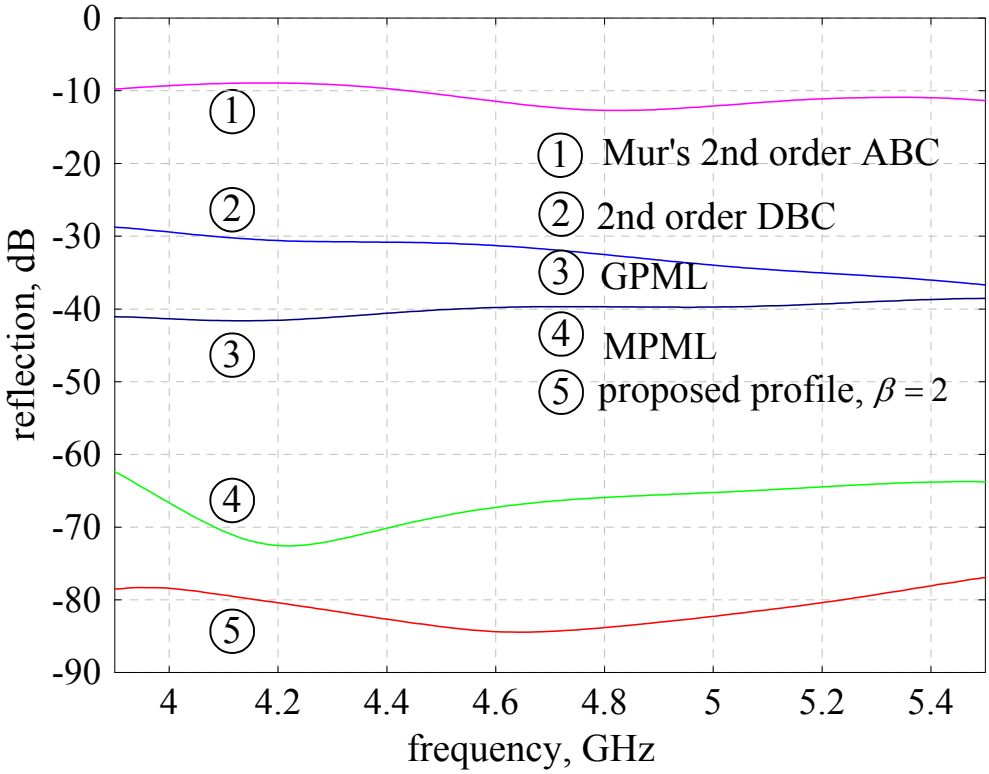

Fig. 6.18. Spectrum of the reflection in the waveguide problem with different ABCs: 1 – Mur's second order ABC, 2 – the second order DBC, 3 – GPML, 4 – MPML, 5 – current profile with $\beta = 2$ ($N_{\text{PML}} = 10$, $R_0 = 10^{-4}$, $\varepsilon_{\max} = 1$, $n = 2$ in all PML cases).

Generally, one can draw the conclusion that thicker PMLs are needed for the termination of 3-D computational domains in the case of open problems modeled by the wave equation than in the case of guiding structures. Compared to the PML termination of the FDTD solution of Maxwell's equations, the number of layers in the IPML-WETD absorber for guiding structures problems are practically the same. For open problems, 4-5 layers more are necessary than in the case of guiding structures. To achieve reflections under 0.1 % in a broad frequency band, at least 12 PML cells are necessary in the case of open problems (with a PEC layer termination).

In brief, for guiding structures 8 to 10 cells thick PML is completely enough, but in open problems, at least 12 to 15 cells are necessary.

The thickness of the IPML-WETD developed here is the same for the same type problem when compared with GPML of J. Fang *et al* (1996) and MPML of B. Chen *et al* (1995). As already mentioned, in the open problem case, the original Berenger's PML for the FDTD solution to Maxwell's equations requires 5-6 layers less in comparison with all other PMLs. Here, it is important to note that in any problem where a presence of scattered/evanescent waves is expected, the performance of any of MPML, GPML or the proposed IPML, is far better than the original Berenger's PML.

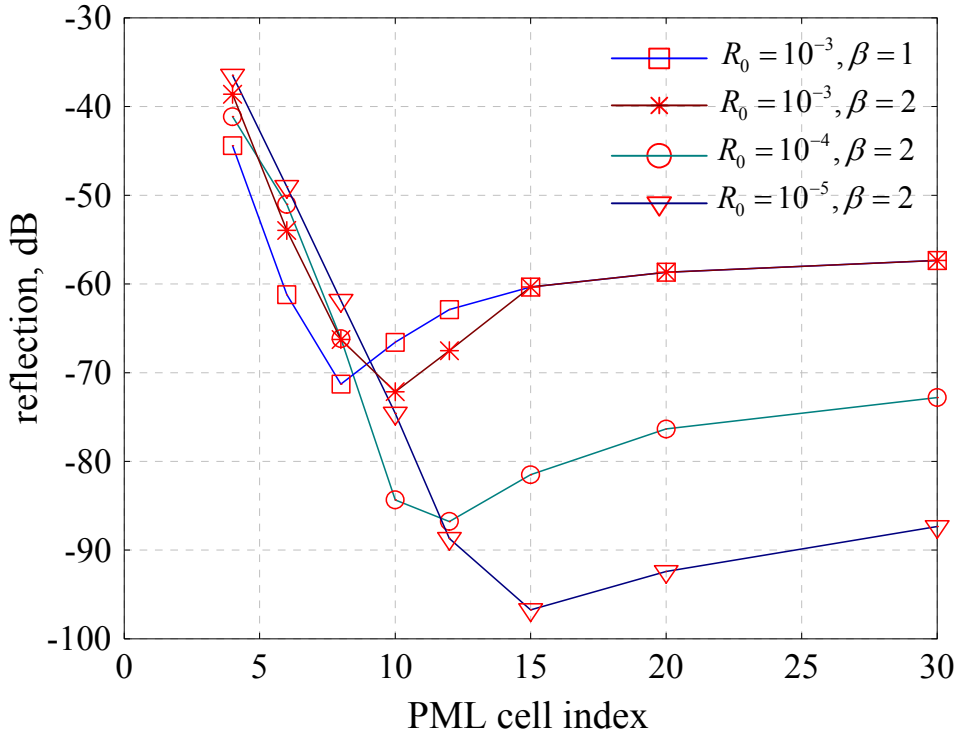

Fig. 6.19. Dependence of the reflection on the thickness of the PML in the partially filled waveguide at $f = 4.7$ GHz ($\varepsilon_{\max} = 1$, $n = 2$) for different theoretical reflection coefficients.

6.5.4 Lossy layer terminations and other PML parameters

The influence of the type of termination layer on the PML performance of the PML ABC has been investigated in the case of waveguide partially filled with dielectric. The results are shown in Fig. 6.20 where the usual termination by a PEC wall is compared to three types of lossy layer terminations:

1.The one-way lossy WE,

2.The lossy Mur's second order ABC, and

3.The lossy second order DBC.

The figure shows that improvement by 5 to 15 dB is easily achievable if a single-layer lossy ABC is used instead of a PEC wall. The one-way lossy WE termination and the lossy second order DBC termination provide the desired broadband performance. It should be mentioned that the lossy DBC termination requires optimization of the two velocities $v_{1\xi}$ and $v_{2\xi}$, and there is no prescription for their choice. This is an intrinsic drawback of all DBC absorbers.

Another parameter, whose influence on the performance of the absorber has been investigated, is $\varepsilon_{\max}$, i.e., the parameter controlling the rate of the evanescent wave absorption in the PML loss factor α_i, $i = x, y, z$. The dependence of the frequency band of the reflection on the value of $\varepsilon_{\max}$ is shown in Fig. 6.21. From the figure it can be seen that increasing the value of $\varepsilon_{\max}$ leads to broadening of the frequency band. However, too large values of $\varepsilon_{\max}$ cause greater numerical dispersion and have to be avoided. The best results are usually

obtained with values of $\varepsilon_{\max}$ in the range of 1 to 3 or at most 4. B. Chen *et al.* (1995) propose values up to 10, but that is for the MPML for the FDTD method when Maxwell's equations are discretized. The experiments conducted so far show that the performance of MPML for FDTD solution to Maxwell's equations is relatively insensitive to the value of $\varepsilon_{\max}$, which is consistent with the results of others. However, this is not the case when the performance of PML for WETD is concerned. In the latter case, the value of $\varepsilon_{\max}$ *must always be greater than zero*. The performance of the IPML-WETD absorber dramatically worsens for $\varepsilon_{\max} = 0$, namely, when the original version of Berenger's PML conductivity profile is used with no PML loss factor included.

The theoretical reflection coefficient at normal incidence R_0, which is a user defined parameter, is the last parameter among the PML variables. Both absorbers (for the FDTD and for the WETD), exhibit moderate sensitivity to its value. Lower values of R_0 correspond to wider frequency band. Also it has to prescribe correctly the desired level of reflections. If a level of –60 dB (0.1 % of the magnitude of the incident wave) is aimed at, the value of R_0 should be prescribed as $R_0 = 10^{-3}$. For all practical purposes, it is enough to choose $R_0 \le 10^{-6}$ for media of permittivity close to that of the air; the numerical experiments show that best PML performance in high-permittivity media is

achieved when the exponent rate of R_0 is multiplied by $\sqrt{\varepsilon_r}$. The dependence of the frequency bandwidth on the reflection coefficient is shown in Fig. 6.22.

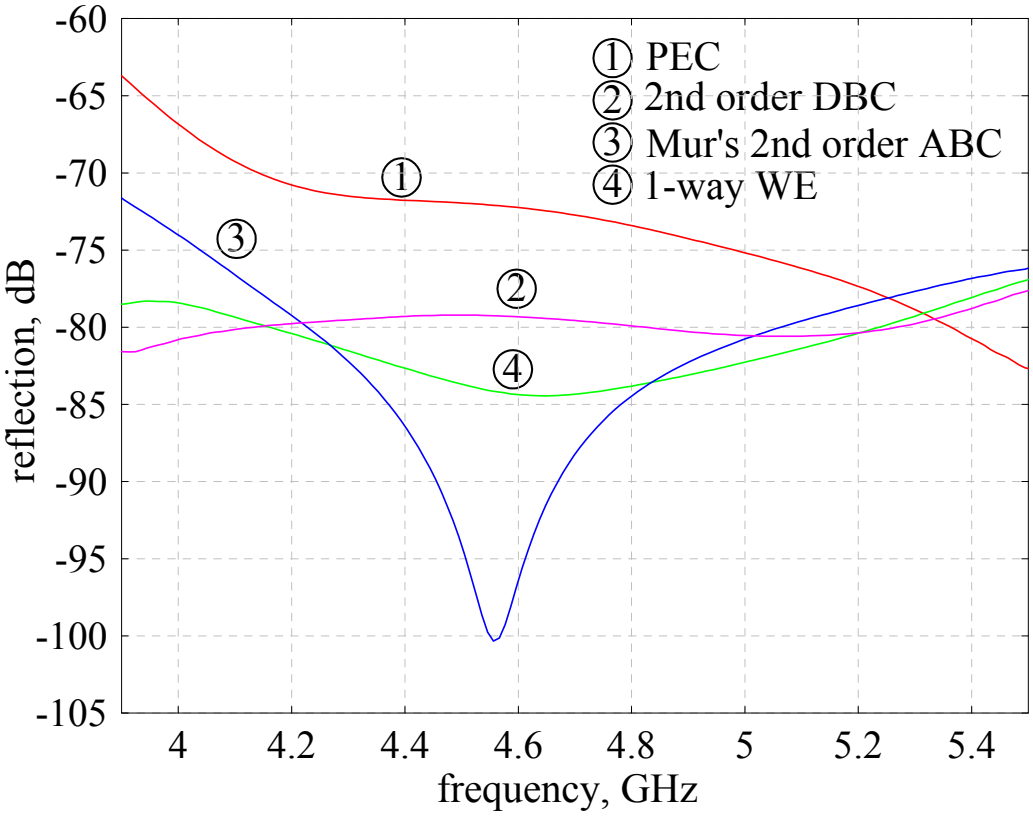

Fig. 6.20. Influence of the type of termination on the PML ABC performance for the waveguide example: 1 – PEC; 2 – second order DBC; 3 – lossy Mur's second order ABC; 4 – one-way lossy WE.

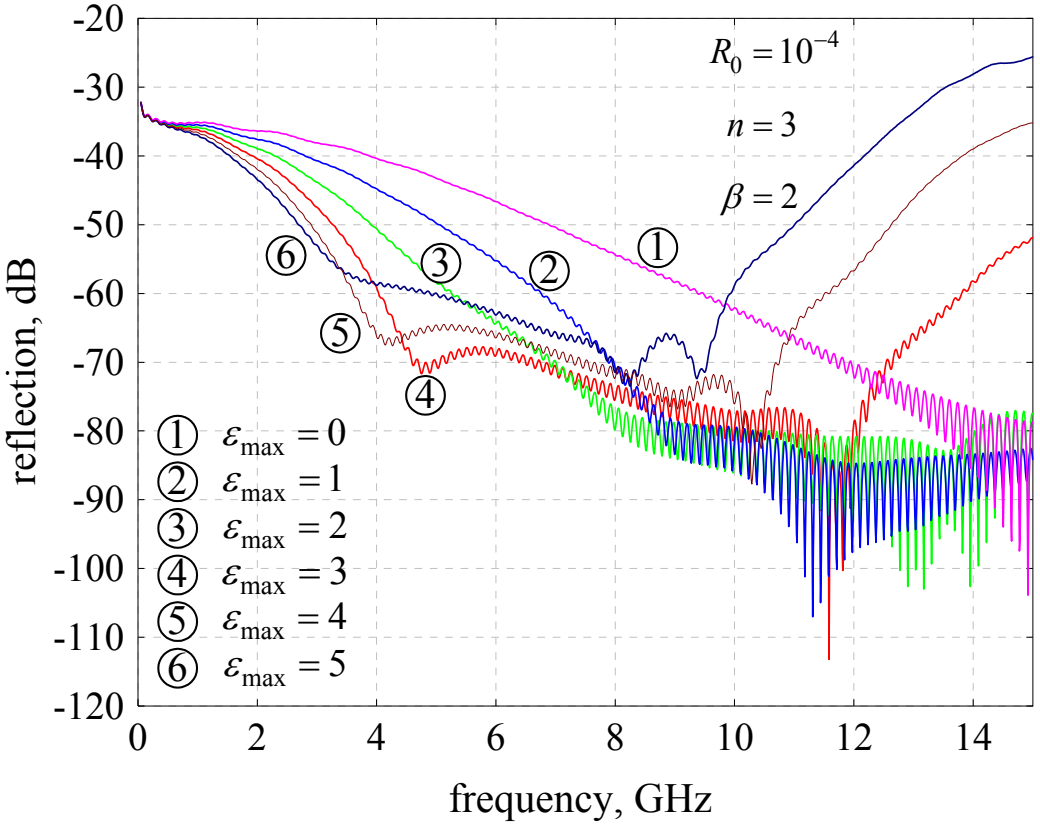

Fig. 6.21. Influence of the parameter $\varepsilon_{\max}$ on the performance of PML ABC in the infinitesimal dipole problem. $N_{PML} = 16$.

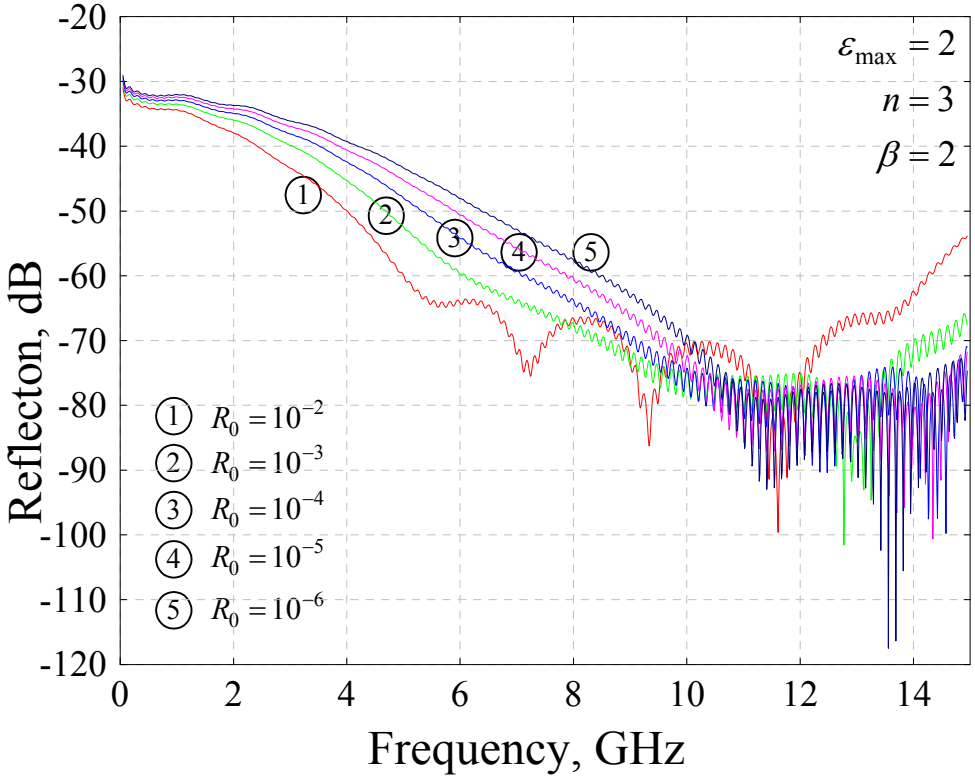

Fig. 6.22. Influence of the parameter R_0 (the reflection coefficient at normal incidence) on the performance of PML ABC in the infinitesimal dipole problem. $N_{PML} = 20$.

6.5.5 Optical waveguide with a two-layer anti-reflection coating

As an example of the application of the PML ABC developed here in photonics, to a 3-D optical structure, a buried optical waveguide terminated by a two-layer anti-reflection (AR) coating is considered. In this case (a lossless inhomogeneous medium), all three components of the magnetic vector potential must be calculated and each of the corresponding auxiliary variables has all three components. The geometry of the waveguide and its AR coating is shown in Fig.6.23. The core and the cladding have refraction coefficients of $n_0 = 3.38$ and $n_c = 3.17$, respectively. The core has rectangular cross section of dimensions $w = 1.6\mu m$ by $h = 0.168\mu m$. The two AR coating layers have thickness of $d_1 = 0.166\mu m$ and $d_2 = 0.267\mu m$. Their corresponding refraction coefficients are $n_1 = 2.33$ and $n_2 = 1.45$.

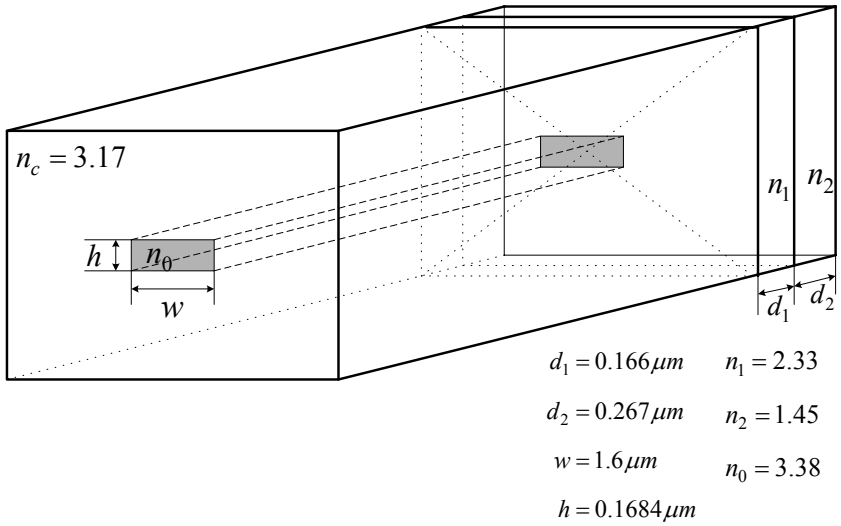

Fig. 6.23 Geometry of a buried optical waveguide terminated by a 2-layer anti-reflection (AR) coating.

The waveguide is excited by a sinusoidal wave of wavelength $\lambda_0 = 1.55\ \mu$m, modulated by the BHW function. The structure is terminated by 20 cells thick PML, located at 15 spatial steps after the end of the second AR coating layer. In all other directions the optical waveguide is terminated by a 6 cells thick PML. Non-uniform grid is used and the minimal spatial step in the structure is $\Delta l_{\min} = 0.0421 \mu m$. The whole computational domain is ($163\,\Delta x$, $124\,\Delta y$, $96\,\Delta z$). In the transverse plane, the core is modeled as $w \times h = 32 \cdot \Delta y \times 4 \cdot \Delta z$, surrounded by a 46-steps cladding of $\Delta y = \Delta z = 0.05$ μm in the $\pm y -$ and $\pm z -$ direction, the last 6 being PMLs. The thickness of the first AR coating is $d_1 = 3 \cdot \Delta x$, the thickness of the second AR coating is $d_2 = 5 \cdot \Delta x$. The structure was simulated by both the FDTD method to Maxwell's equations and by the WETD method. The corresponding spectrum of the reflections from the AR coating is presented in Fig. 6.24 and Fig. 6.25, and is compared to the reflections when the optical waveguide is terminated by air and when the optical waveguide is directly terminated by PML (thus simulating an infinitely long waveguide). A comparison of the reflections spectrum is presented in Fig. 6.25 when the optical waveguide with the two-layer AR coating is simulated by the WETD for the magnetic vector potential and by the FDTD method for Maxwell's equations. The same results obtained from the simulations of the optical waveguide with two-layer AR coating by both methods, show that they are equivalent. The CPU time for the WETD method is about 30 % shorter.

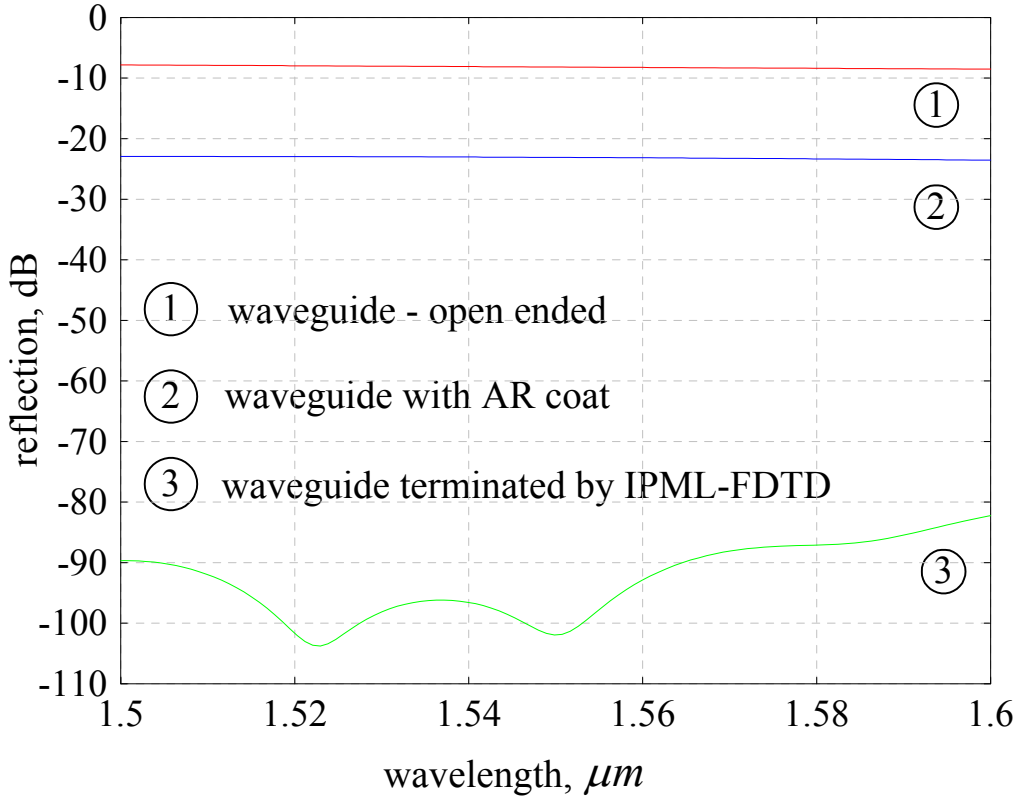

Fig. 6.24. Spectrum of the reflection (by the FDTD method) from: 1 – optical waveguide terminated by air; 2 - optical waveguide terminated by two-layer AR coating; 3 – optical waveguide terminated by IPML-FDTD.

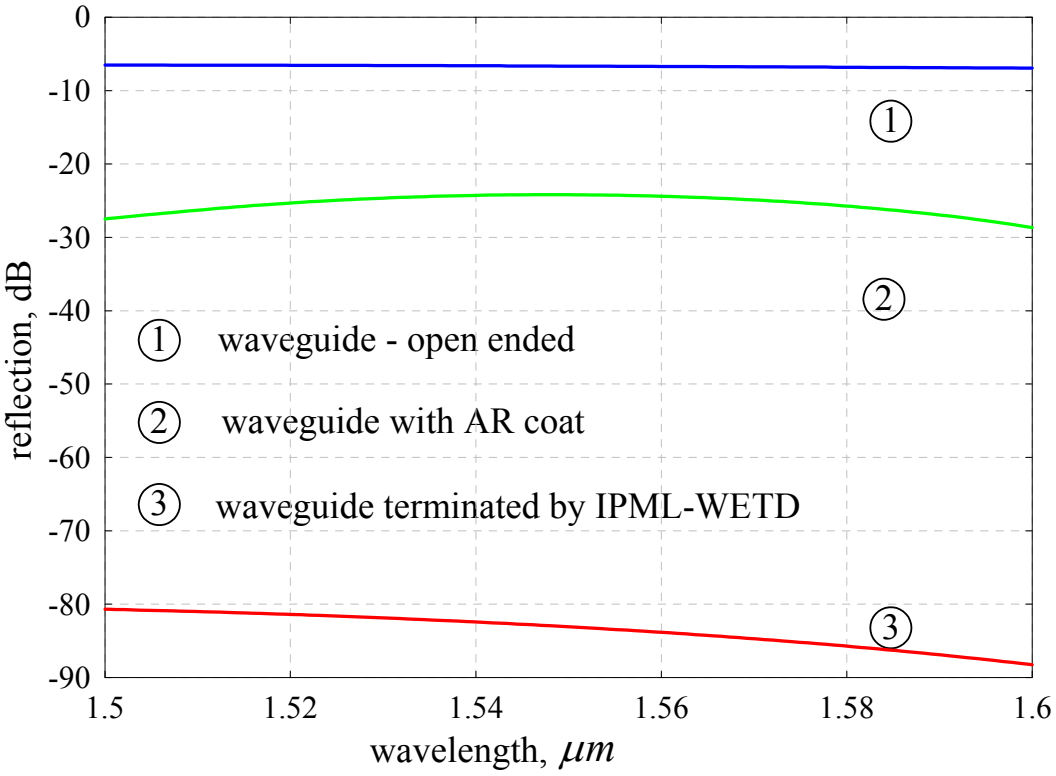

Fig. 6.25. Spectrum of the reflection (by the WETD method) from: 1 – optical waveguide terminated by air; 2 - optical waveguide terminated by two-layer AR coating; 3 – optical waveguide terminated by IPML-WETD.

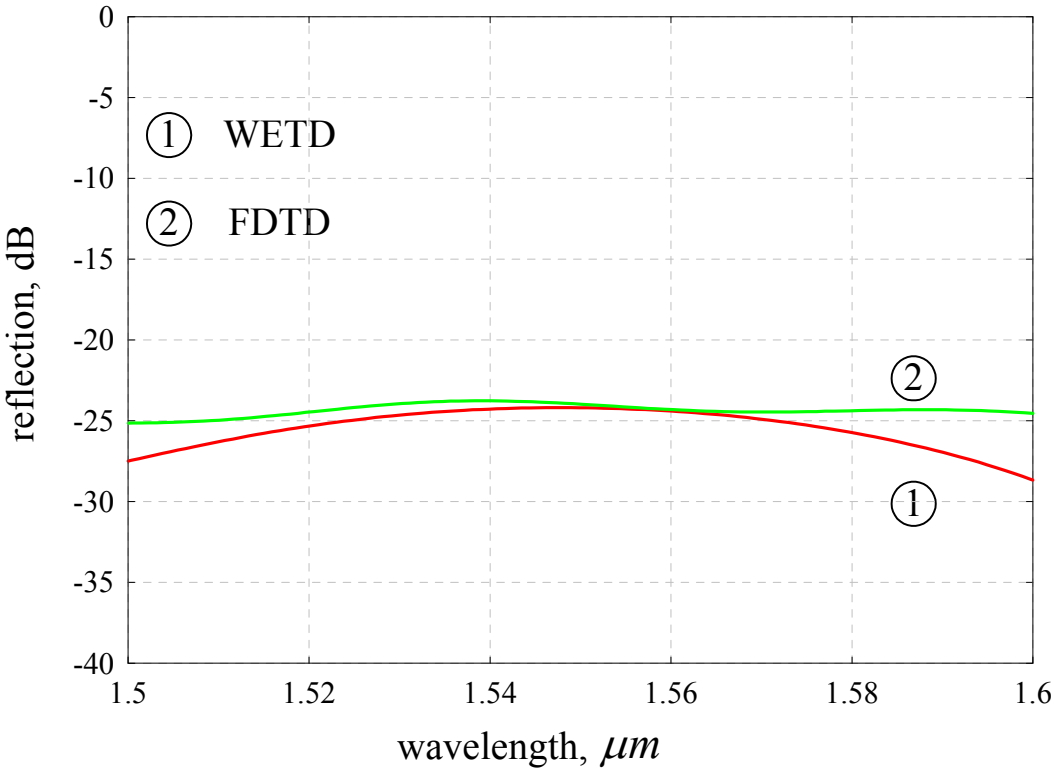

Fig. 6.26. Comparison of the reflections when the buried optical waveguide with a two-layer anti-reflection coating is simulated by: 1 – the WETD method for the magnetic vector potential; 2 – the FDTD method for Maxwell's equations.

Chapter 7

Conclusion

Recent trends in computational electrodynamics include the development of scalar or vector wave equation techniques. They are applied in numerical algorithms both for optical waveguides and devices, and in the microwave and millimetre-wave structure analysis. These new algorithms require a reliable and efficient ABC, which can handle both open problems (i.e. radiation and scattering) and problems involving port terminations (high-frequency circuit problems).

In this thesis, improved PML ABCs for the 3-D scalar wave equation in the time-domain (WETD) in lossless and lossy inhomogeneous media have been developed. To the author's knowledge, this is the first PML ABC developed and successfully implemented in conjunction with the 3-D wave equation in the time domain. It is shown that the conventional PML profiles are not efficient when integrated with the second-order wave equation. A suitable low-reflection broadband PML variable profile is proposed. Its performance is verified and carefully studied in radiation and guided wave problems. The PML variables profiles are modified so that they can grow at different exponent rates. This adds a new degree of freedom in the algorithm and represents a problem-independent

approach to the optimization of the PML performance. Thus improved PML ABCs are developed both for the WETD method and for the FDTD method to the solution of Maxwell's equations. The new profile handles equally well both port terminations and truncations of the computational domain of open problems. The performance of the proposed PML absorber is further improved by the use of simple single-layer ABCs to truncate the PML region. For that, the lossy version of Mur's second order ABC and the lossy version of the second order dispersive boundary condition (DBC) have been developed and implemented. The current implementation handles inhomogeneous dielectrics intersecting the PML boundary. Various numerical simulations have been carried out to validate the theoretical models at microwave and optical frequencies, as well as comparisons to other well-known ABCs are presented.

The author's original contributions in this thesis are enlisted below.

1. The formulation of the PML variable profiles has been modified by allowing the PML conductivity and PML loss factor to grow at different rates. This in effect adds a new degree of freedom in the algorithm. On that basis, an improved Perfect Matched Layer (IPML) ABC for the FDTD solution of Maxwell's equations is developed for orthogonal non-uniform grids and is implemented in a FORTRAN program.

2. The Perfect Matched Layer ABC for the 3-Dimensional wave equation in time-domain (WETD) is formulated and developed on orthogonal non-uniform grids and is implemented in FORTRAN program. New degree of freedom is added in the formulation of the PML variable profiles, so that they are allowed to grow at different rates.
3. New types of termination walls for the PML ABC have been developed and implemented.
4. In depth detailed comparison with commonly used PML ABCs is presented.
5. Prescription for suitable values of all PML parameters is given based on extensive numerical experiments.

In author's opinion, the most important contribution is the introduction of the new degree of freedom in the definition of the PML variables profiles This represents a problem-independent approach to the improvement and optimization of the PML performance, in contrast to the attempts to optimize one PML variable in a problem-specific environment. Finding PML variable profiles suitable for the 3-D wave equation in the time domain was crucial to the primary goal of this research: a development of reliable and efficient ABCs for the WETD. It is important to note also that the PML ABC developed in this thesis is not limited to electromagnetic problems only. It can be applied to any physical phenomenon modeled by the general lossy 3-D scalar wave equation, which requires reflection-free boundaries.

From the experience and knowledge gained in the course of this work, the author is convinced that the following research topics should be addressed for further development:

1. More detailed study of the *combined* influence of all PML parameters on its performance is necessary. This issue concerns equally the PML for the FDTD solution to Maxwell's equations and the PML for the wave equation in the time domain. There are few attempts in this direction (only regarding the FDTD method to the solution of Maxwell's equations), but they include usually one of the PML parameters in a problem-specific environment. Rigorous mathematical formulation of the problem is needed such that *all* PML parameters are included in the model, as well as the influence of the material parameters of the medium, and the intrinsic finite-difference discretization error of third-order.
2. Generalization of the IPML-WETD for anisotropic and especially for dispersive media should be addressed.
3. All the microwave and optical structures considered in this thesis are linear. Further work should be realized to apply the IPML ABC for non-linear media as those are frequently met in photonics applications.

BIBLIOGRAPHY

M.A. AlSunaidi, W. ElSallal (1999) – A PML-FDTD formulation for the simulation of optical structures, *Microwave and Optical Technology Letters*, vol. 22, no.5, Sep 5 1999, pp. 355-358.

J.P. Berenger (1994) – A perfectly matched layer for the absorption of electromagnetic waves, *J. of Comp. Physics,* vol. 114, pp. 185-200.

J.P. Berenger (1996) – Perfectly matched layer for the FDTD solution of wave-structure interaction problems", *IEEE Trans. on Antennas and Propagation*, vol. 44, no. 1, pp. 110-117.

Z. Bi, K.L. Wu, C. Wu, and J. Litva (1992) – A dispersive boundary condition for microstrip component analysis using FDTD method, *IEEE Trans. on Microwave Theory and Techniques*, vol. 40, no. 4, pp. 774-777.

M, Cai, H. Zhou, N.N. Ljepojevic (1996) –Ideal absorption condition for FDTD method in isotropic lossy dispersive media, *2nd High Frequency Postgraduate Student Colloquium,* Centre for Comput. & Math. Modelling, South Bank Univ., London, UK, pp. 51-57.

B. Chen, D.G. Fang and B.H. Zhou (1995) – Modified Berenger PML absorbing boundary condition for FD-TD meshes, *IEEE Microwave and Guided Wave Letters*, vol. 5, no. 11, pp. 399-401.

W.C. Chew, J.M. Jin and E. Michielssen (1997) – Complex coordinate system as a generalized absorbing boundary condition, *IEEE Antennas and Propagation Society International Symposium,* Digest, vol. 3, pp. 2060-2063.

W.C. Chew and J.M. Jin (1996) – Perfectly matched layers in the discretized space: An analysis and optimization, *Electromagnetics*, vol. 16, pp.325-340.

W.C. Chew and W.H. Weedon (1994) – A 3D perfectly matched medium from modified Maxwell's equations with stretched coordinates, *Microwave and Optical Technology Letters*, vol.7, no. 13, pp.599-604.

A. Cuccinotta, G. Pelosi, S. Selleri, L. Vincetti and M. Zoboli (1999) –Perfectly matched anisotropic layers for optical waveguide analysis through the finite-element beam-propagation method, *Microwave and Optical Technology Letters*, vol. 23, no. 2, pp. 67-69.

B. Engquist and A. Majda (1977) –Absorbing boundary condition for the numerical simulation of waves*, Mathematical Computation*, vol.31, pp. 629-651.

D.G. Fang (1998) – *Electromagnetics*, Lecture notes, Nanjing University of Science and Technology, China.

J. Fang, Zh. Wu (1995) – Generalized perfectly matched layer – An extension of Berenger's perfectly matched layer boundary condition, *IEEE Microwave and Guided Wave Letters*, vol. 5, no. 12, pp. 451-453.

J. Fang and Zh. Wu (1996) – Generalized perfectly matched layer for the absorption of propagating and evanescent waves in lossless and lossy media,

IEEE Trans. on Microwave Theory and Techniques, vol. 44, no. 12, pp. 2216-2222.

S.D. Gedney (1996) – An anisotropic perfectly matched layer absorbing medium for the truncation of FDTD lattices, *IEEE Trans. On Antennas and Propagation*, vol. 44, pp. 1630-1639.

M.A. Gribbons, W.P. Pinello and A.C. Cangellaris – A stretched coordinate technique for numerical absorption of evanescent and propagating waves in planar waveguiding structures, *IEEE Trans. on Microwave Theory and Techniques*, vol. 43, no. 12, pp. 2883-2889.

N. Georgieva (2001) – Construction of solutions to electromagnetic problems in terms of two collinear vector potentials, accepted for publication in *IEEE Trans. on Microwave Theory and Techniques*.

N. Georgieva (1997) – Studies on numerical time-domain methods for the analysis of transient electromagnetic fields, *Ph.D. thesis*, The University of Electro-Communications, Japan.

N. Georgieva and Y. Rickard (2000) – The application of the wave potential functions to the analysis of transient electromagnetic fields, *IEEE MTT-S Int. Symposium Digest*, June 2000, vol. 2, pp. 1129-1132.

N. Georgieva and Y. Rickard (1999) – Time domain modelling of electromagnetic field propagation via wave potentials," *XXVIth General Assembly of the International Union of Radio Science (URSI)*, August 1999, Toronto, Abstracts Digest pp. 178.

N. Georgieva and E. Yamashita (1998) – Time-domain vector-potential analysis of transmission line problems, *IEEE Trans. on Microwave Theory and Techniques*, vol. 46, no. 4, pp. 404-410.

M.A. Gribbons, W.P. Pinello and A.C. Cangellaris (1995) – A stretched coordinate technique for numerical absorption of evanescent and propagating waves in planar waveguiding structures, *IEEE Trans. on Microwave Theory and Techniques*, vol. 43, no. 12, pp. 2883-2889.

R.F. Harrington (1961) – *Time-Harmonic Electromagnetic Fields*, New York: McGraw Hill, pp.158-161.

R.F. Harrington (1968) – *Field Computation by Moment Methods*, New York: Macmillan.

F.J. Harris (1978) – On the use of windows for harmonic analysis with the discrete Fourier transform, *Proc. IEEE*, vol. 66, no. 1, pp. 51-83.

R. Holland (1994) – Finite-difference time-domain (FDTD) analysis of magnetic diffusion, *IEEE Trans. on Electromagnetic Compatibility*, vol. 36, pp. 32-39.

W.P. Huang, S.T. Chu, A. Goss, and S.K. Chaundhuri (1991a) – A scalar finite-difference time-domain approach to guided-wave optics, *IEEE Photonics Technology Letters*, vol. 3, no. 6, pp. 524-526.

W.P. Huang, S.T. Chu, and S.K Chaundhuri (1991b) – A semivectorial finite-difference time-domain method, *IEEE Photonics Technology Letters*, vol. 3, no. 9, pp. 803-806.

W.P. Huang, C.L. Xu, and J. Chrostowski (1993) – A time-domain propagating scheme for simulation of dynamics of optical guided-wave devices, *IEEE Photonics Technology Letters*, vol. 5, no. 4, pp. 1071-1073.

W.P. Huang, C.L. Xu and K. Yokoyama (1996) – The perfectly matched layer boundary condition for modal analysis of optical waveguides: leaky mode calculations, *IEEE Photonics Technology Letters*, vol.8, no. 5, pp. 652-654.

D. Johnson, C. Furse and A. Tripp (2000) – Application and optimization of the Perfectly Matched Layer Boundary Condition for geophysical simulations, *Microwave and Optical Technology Letters*, vol. 25, no.4, May 20 2000, pp.253-55.

D.S. Katz, T. Thiele, Allen Taflove (1994) – Validation and extension to three dimensions of the Berenger's PML ABC for FD-TD Meshes, *IEEE Microwave and Guided Wave Letters*, vol. 4, no.8, pp. 268-270.

M. Koshiba, Y. Tsuji, and M. Hikari (2000) – Time-domain beam propagation method and its application to photonic crystal circuits, *IEEE Photonics Technology Letters*, vol. 18, no. 1, pp. 102-110.

L. Knockaert, D. De Zutter (2000) – On the stretching of Maxwell's equations in general orthogonal coordinate systems and the PML, *Microwave and Optical Technology Letters*, vol. 24, no.1, pp.31-34.

D. Krupezevic, V. Brankovic, F. Arndt (1993) – The wave-equation FD-TD for the efficient eigenvalue analysis and S-matrix computation of waveguide structures, *IEEE Trans. on Microwave Theory and Techniques*, vol. 41, no. 12, pp. 2109-2115.

K. Kunz and R Luebbers (1993) – *Finite-Difference Time-Domain Method for Electromagnetics*, CRC Press.

G. Lazzi (2001) – Unconditionally stable D-H FDTD formulation with anisotropic PML boundary conditions, *IEEE Microwave and Wireless Components Letters*, vol. 11, no. 4, pp. 149-151.

G. Lazzi, C.M. Furse, O.P. Gandhi (1997a) – Optimization and design of conductivity profiles for the PML boundary condition and its application to bioelectromagnetic problems, *IEEE Antennas and Propagation Society International Symposium,* Digest, vol. 1, pp. 486 –489.

G. Lazzi, O.P. Gandhi (1997b) – Inversion theory as applied to the optimization of conductivity profile for PML absorbing boundary condition for FDTD code, *Electronics Letters*, vol. 33, no. 6, pp. 502-503.

G. Lazzi, O.P. Gandhi (1997c) – On the optimal design of the PML absorbing boundary condition for the FDTD Code, *IEEE Trans. on Antennas and Propagation*, vol. 45, no. 5, pp. 914-916.

E.A. Marengo, C.M. Rappaport and E. L. Miller (1999) – Optimum PML ABC conductivity profile in FDTD, *IEEE Trans. on Magnetics*, vol. 35, no. 3, May 1999, pp. 1506-1509.

P. Monk and E. Suli (1994) – A convergence analysis of Yee's scheme on non-uniform grid, *SIAM J. on Numerical Analysis*, vol. 31, pp. 393-412.

G. Mur (1981) – Absorbing boundary conditions for the finite-difference approximation of the time-domain electromagnetic-field equations, *IEEE Trans. on Electromagnetic Compatibility*, vol. EMC-23, no.4, pp.377-382.

E.A. Navarro, N.T. Sangari and J. Litva (1996) – Some considerations on the accuracy of the non-uniform FDTD method and its applications to waveguide analysis when combined with the perfectly matched layer technique, *IEEE Trans. on Microwave Theory and Techniques*, vol. 44, pp. 1115-1124.

E.A. Navarro, C. Wu, P.Y. Chung and J. Litva (1995) – Application of PML super-absorbing boundary condition to non-orthogonal FDTD method, *IEE Electronics Letters*, 30(20), pp. 1654-1656.

J. Peng, C.A. Balanis (1998) – A generalized reflection-free domain-truncation method: transparent absorbing boundary, *IEEE Trans. on Antennas and Propagation,* vol. 46, no. 7, pp. 1015-1022.

O.M. Ramahi (1999) – Absorbing boundary conditions for the three-dimensional vector wave equation*, IEEE Trans. on Antennas and Propagation*, vol. 47, no. 11, pp. 1735-1736.

C.M. Rappaport (1995) – Perfectly matched absorbing boundary conditions based on anisotropic lossy mapping of space, *IEEE Microwave and Guided Wave Letters*, vol. 5, no. 3, pp. 90-92.

C.M. Rappaport (1996) – Interpreting and improving the PML absorbing boundary condition using anisotropic lossy mapping of space, *IEEE Trans. on Magnetics*, vol. 32, no. 3, pp. 968-974.

N. Sachdeva, N. Balakrishnan, S.M. Rao (2000) – A new ABC for FDTD, *Microwave and Optical Technology Letters*, vol. 25, no.2, pp.86-90.

Z.S. Sacks, D.M. Kingsland, R. Lee, Jin-Fa Lee (1995) – A perfectly matched anisotropic absorber for use as an absorbing boundary condition, *IEEE Trans. on Antennas and Propagation*, vol.43, no. 12, pp. 1460 –1463.

G. Shen; G. Zhou; Y. Chen; B. Beker, (2000) – Analysis and design of cylindrical multilayered MMICs using a unified non-uniform FDTD algorithm, *IEEE Antennas and Propagation Society International Symp*, Digest, vol. 4, pp. 2008 – 2011.

J. Strikwerda (1989) – *Finite Difference Schemes and Partial Differential Equations*, Wadsworth & Brooks, Pacific Grove, California.

B. Stupfel and R. Mittra (1996) – Numerical absorbing boundary conditions for the scalar and vector wave equations, *IEEE Trans. on Antennas and Propagation,* vol. 44, no. 7, pp. 1015-1022.

D.M. Sullivan (1998) – A simplified PML for use with the FDTD method, *IEEE Microwave and Guided Wave Letters,* vol. 6, no. 2, pp. 97-99.

A. Taflove (1995), *Computational Electrodynamics: the Finite-Difference Time-Domain Method*, Artech House, Boston.

A. Taflove and M.E. Brodwin (1995) – Numerical solution of steady-state electromagnetic scattering problems using the time-dependent Maxwell's equations, *IEEE Trans. on Microwave Theory and Techniques*, vol. 23, pp. 623-630.

J. Tang, K.D. Paulsen and S.A. Haider (1998) – Perfectly matched layer mesh terminations for nodal-based finite-element methods in electromagnetic scattering, *IEEE Trans. on Antennas and Propagation*, vol. 46, no. 4, pp. 507-516.

F.L. Teixeira, W.C. Chew (1998a) – A general approach to extend Berenger's ABC to anisotropies and dispersive media, *IEEE Trans. on Antennas and Propagation*, vol. 46, no. 9, pp. 1386-1387.

F.I. Teixeira and W.C. Chew (1998b) – Analytical properties of the anisotropic PML constitutive tensors in curvilinear coordinates, *IEEE Antennas and Propagation Society International Symposium,* Digest, vol. 2, pp. 1266-1269.

F.L. Teixeira, W.C. Chew (1999) – On causality and dynamic stability of perfectly matched layers for FDTD simulations*, IEEE Trans. on Microwave Theory and Techniques*, vol. 47, no. 6, pp. 775-785.

T. Uno; Yiwei He, S. Adachi (1997) – Perfectly matched layer absorbing boundary condition for dispersive medium, *IEEE Microwave and Guided Wave Letters*, vol. 7, no. 9, pp. 264 –266.

S.C. Winton and C.M. Rappaport (2000) – Specifying PML conductivities by considering numerical reflection dependencies, *IEEE Trans. on Antennas and Propagation*, vol. 48, no. 7, pp. 1055-1063.

T. Yassui, M. Koshiba, Y. Tsuji (1999) – A wide-angle finite element beam propagation method with perfectly matched layers for nonlinear optical waveguides, *J. of Lightwave Technology*, vol. 17, no. 10, pp.1909-1915.

K.S. Yee (1966) – Numerical solution of initial boundary value problems involving Maxwell's equations in isotropic media, *IEEE Trans. on Antennas and Propagation*, vol. 14, pp. 302-307.

S. Yoneta, M. Koshiba and Y. Tsuji (1999) – Combination of BPM and FEM for optical beam propagation analysis, *J. of Lightwave Technology*, vol. 17, no. 11, pp. 2398-2404.

An Ping Zhao (1998a) – Application of the material-independent PML absorbers to the FDTD analysis of electromagnetic waves in nonlinear media, *Microwave and Optical Technology Letters,* vol. 17, no.3, pp.164-168.

An Ping Zhao (1998b) – Generalized material-independent PML absorbers used for the FDTD simulation of electromagnetic waves in 3-D arbitrary anisotropic dielectric and magnetic media, *IEEE Trans. on Microwave Theory and Techniques*, vol. 46, no.10, pp. 1511-1513.

An Ping Zhao and A.V. Räisänen (1998a) – Extension of Berenger's PML ABC to arbitrary anisotropic magnetic media, *IEEE Microwave and Guided Wave Letters*, vol. 8, no.1, pp. 15-17.

An Ping Zhao and M.A. Rinne (1998b) – Theoretical proof of the material-independent PML absorbers used for arbitrary anisotropic media, *Electronics Letters*, vol. 34, pp. 48-49.

An Ping Zhao, J. Juntunen and A.V. Räisänen (1999) – An efficient FDTD algorithm for the analysis of microstrip patch antennas printed on a general

anisotropic dielectric substrate, *IEEE Trans. on Microwave Theory and Techniques*, vol. 47, no.7, pp.11142-46.

Li Zhao and A.C. Cangellaris (1996a) – A general approach for the development of unsplit-time-domain implementations of perfectly matched layers for FDTD grid truncation, *IEEE Microwave and Guided Wave Letters*, vol. 6, no. 5, pp. 209-211.

Li Zhao and A.C. Cangellaris (1996b) – GT-PML: Generalized theory of perfectly matched layers and its application to the reflectionless truncation of finite-difference time-domain method, *IEEE Trans. on Microwave Theory and Techniques*, vol. 44, no. 12, pp. 2555-2563.

D. Zhou, W.P. Huang, C.L. Xu, D.G. Fang and B. Chen (2001) – The perfectly matched layer boundary condition for scalar finite-difference time-domain method, *IEEE Photonics Technology Letters*, vol.13, no.5, pp. 454-456.

List of Publications Related to the Thesis

1. Yotka Rickard, N. Georgieva and W. -P. Huang, "Application and optimization of PML ABC for the 3-D wave equation in the time domain", accepted for publication in *IEEE Trans. On Antennas and Propagation,* Dec 2002.

2. Yotka Rickard, N. Georgieva and W. -P. Huang, "A perfectly matched layer for the 3-D wave equation in the time domain", accepted for publication in *IEEE Microwave and Wireless Components Letters,* May 2002.

3. Yotka Rickard and N. Georgieva, "Performance study of an improved PML ABC for Finite-Difference Time-Domain Techniques in Electrodynamics", submitted for the XXVIIIth General Assembly of the International Union of Radio Science (URSI), 2002.

4. N. Georgieva and Y. Rickard, "The application of the wave potential functions to the analysis of transient electromagnetic fields", *IEEE MTT-S Int. Symposium Digest* (Boston, Massachusetts), June 2000, vol. 2, pp. 1129-1132.

5. N. Georgieva and Y. Rickard, "Time domain modelling of electromagnetic field propagation via wave potentials," *XXVIth General Assembly of the International Union of Radio Science (URSI)*, August 1999, Toronto, Abstracts Digest pp. 178.

Abbreviations Index